Aus der Klinik für Gastroenterologie, gastrointestinale Onkologie und Endokrinologie
(Prof. Dr. med. V. Ellenrieder)
der Medizinischen Fakultät der Universität Göttingen

Expression of gemcitabine metabolizing enzymes in different pancreatic cancer model systems

INAUGURAL-DISSERTATION

zur Erlangung des Doktorgrades
der Medizinischen Fakultät der
Georg-August-Universität zu Göttingen

vorgelegt von

Lisa Knoll

aus

Göttingen

Göttingen 2022

Dekan:	Prof. Dr. med. W. Brück

Betreuungsausschuss

Betreuer/in	Prof. Dr. Dr. Albrecht Neeße
Ko-Betreuer/in:	Prof. Dr. Wolfram Hubertus Zimmermann

Prüfungskommission

Referent/in	Prof. Dr. Dr. Albrecht Neeße
Ko-Referent/in:	Prof. Dr. med. Wolfram Hubertus Zimmermann
Drittreferent/in:	Prof. Dr. Margarete Schön

Datum der mündlichen Prüfung: 19.04.2023

Hiermit erkläre ich, die Dissertation mit dem Titel "Expression of gemcitabine metabolizing enzymes in different pancreatic cancer model systems" eigenständig angefertigt und keine anderen als die von mir angegebenen Quellen und Hilfsmittel verwendet zu haben.

Göttingen, den 12.04.2022 ……

(Unterschrift)

Contents

List of Figures

List of Tables

List of Abbreviations

AB	antibody
ADM	acinar-to-ductal metaplasia
ap	antigen-presenting
BET	bromodomain and extra-terminal motif
BRCA 1/2	breast cancer gene 1/2
BS	blocking solution
CAF	cancer-associated fibroblast
CIS	carcinoma *in situ*
CD	cluster of differentiation
CDA	cytidine deaminase
CM	conditioned medium
COL	collagen
CTP	cytidine triphosphate
CXCL12/14	Chemokine (C-X-C motif) ligand 12/14
DCK	deoxycytidine kinase
DCTD	deoxycytidylate deaminase
dFdC	2',2'-difluoro 2'-deoxycytidine
dFdCMP	2',2'-difluoro 2'-deoxycytidine monophosphate
dFdCDP	2',2'-difluoro 2'-deoxycytidine diphosphate
dFdCTP	2',2'-difluoro 2'-deoxycytidine triphosphate
dFdU	2',2'-difluoro 2'-deoxyuridine
DGVS	German Society for Gastroenterology, Digestive- and Metabolic Diseases *(deutsch „Deutsche Gesellschaft für Gastroenterologie, Verdauungs- und Stoffwechselkrankheiten")*
DME	drug metabolizing enzymes
DNA	desoxyribonucleic acid
ECM	extracellular matrix
EMT	epithelial-mesenchymal transition
ENT	equilibrative nucleoside transporter
FOLFIRINOX	folinic acid (leucovorin), 5-fluoruracil, irinotecan, oxaliplatin
Foxn1^{nu}	foxhead box n1, nude
GEKID	Association of Population-based Cancer Registries in Germany *(deutsch „Gesellschaft der epidemiologischen Krebsregister in Deutschland e.V.")*
GEMM	genetically engineered mouse model
GME	gemcitabine metabolizing enzymes
h	human
H&E	hematoxylin and eosin
HA	hyaluronic acid
Hh	hedgehog

HHIP	Human hedgehog interacting protein
i	inflammatory
IHC	immunohistochemistry
IL	interleukin
Kras	*kirsten rat sarcoma viral oncogene*
KPC	LSL-Kras$^{G12D/+}$;LSL-Trp53$^{R172\ H/+}$; Pdx-1-Cre
LOX	lysyl oxidase
LSL	Lox-STOP-Lox
m	mouse
MDSC	marrow-derived stem cell
MT	Masson's trichrome
my	myofibroblast-like
NIH	National Cancer Institute
NT5C1A	5'-nucleotidase, cytosolic 1A
o/n	overnight
OS	overall survival
OTM	orthotopically transplanted mouse
PanIN	pancreatic intraepithelial neoplasm
PDAC	pancreatic ductal adenocarcinoma
PDX	patient-derived xenograft
PFS	progression-free survival
PRT	primary resected tissue
PSC	pancreatic stellate cell
qRT-PCR	quantitative realtime-polymerase chain reaction
RKI	Robert-Koch Institute *(deutsch „Robert Koch-Institut")*
RNA	ribonucleid acid
RR	ribonucleotide reductase
RT	room temperature
SPARC	secreted protein acidic and rich in cysteine
TAM	tumor-associated macrophage
TCP	tissue-coated plastic
TGF-β	transforming growth factor-β
TME	tumor microenvironment
USA	United States of America
VDR	vitamin D receptor
2D	two-dimensional
3D	three-dimensional
5-FU	5-fluoruracil
α-SMA	α-smooth muscle actin

1 Introduction

Despite efforts in molecular and clinical research, pancreatic cancer remains a lethal disease in Western countries and across the world (Rahib et al. 2014; Quante et al. 2016). It can originate from different parts of the pancreas. However, over 90 % of the most common subtype found in patients arises from the exocrine gland and is termed pancreatic ductal adenocarcinoma (PDAC)(Biankin et al. 2012).

1.1 Pancreatic ductal adenocarcinoma

1.1.1 Epidemiology and Clinical practice

In 1980, the relative 5-year overall survival (OS) for PDAC was 3.4 % in the United States of America (USA) (NIH 2021). After almost fourty years, the 5-year OS is still below 9 % (Siegel et al. 2019). Originally predicted to become the tenth most common cancer, PDAC is dismally foreseen to be the fifth most common cancer type and the second leading cause of cancer-related deaths in the USA by 2030 (Rahib et al. 2014; Quante et al. 2016). With regards to Germany, PDAC had an incidence rate of 18,400 men and women in 2016, and this is predicted to increase to 20,000 new cases in 2020 (RKI and GEKID, 2020). Intriguingly, the mortality rate kept the balance, noting approximately 18,000 deaths in 2016 (RKI and GEKID, 2020). Whereas women are diagnosed at an average age of 76, men are diagnosed four years earlier (RKI and GEKID, 2020). Overall, the relative 5-year OS was 9 % for both genders making PDAC the fourth most common cause of cancer death in Germany in 2016 (RKI and GEKID, 2020). Poor prognosis of PDAC contrasts promising new therapy options for other cancer entities, e. g. breast cancer, or effective screening procedures, e. g. colorectal cancer that have improved outcome of patients suffering from these solid malignancies (Edwards et al. 2010; Akram et al. 2017).

In general, common risk factors for PDAC development are smoking, obesity, alcohol consumption and chronic pancreatitis (RKI and GEKID, 2020). Furthermore, diabetes is a common risk factor and also a comorbidity or potentially an early symptom in about 50 % of all patients with a stage I or II PDAC (Okano 2014). As type two diabetes is nowadays commonly diagnosed in about 8 % of the German adult population, it is impossible to screen all diabetes patients for the presence of PDAC (Jacobs and Rathmann, 2019). Additional clinical symptoms include jaundice, venous thromboses and back pain (Modolell et al. 1999; Porta et al. 2005). Moreover, patients experience an unintentional weight loss which is, among other factors such as loss of appetite, caused by malabsorption of nutrients. Since pancreatic cancer exhibits a familial incidence of 2-10 %, individuals with one or two first degree relatives have a 6- to 18-fold increased risk (Winter et al. 2006).

Due to the retroperitoneal location, lack of specific symptoms, and lack of screening for clinical biomarkers, about 80 % of all patients exhibit metastatic spread or locally advanced disease by the time of diagnosis (Oberstein and Olive 2013; Adamska et al. 2017). Therefore, only 20 % of all patients are eligible for surgical resection which is currently the only curative treatment possibility (Sohn et al. 2000). Depending on the location of the tumor, different surgical procedures can be performed. Since microscopically (R1) and macroscopically (R2) visible tumors at the pancreatic margins are correlated with a reduced survival, the necessity of tumor free pancreatic margins (R0) marks the difficulty and complexity of surgical resection (Sohn et al. 2000). As an example, patients graded with R1 or R2 pancreatic tumors revealed a median survival of 12 months compared to R0 resected patients who showed a median survival of 19 months (Sohn et al. 2000). Moreover, both eligibility and outcome of surgery are highly dependent on patients' performance, and patients with tumors infiltrating into surrounding structures are not considered resectable (Adamska et al. 2017). Even after successful R0-resection, 40 % of patients present with tumor reoccurrence after 6-24 months, and only 25 % of patient survive the first five years after resection (Kedra et al. 2001; Hishinuma et al. 2006).

Thus, a need for adjuvant chemotherapy has been proposed and led to two trials demonstrating the efficacy of 5-fluoruracil (5-FU) in combination with folinic acid and gemcitabine monotherapy (Neoptolemos et al. 2001; Oettle et al. 2007). Though these regimens remain exclusively listed in the S3-guidelines for pancreatic cancer in Germany, 5-FU combined with folinic acid is scarcely used today in the clinical setting due to high toxicity (Neoptolemos et al. 2010; DGVS 2013). Later studies showed that the combination of gemcitabine plus an oral fluoropyrimide, capecitabine, resulted in a longer OS compared to gemcitabine monotherapy (Neoptolemos et al. 2017). Moreover, a modified scheme of FOLFIRINOX (combination of fluoruracil, leucovorin, irinotecan and oxaliplatin) demonstrated a significant advantage over gemcitabine monotherapy and is now only applied in patients with very good performance status in the adjuvant setting (Conroy et al. 2018).

Unresectable patients are eligible for palliative chemotherapy, and again the therapy regimen is dependent on patients' performance (Adamska et al. 2017). Approved in 1997, the chemotherapeutic drug gemcitabine has been a first-line regimen for pancreatic cancer patients. However, a median OS of 5.65 months was one of the grim perspectives which prompted further development of drugs with a higher efficacy (Burris et al. 1997). Thus, recent studies have investigated multiple approaches: The combination therapy of gemcitabine and erlotinib, a growth factor inhibitor, has been approved by the federal drug administration (FDA) to treat pancreatic cancer (Moore et al. 2007). However, this combination is hardly applied today as more suitable treatment options have emerged: Firstly, results of a phase III trial demonstrated a prolonged OS in patients when treated with the combination of gemcitabine plus albumin-bound paclitaxel, nab-paclitaxel (Von Hoff et al. 2013). Secondly, FOLFIRINOX resulted also in a higher OS than gemcitabine in the palliative setting (Conroy et al. 2011). Again, this regimen is only applied in patients with a good performance status due to a relatively high toxicity.

Overall, unspecific symptoms, late diagnosis at advanced stages and the pronounced chemo-resistance are hallmark features of PDAC patients reflecting their poor prognosis overall.

1.1.2 Pathogenesis

Due to the anatomic location of the pancreas, acquisition of biopsies from precursor lesions has not been feasible. Thus, the first model of tumor progression was postulated by Hruban et al. in 2000, almost ten years after a similar model was first published for colon cancer (Vogelstein et al. 1988). The most recent model of pancreatic cancer tumorigeneses is illustrated in Figure 1.

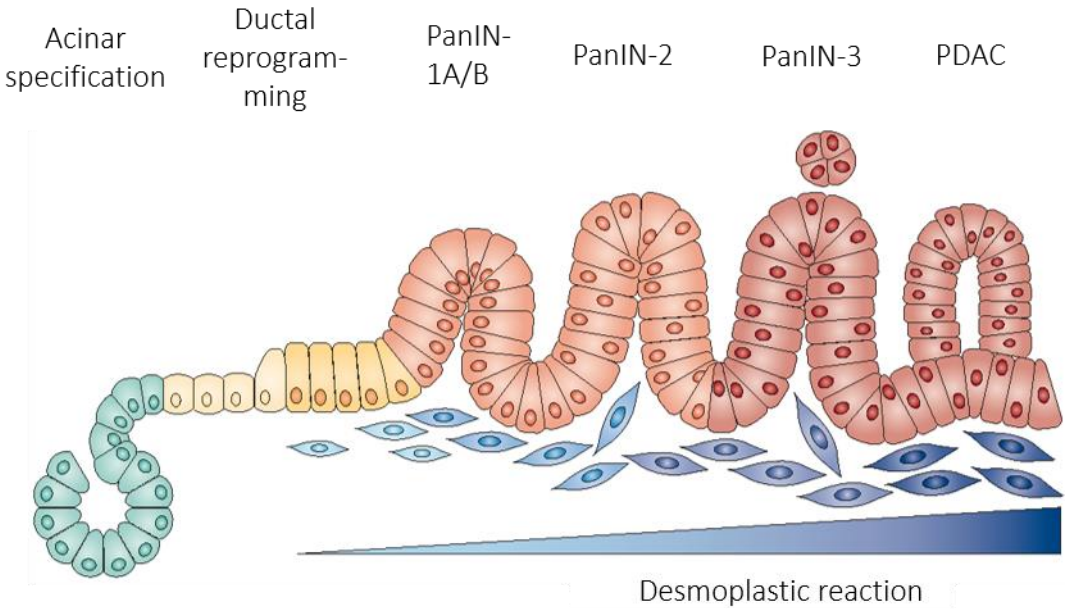

Figure 1: Progression from normal epithelium to invasive PDAC. Pancreatic cancer can arise from both acinar cells and duct cells harboring genetic alterations. According to nuclear atypia and polarization, precursor lesions can be distinguished histopathologically. Progression of precursor lesions is accompanied by a desmoplastic reaction. Modified from Morris et al. 2010. The figure is used with kind permission from Nature Reviews Cancer. *(PanIN = pancreatic intraepithelial neoplasia)*

PDAC can arise from both acinar and ductal cells (Hruban et al. 2000; Huang et al. 2015). Interestingly, recent findings suggest that precursor lesions arising from duct cells demonstrate a more rapid progression towards an invasive carcinoma and a less favorable tumor phenotype than lesions with the same mutations, but originating from other cells types within the pancreas (Lee et al. 2019).

As a result of inflammatory processes, acinar cells are believed to transdifferentiate into duct cells, subsequently leading to the formation of acinar-to-ductal metaplasia (ADM) (Reichert and Rustgi 2011). Either ADM or early genetic alterations in duct cells, e. g. telomere length shortening, lead to precursor lesions termed pancreatic intraepithial neoplasia (PanINs) (Winter et al. 2006). According to their grade of dysplasia, PanIN lesions can be categorized into different

stages: PanIN-1A, PanIN-1B, PanIN-2 and PanIN-3, also referred to as carcinoma *in situ* (CIS). Earlier during progression, PanIN-1A lesions exhibit tall columnar cells with basal nuclei developing to papillary structures in PanIN-1B lesions (Hruban et al. 2000). Loss of nuclei polarity and nuclei crowding are observed in PanIN-2, while additional nuclear and cytosolic abnormalities, but an intact basal membrane, are characteristic for the high grade lesion PanIN-3 and CIS (Hruban et al. 2000; Hingorani et al. 2003; Winter et al. 2006). Besides PanINs, pancreatic precursor lesions can exhibit a cystic morphology, subcategorized into intraductal papillary mucinous neoplasm (IPMN), and mucinous cystic neoplasm (MCN) (Esposito et al. 2012). While the former is increasingly found in elderly patients and exhibits a mean frequency of invasive cancer of approximately 30 %, the latter demonstrates a prevalence of 15 % (Tanaka et al. 2012; Kromrey et al. 2018). However, these lesions are scarcely found compared to PanIN (Esposito et al. 2012).

Molecular characteristics have identified several genetic alterations including mutations, activation of oncogenes and inactivation of tumorsuppressor genes. Furthermore, aberrant activation of signaling pathways, such as of the ERK-pathway, are crucial for the final progression to an invasive PDAC (Feldmann and Maitra 2008). It is known that the amount of alterations progressily increases with the histological atypia, although certain molecular alterations occur at distinct stages (Hruban et al. 2000; Winter et al. 2006). At early stages, the activating mutation of the protooncogene *Kirsten rat sarcoma viral oncogene* (*KRAS*) is found in 30 % of PanIN lesions (Feldmann and Maitra 2008). The substitution from glycine to aspartic acid in the KRAS protein leads to loss of GTPase activity, and subsequently to constant KRAS signaling and activation of downstream signaling pathways important in cell proliferation and survival (Almoguera et al. 1988; Hingorani et al. 2003). Found in 90-95 % of all patients with invasive carcinomas, it is considered to be the most frequent mutation of an oncogene in PDAC (Feldmann et al. 2007). Intermediate stages demonstrate loss of the *cyclin dependent kinase inhibitor 2A* (*CDKN2A*) gene, coding for both proteins $p16^{INK4}$ and $p19^{ARF}$ (Feldmann and Maitra 2008). Consequently, overexpression of the protein cycline D1 results in cell cycle deregulation and uncontrolled proliferation (Hruban et al. 2000). Notably, as 95 % of all patients exhibit this alteration, it is marked to be the most frequent mutation of a tumor suppressor in PDAC (Feldmann and Maitra 2008). At late stages, loss of the tumor suppressor genes *TP53* and *deleted in pancreatic carcinoma, locus 4* (*DPC4*) occur in CIS (Hahn et al. 1996; Maitra et al. 2003). Intensive research identified various epigenetic changes, e. g. methylation of the human hedgehog interacting protein (HHIP), and novel targets associated with poor survival (Martin et al. 2005; Biankin et al. 2012). Besides these frequent mutations found in most patients, pancreatic cancers might exhibit up to 60 additional low frequency genetic alterations (Jones et al. 2008), and this heterogeneity may also account for the poor efficacy of chemotherapeutic drugs in patients.

1.1.3 Tumor microenvironment

During tumor progression, inflammatory signals do not only promote the transition from normal epithial cells to invasive tumor cells, but also a desmoplastic reaction of the surrounding

tissue is observed. Changes are characterized by abundant connective tissue accumulation, activated fibroblasts, immune cells and lack of perfused vessels (Neesse et al. 2011). The presence of a pronounced desmoplasia is a hallmark feature of pancreatic cancer. Therefore, the tissue surrounding the tumor is often referred to as the tumor microenvironment (TME) (Mahadevan and Von Hoff 2007) (Figure 2).

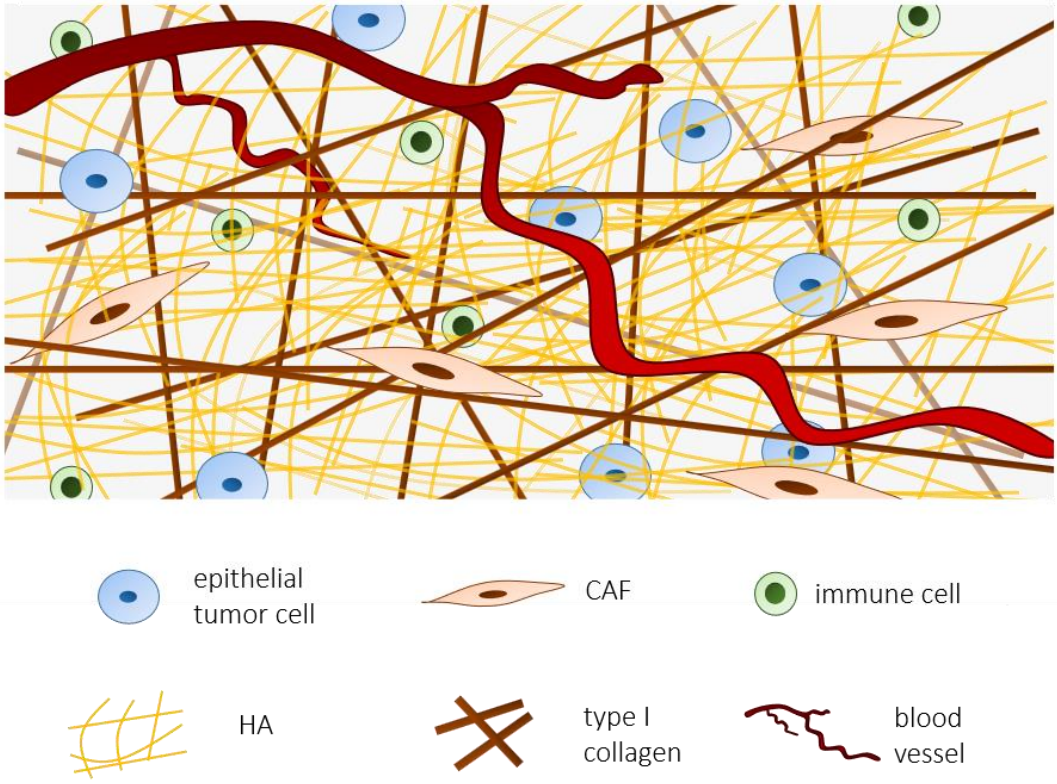

Figure 2: The pancreatic TME. The desmoplastic reaction is a hallmark feature of pancreatic cancer exhibiting proliferation of CAFs and their abundant production of extracellular matrix (ECM) components. *(CAF = cancer associated fibroblast; HA = hyaluronic acid)*

Several studies have investigated the role of various components of the TME and the influence upon patients' outcome. Indeed, subtyping of stroma might be important for future therapeutic approaches, paving another way towards personalized medicine (Olive et al. 2009; Nicolle et al. 2017; Neesse et al. 2019). Pancreatic tumor stroma can be subcategorized into "normal" vs. "activated" when the transcriptional expression pattern is analyzed. Intriguingly, the "activated" stromal subtype was shown to be associated with a shorter survival in both mice and humans stressing the need for further extended evaluation of both acellular and cellular components of the TME (Erkan et al. 2008; Laklai et al. 2016; Neesse et al. 2019).

1.1.3.1 Cancer-associated fibroblasts

In normal pancreatic tissue, quiescent pancreatic stellate cells (PSCs) are the main fibroblast type. Upon tumorigenesis, activated PSCs are the main source of cancer-associated fibroblasts (CAFs), however, also various other cell types such as endothelial cells or bone marrow-derived

stem cells (MDSCs) have been postulated as a source of CAFs (Apte et al. 2004; Garcia et al. 2012; Öhlund et al. 2014). Due to to this heterogeneity of origin, CAFs exhibit both tumor-promoting and tumor-restrainig properties (Elyada et al. 2019). As an example, presence of activated fibroblasts is associated with a stem cell phenotype of cancer cells, a higher invasion rate and chemoresistance, but reduced apoptotic rate (Vonlaufen et al. 2008; Feig et al. 2012). In addition, previous studies suggest a drug scavenging effect of fibroblasts, thus reducing the amount of chemotherapeutic drugs that act on tumor cells (Hessmann et al. 2018). In the absence of CAFs, tumors demonstrate enhanced vascularization and, therefore, increased drug delivery (Olive et al. 2009). Unexpectedly, CAF-depleted tumors also show a more undifferentiated tumor histology and shorter survival, providing evidence for tumor restraining properties of CAFs (Özdemir et al. 2014; Rhim et al. 2014; Neesse et al. 2015). Furthermore, CAFs interact with tumor cells directly through paracrine secretion of different factors, such as chemokine (C-X-C motif) ligand 12 and 14 (CXCL12/CXCL14), as well as indirectly through the synthesis of extracellular matrix (ECM) components such as HA and collagen which both influence proliferation and chemoresistance of cancer cells (Bhowmick et al. 2004; Egeblad et al. 2010; Sironen et al. 2011). Moreover, tumor-stroma interaction results in an upregulation of the secreted protein acidic and rich in cysteine (SPARC) in fibroblasts, an important matricellular protein and marker of activated stroma, resulting in an abundant synthesis of collagen (Sato et al. 2003; Moffitt et al. 2015). Interestingly, ablation of SPARC in a novel mouse model reduces the amount of collagen but does not accelerate PanIN or tumor progression (Ramu et al. 2019). Furthermore, the small glycoproteine podoplanin was found to be expressed on the surface of CAFs recently (Quintanilla et al. 2019). Interestingly, high expression of podoplanin in cancer cells was among other consequences connected to an increase in epithelial-mesenchymal transition (EMT) and associated with poor survival in breast, lung and pancreatic cancer (Martín-Villar et al. 2006; Quintanilla et al. 2019). Thus, it is proposed to be a novel marker for tumor aggressiveness.

1.1.3.2 Collagen

In contrast to normal pancreatic tissue, expression of type I collagen is significantly increased in pancreatic cancer, predominantly produced by activated PSCs (Imamura et al. 1995; Apte et al. 2004). Together with HA, type I collagen is responsible for a high intratumoural pressure, leading to impaired drug delivery (Chauhan et al. 2013). It is also found to promote proliferation and reduce apoptosis levels in cancer cell lines, thus being positively correlated with tumor growth (Armstrong 2004; Egeblad et al. 2010). Moreover, studies propose a negative correlation between expression levels and OS (Whatcott et al. 2015). After studies found a high expression of the enzyme lysyl oxidase (LOX) in a hypoxic environment important for collagen development, combined treatment of transgenic *LSL-Kras*$^{G12D/+}$;*LSL-Trp53*$^{R172\ H/+}$; *Pdx1-Cre* (KPC) mice with gemcitabine plus a LOX-inhibitor resulted in longer survival and reduced metastatic spread (Miller et al. 2015).

1.1.3.3 Hyaluronic acid

HAs are unbranched, long-chained glycosaminoglycans comprising thousands of dissacharides. Due to their biochemical properties, HAs are capable of retaining a great amount of water. Subsequently, HA is one decisive factor held responsible for the high intratumoral pressure which leads to the collapse of blood vessels, restricted drug delivery and change in gene expression of tumor cells (Sironen et al. 2011; Provenzano et al. 2012; Jacobetz et al. 2013). Previous studies indicate a shorter survival upon enhanced expression of HA (Cheng et al. 2013; Whatcott et al. 2015). Intriguingly, depletion of HA via the Smoothened inhibitor IPI-926 leads to a decompression of blood vessels paired with increased drug delivery and better response to gemcitabine in murine models (Jacobetz et al. 2013). In a phase II clinical trial, patients exhibiting high levels of HA undergoing combined treatment of a hyaluronidase (PEGPH20) plus gemcitabine/nab-paclitaxel showed a higher OS and progression-free survival (PFS) (Hingorani et al. 2018). However, the subsequent phase III clinical trial did not corroborate phase II trials. As no improvement in OS and PFS was reported, and a higher rate of adverse events occurred in the treatment arm, no further therapeutic approaches regarding HA depletion are likely (Van Cutsem et al. 2020). However, the question of whether HA expression influences protein expression in gemcitabine-related genes remains unexplored to this point.

1.2 Different model systems in PDAC research

A detailed molecular understanding of PDAC evolution and progression is crucial for the development of novel diagnostic and therapeutic possibilities. Over decades, several *in vitro* and *in vivo* approaches have revealed the complex nature of pancreatic cancer. Easy and fast to use, two-dimensional (2D) cell culture systems are wildly established to answer important biological questions. Importantly, these are highly simplified tumor models which inaccurately recapulate biological and therapeutic hallmarks. The majority of advanced clinical trials possibly failed in PDAC because most drug research was based upon findings in cell line studies (Thota et al. 2017). A better understanding of tumor biology has been reached by multiple approaches towards three-dimensional (3D) cell culture systems which are still in development (Edmondson et al. 2014; Simian and Bissell 2017). Besides *in vitro* studies, different *in vivo* mouse models of pancreatic cancer have been established adding great value to preclinical science, especially regarding the faithful representation of the TME and testing of potential new drugs (Frese and Tuveson 2007).

1.2.1 KPC mice

One genetically engineered mouse model (GEMM) that closely recapitulates the development from non-neoplastic epithelial cells to fully invasive PDAC is the KPC mouse model first described by Hingorani et al. in 2005. $Kras^{G12D}$ and $Trp53^{R172H}$ alleles are altered leading to an exchange of amino acids (glycine to aspartic acid at codon 12 or arginine to histidine at codon

172) within the proteins, thus promoting initiation and progression of PDAC after active transcription (Hingorani et al. 2003; Olive et al. 2004). Upstream of the mutations named above, a *Lox-STOP-Lox* (LSL) cassette is inserted to prohibit initial expression at the 5'-end (Hingorani et al. 2005). Hence, only the wild type allele is expressed (Hingorani et al. 2003; Hingorani et al. 2005). For pancreas-specific expression of mutated genes, a Cre-recombinase, functionally similar to topoisomerase I, is linked to promotor regions of transcription factors only expressed in pancreatic progenitor cells (Van Duyne 2001). So far, two genes, *Pdx/Ipf1* activated on day 8.5 and, slightly later, *p48/ptf1* activated on day 9.5 of embryonic development, have been characterized as pancreas-specific promoters (Kawaguchi et al. 2002; Hingorani et al. 2003).

In general, the KPC model is currently the mouse model recapitulating the human disease the closest. KPC mice exhibit the full spectrum of histopathological precursors towards the development of frank invasive cancers, allowing for the possibility of investigating precursor lesions and different differentiation levels of PDAC (Singh et al. 2015; Lee et al. 2016). Similar to human cancers, KPC tumors frequently metastasize in the liver followed by the lung and lymph nodes (Olive et al. 2004). Moreover, KPC mice feature a pronounced TME, immune cell infiltrations and a distinct hypovascularity that can be studied and experimentally probed (Sharpless and DePinho 2006; Lee et al. 2016). In addition, clinical signs such as malignant ascites, biled duct obstruction and jaundice are regularly found in KPC mice (Hingorani et al. 2005). Taken together, the KPC mouse model is the most widely used GEMM in PDAC research that has contributed to a deeper understanding of molecular and cellular mechanisms as well as therapeutic strategies in PDAC.

1.2.2 Orthotopically transplanted mice

Due to the challenges of breeding the desired genotype, high costs, and slow tumor developments over several months, other *in vivo* mouse models have been used for PDAC research (Sharpless and DePinho 2006; Jiang et al. 2014; Lee et al. 2016). For instance, the injection of cancer cells into the tail of the pancreas of immunodeficient or immunocompetent mice is both more feasible and less expensive compared to KPC mice, generating a tumor in orthotopically transplanted mice (OTMs) (Jiang et al. 2014). If cancer cells and the recipient mouse exhibit the identical genetic background, a syngenic mouse model can be generated. This is the case for *in vitro* KPC tumor cells and C57/B6 mice (Sharpless and DePinho 2006).

OTM models offer several advantages over the conventional subcutaneous xenograft models: First, these tumors recapitulate histological and clinical features like local invasion, angiogenesis and metastatic spread (Feldmann and Maitra 2008; Jiang et al. 2014). Secondly, experiments can be perfomed at a large-scale at the same time and tumors normally develop rapidly within a few weeks (Jiang et al. 2014). Hence, this model is commonly used for initial screening of potential chemotherapeutic drugs to investigate the effects on the TME and metastasis formation (Sharpless and DePinho 2006; Feldmann and Maitra 2008).

1.2.3 PDX mice

First introduced by Rygaard and Poulsen in 1969, a novel approach towards personalized medicine is the subcutatenous transplantation of human primary resected tissue (hPRT) of patients into immunodeficient mice, often referred to as patient-derived xenograft (PDX) mice. Because of the feasibility of this model, PDX mice are commonly used for preclinical drug studies including the investigation of pharmacodynamics and effects on tumor size or tumor volume (Kelland 2004; Feldmann and Maitra 2008). Transplantation of tumor bulk tissue into nude mice allows research on tumors which maintain their original 3D structure (Hessmann et al. 2020). In addition, the molecular subtypes (classical and basal-like) are at least partially represented (Collisson et al. 2011; Lomberk et al. 2018). Strikingly, studies indicate that cellular components of the immune system are increasingly located within tumors compared to normal tissue and might further promote tumorigenesis (Wörmann et al. 2014). PDX mice demonstrate a loss of essential hallmarks such as a strong immune response and pronounced TME, thus, the absence of these hallmarks might be responsible for unexplained tumor shrinkage rather than cytotoxic effects of administered chemotherapies (Kelland 2004; Rubio-Viqueira et al. 2006). However, as the human TME is gradually replaced by stroma of murine origin during passaging, there is a chance to specifically investigate the crosstalk between stromal and epithelial compartments *in vivo* (Bradford et al. 2013; Delitto et al. 2015) including the possibility of this model to evaluate drug efficacy (Aparicio et al. 2015; Witkiewicz et al. 2016; Hessmann et al. 2020).

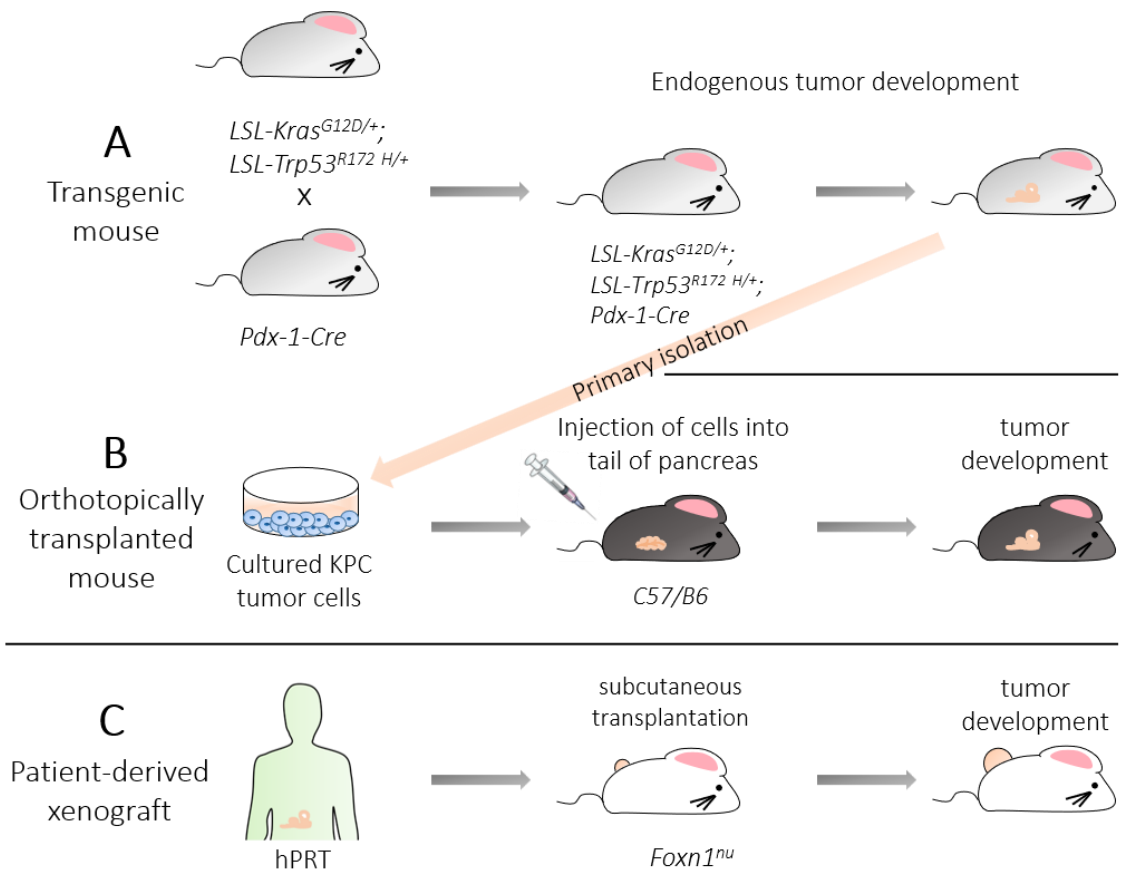

Figure 3: Different mouse models of PDAC. (A) In the transgenic KPC mouse model, tumor development is induced in mutation-bearing and Cre-recombinase-expressing mice. (B) Previously isolated 2D-cultured KPC cells are orthotopically transplanted into C57/B6 mice, resulting in the generation of a syngenic pancreatic tumor. (C) Patient-derived xenografts (PDX) are established by subcutaneous transplantation of human primary resected tissue (hPRT) into immunodeficient Foxn1^{nu} mice. *[LSL = Lox-STOP-Lox; (KPC = LSL-Kras$^{G12D/+}$;LSL-Trp53$^{R172H/+}$;PDX-1-Cre); Foxn1^{nu} = Foxhead box n1, nude; hPRT = human primary resected tissue]*

1.2.4 Organoids

The term organoid cultures, or short organoids, has been defined multiple times over the last few years. In general, organoids are tissue- or cell line-derived cells which exhibit an organ-like structure and gene expression (Simian and Bissell 2017). The development of the technique started in 1963 when Swarm and colleagues observed the survival of a murine chondrosarcoma after subcutaneous transplantation to inbred mice. Subsequently, the ECM of the chondrosarcoma was characterized, a gel compromising its components was generated and named after the first investigators Engelbrecht, Swalm and Holm (EHS)-matrix (Swarm 1963; Simian and Bissell 2017).

The most important advantage of 3D culture systems is the additional dimension in which cells are able to interact with each other (Edmondson et al. 2014). Notably, 3D-cultured cells demonstrate a polarization and tissue-specific cytodifferentiation more similar to *in vivo* tissue (Barcellos-Hoff et al. 1989; Simian and Bissell 2017). Besides a more natural cell morphology in 3D,

the composition of the cell population itself also differs between the culture systems. In contrast to homogenous, mostly proliferating cell populations in 2D, 3D culture exhibits different cell stages including proliferating, quiescient, hypoxic and necrotic cells within the same culture (Baharvand et al. 2004; Edmondson et al. 2014). This heterogeneity of cells is based on the formation of clusters within 3D, subsequently leading to an uneven accessibility to oxygen and nutrients (Edmondson et al. 2014).

Importantly, the culture method strongly influences the expression of various genes, including transcripton factors, surface receptors, signaling molecules and factors essential for drug response (Baharvand et al. 2004; Edmondson et al. 2014). Compared to 2D, cells maintained in 3D reveal a more comparable gene expression pattern to the original tissue, thus mimicking the genuine biological behavior of the tumor more closely (Birgersdotter et al. 2007). For instance, genes involved in inflammation processes, apoptosis factors and immune responses are enriched in 3D compared to 2D (Baharvand et al. 2004; Birgersdotter et al. 2007; Edmondson et al. 2014). Taking this into account, it is not surprising that a great amount of potential drugs tested in 2D cell cultures eventually failed in clinical trials due to a lack of efficacy and toxicity (Lee et al. 2013). However, as 2D cell culture is feasible and affordable, it is still the most common platform used for drug testing today (Edmondson et al. 2014).

The advent of organoid cultures resulted in numerous preclinical studies in pancreatic cancer research. Organoids are now regarded as a key approach to improve the understanding of molecular mechanisms and to develop more efficient screenings for potential chemotherapeutic drugs (Boj et al. 2015; Hou et al. 2018; Tiriac et al. 2018). Both murine and human resected normal pancreatic tissue, PanIN lesions and invasive PDAC can be grown and cultivated in organoid cultures (Boj et al. 2015). It has been shown that these cultures closely resemble the distinct morphology and histopathology of the distinct stages in tumor progression (Boj et al. 2015; Huang et al. 2015). Moreover, orthotopic transplantation of organoids into mice exhibit an abundant desmoplastic reaction and show distinct stages of PDAC development (Boj et al. 2015). Due to the lower costs and relatively rapid outgrowth, this model displays an attractive alternative when GEMMs are not available (Gurski et al. 2010; Boj et al. 2016). Therapeutic approaches in 3D organoids demonstrate a higher drug resistance than corresponding 2D cell culture (Hou et al. 2018). Organoids accurately predicted drug sensitivity in patients, and longitudinal molecular and therapeutic examinations might identify newly occurring mutations and chemo-refractory tumors, thus leading to an adjustment of therapy (Tiriac et al. 2018). The possibility of generating organoid cultures in high-throughput screenings ultimately marks an important step towards personalized medicine (Boj et al. 2015; Hou et al. 2018; Tiriac et al. 2018; Frappart et al. 2020).

1.3 Gemcitabine

1.3.1 Drug metabolism and function

Around 80 % of all patients with newly diagnosed pancreatic cancer qualify for palliative treatment. Different therapy regimes have been established over the last few decades. The prodrug 2',2'-difluoro 2'-deoxycytidine (dFdC), known as gemcitabine, has been administered as a standard chemotherapy drug since 1997 (Burris et al. 1997; Neesse et al. 2015), and has been combined with nab-paclitaxel more recently (Von Hoff et al. 2013). Biochemically, gemcitabine is an analogue to the nucleoside cytidine, substituted with two fluor atoms at 2' carbon of deoxycytidine essential for its antitumoural activity (Mini et al. 2006) (Figure 4A).

Being hydrophilic in nature, dFdC uptake is achieved by isoforms of the equilibrative nucleoside transporters (ENTs), such as ENT1, located in the cell membrane (Mini et al. 2006) (Figure 4B). The initial step, which is also considered to be the rate-limiting step of the prodrug gemcitabine undergoing activation, is its phosphorylation to 2', 2'-difluoro 2'-deoxycytidine monophosphate (dFdCMP) catalyzed by deoxycytidine kinase (DCK) (Mini et al. 2006).

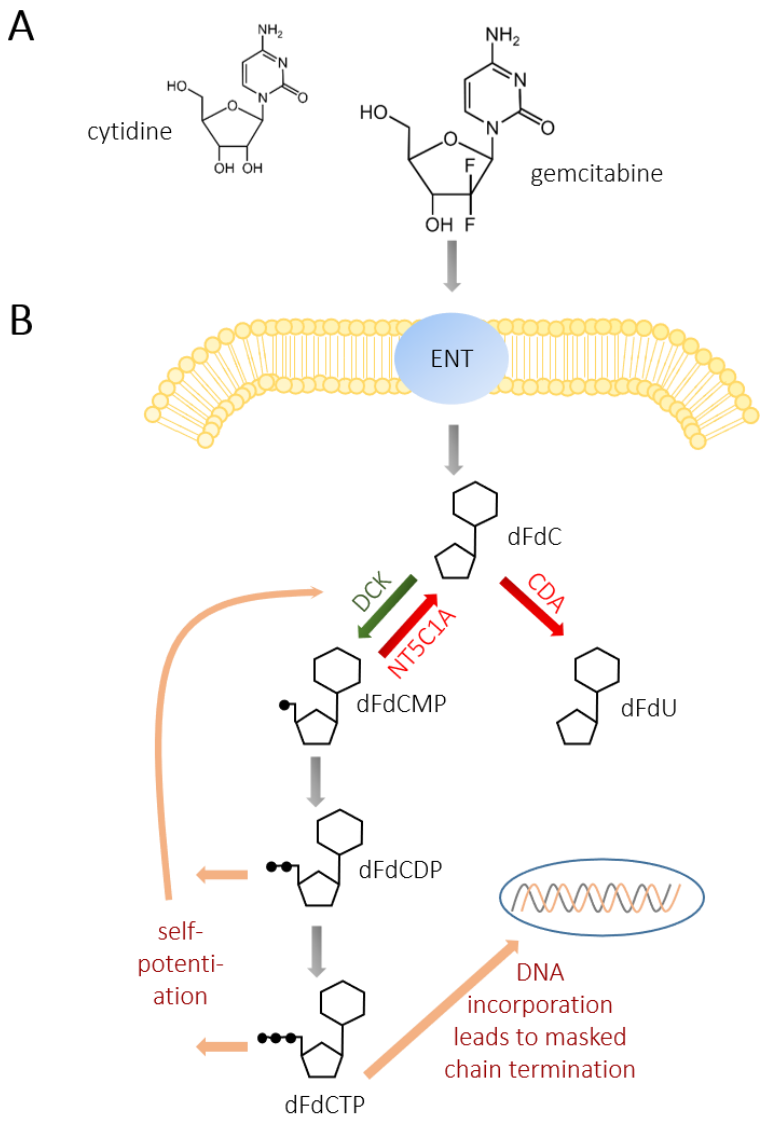

Figure 4: Structure, metabolism, and function of gemcitabine. (A) Gemcitabine is a nucleoside analogue substituted with two fluor atoms at 2' carbon. (B) Following the influx via ENT transporters, dFdC is metabolized to its active form by phosphorylation to dFdCTP, subsequently leading to various modes of action. Gemcitabine is inactivated through NT5C1A and CDA. *[CDA = cytidine deaminase; DCK = deoxycitidine kinase; dFdC = 2',2'-difluoro-2'-deoxycitidine (prodrug); dFdCMP/dFdCDP = 2',2'-difluoro-2'-deoxycitidine monophosphate/diphosphate (intermediate metabolites); dFdCTP = 2',2'- difluoro-2'-deoxycitidine triphosphate (active metabolite); dFdU = 2',2'-difluoro-2'-deoxyuridine (inactive metabolite); ENT = equilibrative nucleoside transporter; NT5C1A = nucleotidase 5', cytosolic 1A]*

Subsequent phosphorylation leads to the active metabolite 2',2'-difluoro 2'-deoxycytidine triphosphate (dFdCTP), unfolding antitumoural activity specifically in the S-phase of the cell-cycle (Mini et al. 2006). Termed as masked-chain-termination, dFdCTP is incorporated into desoxyribonucleic acid (DNA), and after subsequent addition of one deoxynucleotide, chain elongation is stopped (de Sousa Cavalcante and Monteiro 2014). Besides the protection by the final added deoxynucleotide from removal by DNA repair enzymes, gemcitabine metabolites mediate self-potentiation (Heinemann et al. 1990). Through inhibiting both the ribonucleotide reductase

(RR) by dFdCDP and DNA-polymerase by dFdCTP, respectively, CTP production and incorporation into DNA is reduced and DCK activity is upregulated leading to an increase in dFdCMP concentration and influx of dFdC into the cell (Heinemann et al. 1990; Mini et al. 2006).

Prior to the inactivation to the inactive metabolite 2',2'-difluoro 2'-deoxyuridine (dFdU) by cytidine deaminase (CDA), dephosphorylation to dFdCMP is catalyzed by cytosolic 5'-nucleotidases, especially subgroup 1A (NT5C1A) (Mini et al. 2006; Patzak et al. 2019). Importantly, high expression levels of both enzymes are correlated with a reduced OS and therapeutic response in pancreatic cancer preclinical models and PDAC patients because of higher inactivation rates of the active metabolite of gemcitabine (Bengala et al. 2005; Patzak et al. 2019).

1.3.2 Pharmacogenetics – a new chance?

Recently established chemotherapeutic treatments such as the FOLFIRINOX regime or gemcitabine in combination with nab-paclitaxel are more efficient but also more toxic compared to gemcitabine monotherapy (Conroy et al. 2011; Von Hoff et al. 2013). Chemoresistence of PDAC relies not only on biophysical tumor properties such as the stiff tumor stroma with compressed vessels, but also on a highly heterogeneous genetic and transcriptional program of tumor cells. It is suggested that the gene expression patterns account for up to 95 % of variation in drug responses of patients (Wong et al. 2009; Neesse et al. 2019). The evolving field of pharmacogenetics investigates the influence of gene expression on responses to certain drugs (Wong et al. 2009). Considering the efficient antitumoral effects that gemcitabine has shown during *in vitro* studies, it might be beneficial to classify PDAC patients according to expression of gemcitabine metabolizing enzymes (GME) (de Sousa Cavalcante and Monteiro 2014). Previous studies demonstrated that high expression of the activating enzyme DCK and low expression of inactivating enzymes NT5C1A and CDA correlated with a higher sensitivity to gemcitabine, thus leading to a longer OS, respectively (Bergman et al. 1999; Bengala et al. 2005; Patzak et al. 2019). Moreover, high expression of both ENT1 and DCK correlated with a prolonged OS in patients with advanced PDAC (Maréchal et al. 2012; Greenhalf et al. 2014). Therefore, application of drugs according to distinct expression patterns of drug metabolizing enzymes (DME) should be explored since pancreatic cancer still lacks tailored therapeutic strategies (Yauch and Settleman 2012).

1.4 Aims of this study

Pancreatic cancer is one of the most challenging cancer entities to treat. The expression of DME might determine the response to chemotherapeutic drugs. However, it is unknown by which mechanisms the expression of DME is controlled and whether the expression differs in various preclinical experimental models.

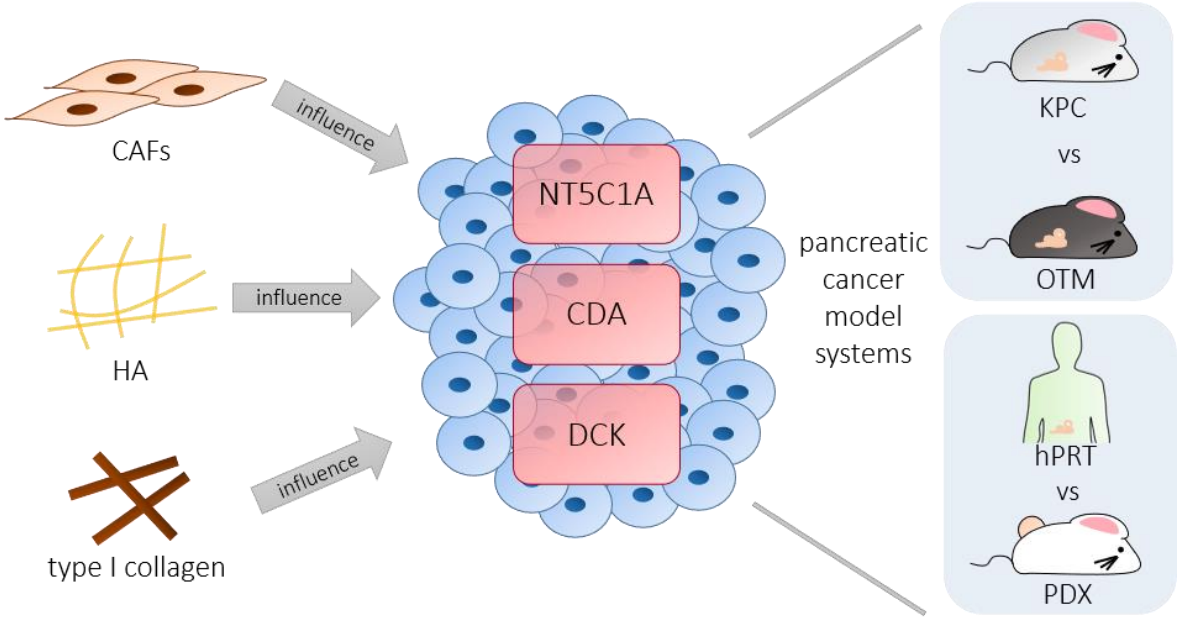

Figure 5: Influence of stromal compartments on gemcitabine metabolizing enzymes. Stromal components might have the potential to alter gene and protein expression of tumor cells. We hypothesize that stromal components might have an impact on the expression of gemcitabine metabolizing enzymes, thus promoting chemoresistance in different pancreatic cancer model systems. *[CAF= cancer associated fibroblast; CDA = cytidine deaminase; DCK= deoxycitidine kinase; HA = hyaluronic acid; (KPC = LSL-Kras$^{G12D/+}$;LSL-Trp53$^{R172H/+}$;PDX-1-Cre); NT5C1A= nucleotidase 5', cytosolic 1A; OTM = orthotopically transplanted mouse; PDX = patient-derived xenograft; hPRT = human primary resected tissue]*

We hereby hypothesize that the expression of DME, in particular GME, is associated with the amount and composition of the tumor stroma. To test this, (i) enzyme expression of NT5C1A, CDA and DCK are investigated in KPC mice, OTMs, hPRT and PDX mice. Furthermore, (ii) stainings of stromal components for HA, type I collagen and podoplanin are conducted and correlated to GME expression. By using in vitro approaches, (iii) conditioned medium experiments and (iv) type I collagen-coated plates are used to investigate whether re-introduction of different stromal components changes the expression of GME. Finally, (v) GME expression is investigated in KPC SPARC^{WT} and KPC SPARC$^{-/-}$ mice to approach the role of type I collagen. These experiments aim to investigate the role of stromal components on the expression of GME, thus possibly providing an explanation of the varying responses of different preclinical model systems to gemcitabine.

2 Material and Methods

2.1 Material

2.1.1 Lab equipment

Table 1: General lab equipment

Equipment	Company	Location
Anesthetic vaporizer	Sigma delta Penlon Ltd.	Abingdon, UK
Aspirator – Grant-bio FTA-1	Grant Instruments	Cambridge, UK
Autoclave – FVA2/A1 Fedegari group	ibs/ tecnomara GmbH	Fernwald, Germany
Beaker/Erlenmeyer flask – Schott DURAN®	DWK Life Sciences GmbH	Wertheim/Main, Germany
Benchtop Orbital Shaker – MaxQ™ 4450	Thermo Fisher Scientific	Waltham, MA, USA
Biological safety cabinet, class II – Thermo Scientific™ Safe 2020	Thermo Electron LED GmbH	Langenselbold, Germany
Cell Counter - Cellometer® Auto 1000, with single use cell counting chambers	Nexcelom Bioscience LLC.	Lawrence, MA, USA
Centrifuge – Heraeus Megafuge 16/ Multifuge X1R	Thermo Fisher Scientic	Waltham, MA, USA
Centrifuge – Universal 320R	Andreas Hettich GmbH & Co. KG	Tuttlingen, Germany
CO_2 incubator - HERAcell® 240i	Thermo Fisher Scientific	Waltham, MA, USA
Cryo boxes with grid inserts - Labsolute®	Th. Geyer GmbH & Co. KG	Renningen, Germany
Dewar flask for liquid nitrogen – KGW- Isotherm	Karlsruher Gastechnisches Werk – Schieder GmbH	Karlsruhe, Germany
Digital camera – cyber-shot DSC-RX100	Sony Europe Limited	Surrey, UK
Dry bath incubator – BSH 5002-E	Benchmark Scientic, Inc.	Edison, NJ, USA
Fluid aspiration system – BVC control	Vacuubrand GmbH & Co. KG	Wertheim, Germany
Forceps and dissecting scissors	Karl Hammacher GmbH	Solingen, Germany
Freezer – Mediline/ Fridge – Profi line/ Fridge and freezer – glass line	Liebherr-International Deutschland GmbH	Biberach an der Riß, Germany
Glass bottles 100 ml, 250 ml, 500 ml, 1l - Schott DURAN®	DWK Like Sciences GmbH	Wertheim/Main, Germany
Graduated cylinders – SILBER-BRAND ETERNA – 100 ml, 500 ml, 1l	BRAND GmbH + Co. KG	Wertheim, Germany
Heated Paraffin Embedding Module – EG1150 H with cold plate – HistoCore Arcadia C	Leica Biosystems Nussloch GmbH	Nussloch, Germany

High resolution ultrasound system – Visual Sonics Vevo2100, including imaging stage, anesthesia line, and micro scan transducer (MS-550-D. 22-55 MHz)	FUJIFILM VisualSonics *Inc.*	Toronte, Canada
Horizontal gel electrophoresis system – 41-2025	PEQLAB Biotechnologie GmbH	Erlangen, Germany
Hot plate – 062	Labotect Labor-Technik-Göttingen GmbH	Rosdorf, Germany
Ice bath – 1-6030	NeoLab Migge GmbH	Heidelberg, Germany
Ice machine - Scotsman® AF80	Scotsman Ice Srl	Milano, Italy
Imaging system – ChemiDoc™ XRS+	Bio-Rad Laboratories GmbH	Munich, Germany
Immunostaining slide rack and slides – Thermo Scientic™ Shandon Sequenza™	Thermo Shandon Limited, Subsidiary of Thermo Fisher Scientific	Runcorn, UK
Incubator – UF260/UN55pa	Memmert GmbH & Co. KG	Schwabach, Germany
INTAS UV system	Intas Science Imaging Instruments GmbH	Goettingen, Germany
Liquid nitrogen cell storage canister – Bio-cane™ 47	Thermo Fisher Scientific	Waltham, MA, USA
Magnetic stirrer – RH basic	IKA®- Werke GmbH & Co. KG	Staufen, Germany
Microscope – Axiovert 25	Carl Zeiss AG	Oberkochen, Germany
Microscope – BX43F/ CKX53	Olympus Corporation	Tokyo, Japan
Microwave – NN-E209W	Panasonic Marketing Europe GmbH	Hamburg, Germany
Microwave heatpad for animals - snuggleSafe®	SnuggleSafe Lenric C21	West Sussex, UK
Mini gel tank – Invitrogen, for Western blot analysis with mini blot module – B1000	Thermo Fisher Scientific	Waltham, MA, USA
Multi-functional orbital shaker – Grant-bio PSU-20i	Grant Instruments	Cambridge, UK
Oxygen generator – Aeroplus 5	Kroeber Medizintechnik GmbH	Dieblich, Germany
pH meter – FiveEasy Plus	METTLER TOLEDO AG	Schwerzenbach, Switzerland
Pipette filler - pipetus® akku	Hirschmann Laborgeräte GmbH & Co. KG	Eberstadt, Germany
Pipettes - Research plus (10 µl, 20 µl, 100 µl, 200 µl, 1000 µl), Multipette® plus	Eppendorf AG	Hamburg, Germany
Plate spinner – PerfectSpin P	PEQLAB Biotechnologie GmbH	Erlangen, Germany
PowerPac™ HC for gelelectrophoresis and Western blot analysis	Bio-Rad Laboratories GmbH	Munich, Germany
Real-time PCR system – Applied Biosystems StepOnePlus™	Thermo Fisher Scientific	Waltham, MA, USA

Residual gas filter - CONTRAfluranTM	ZeoSys GmbH	Berlin, Germany
Rotary Microtome - RM2265 with flattening table for histopathology – HI 1220	Leica Biosystems Nussloch GmbH	Nussloch, Germany
Shaver – ER-PA10	Panasonic Corporation	Osaka, Japan
Thermal cycler – T100™	Bio-Rad Laboratories GmbH	Munich, Germany
ThermoMixer® compact	Eppendorf AG	Hamburg, Germany
Timer – WB-388	Oregon Scientific	Gennevilliers, France
Tissue lyser – Qiagen with stainless steel beads, 5 mm	RETSCH GmbH	Haan, Germany
Tissue processor – TP1020	Leica Biosystems Nussloch GmbH	Nussloch, Germany
Ultrapure water system - arium® pro	Sartorius AG	Goettingen, Germany
Ultrasonic homogenizer – Sonopuls HD70	BANDELIN Electronic GmbH & Co. KG	Berlin, Germany
Vortex mixer – REAX2000	Heidolph Instruments GmbH & Co. KG	Schwach, Germany
Waterbath WNB 14	Memmert GmbH & Co. KG	Schwach, Germany

2.1.2 Consumables

Table 2: Consumables

Consumable	Catalogue number	Supplier	Location
Adhesion slides for IHC - SuperFrost® Plus	J1800AMNZ	Gerhard Menzel B.V. & Co. KG	Braunschweig, Germany
Cell culture multiwall plate, 24 well/ 96 well, F-bottom	662160/ 655180	Greiner Bio-One GmbH	Frickenhausen, Germany
Cell scraper, 25cm	83.1830	Sarstedt, Inc.	Newton, NC, USA
Chamber slide™ system – Lab-Tek®, 8 well, Permanox® slides	177445	Thermo Fisher Scientific	Rochester, NY, USA
Combitips – advanced® 0.5 ml, 1 ml, 2.5 ml, 5 ml/ BIOPUR 1 ml, 5 ml	0030 089.421/ 430/ 448/ 456/ 642/ 669	Eppendorf AG	Hamburg, Germany
CryoPure tube 1.6 ml red	72.380.002	Sarstedt AG & Co.	Nuembrecht, Germany
Desinfectant - Desomed rapid AF	DT-311-010	DESOMED Dr. Trippen GmbH	Freiburg, Germany
Embedding cassettes	9160844	Th. Geyer GmbH & Co. KG	Renningen, Germany
Eye and nose ointment - Bepanthen®	6029009.00.00	Bayer Vital GmbH	Leverkusen, Germany

Filter tips - TipOne® 10/20 µl, 100 µl, 1000 µl	S1120-3810/ S1120-1840/ S1126-7810	STARLAB INTER-NATIONAL GmbH	Hamburg, Germany
Folded filters, 185 mm	311647	Schleicher & Schuell BioScience GmbH,	Dassel, Germany
Gloves – latex/ nitrile - Starguard®	SG-T-M/ SG-C-S	STARLAB Interna-tional GmbH	Hamburg, Germany
Hair removal cream – Veet	8319533	RB Healthcare UK	Hull, UK
Insulin syringes 30 G – BD Micro-Fine™ + Demi	324826	Company, Franklin Lakes, NJ,	USA Micro Amp®
Micro Amp® fast optical 96 well reaction plate (0.1 ml) – Applied biosystems®	4346906	Life Technologies Corporation	Carlsbad, CA, USA
Microscope coverslips 24 x 32 mm	7695 028	Th. Geyer GmbH & Co. KG	Renningen, Ger-many
Microtest plate 96 well, F	2021-08	Sarstedt AG & Co.	Nuembrecht, Ger-many
Microtome blade - Feather® S35	207500000	pfm medical AG	Cologne, Germany
Microtube 0.5 ml, 1.5 ml, 2.0 ml	72.699/ 72.690/ 72.691	Sarstedt AG & Co.	Nuembrecht, Ger-many
Needle Sterican® - 20 G x 2‘, 26 G x 1“	466 7093/ 465 7683	B. Braun Melsungen AG	Melsungen, Ger-many
Optical adhesive covers – applied biosystems®	4360954	Life Technologies Holdings Pte. Ltd.	Singapore
Parafilm®	PM-996	Pechiney Plastic Packiging, Inc.	Menasha, WI, USA
PCR tubes 200 µl - Multi-ply® µStrip Pro	72.990.002	Sarstedt AG & Co.	Nuembrecht, Ger-many
Pipette tips - TipOne® 10 µl, 200 µl, 1000 µl	S1111-3000/ S1113-1006/ S1111-6001	STARLAB Interna-tional GmbH	Hamburg, Germany
Razor blades – Apollo ever-shape blades	9156110	Th. Geyer GmbH & Co. KG	Renningen, Ger-many
Rolled rim bottles 55 x 27 mm	9400240	Th. Geyer GmbH & Co. KG	Renningen, Ger-many
Scalpel	02.001.30.021	Feather Safety Razor Co.	LTD, Osaka, Japan
Serological pipette 2 ml, 25 ml, 50 ml	86.1252.001/ 86.1685.001/ 86.1256.001	Sarstedt AG & Co.	Nuembrecht, Ger-many
Serological pipette 5 ml, 10 ml	606180/ 607180	Greiner Bio-One GmbH	Frickenhausen, Ger-many
Sterilium® classic pure	975512	BODE Chemie GmbH	Hamburg, Germany
Surgical suture material - Ethicon® Vicryl™ Poly-glactin 910	V497	Johnson & Johnson Medical GmbH	Norderstedt, Ger-many
Syringe 5 ml - Injekt®	4606710V	B. Braun Melsungen AG	Melsungen, Ger-many

TC flask T25, T75, T175	83.3910.002/ 83.3911.302/ 83.3912.002	Sarstedt AG & Co.	Nuembrecht, Germany
TC plate, 6 well, standard F	83.3920.005	Sarstedt AG & Co.	Nuembrecht, Germany
Tube 5 ml, 15 ml, 50 ml	60.558.001/ 62.554.502/ 62.547.254	Sarstedt AG & Co.	Nuembrecht, Germany
Ultrasonic gel	ASUSG1	Asmuth GmbH Medizintechnik	Minden, Germany
Weighing boats	9.900 786	Lab Logistics Group GmbH	Meckenheim, Germany
Wound clips – Reflex 9	201-1000	CellPoint Scientific, Inc.	Gaithersbury, MD, USA

2.1.3 Chemicals and reagents

Table 3: Chemicals and reagents

Chemical/Reagent	Catalogue number	Supplier	Location
Acetic acid, glacial	3788.4	Carl Roth GmbH + Co. KG	Karlsruhe, Germany
Albumin Bovine Fraction V, pH 7.0	11930.03	SERVA Electrophoresis GmbH	Heidelberg, Germany
Aqua/Aqua ad iniectabilia	75/12604052/1212/ 6724123.00.00	B. Braun Melsungen AG	Melsungen, Germany
Calcium chloride dihydrate	131232.1210	AppliChem GmbH	Darmstadt, Germany
Citric acid monohydrate p. a.	3958.1	Carl Roth GmbH + Co. KG	Karlsruhe, Germany
dNTP set 100 mM	10297-018	Invitrogen Corp.	Carlsbad, CA, USA
Dulbecco's Phosphate Buffered Saline - gibco®	14190-094	Life Technologies Corporation	Paisley, UK
Embedding wax (Paraffin)	17932A	Engelbrecht GmbH	Edermünde/ Besse, Germany
Eosin Y solution aqueous	HT110232-1L	Merck & Co., Inc.	Kenilworth, NJ, USA
Ethanol - CHEMSOLUTE® 99 % denatured/absolute p. a.	2294.1000, 2212.5000/ 2246.2500	Th. Geyer GmbH & Co. KG	Renningen, Germany
Formaldehyde solution 4 %, buffered, pH 6.9	1.00496.5000	Merck KGaA	Darmstadt, Germany
Glycine	3908.3	Carl Roth GmbH + Co. KG	Karlsruhe, Germany
Goat serum (normal)	X0907	Dako Denmark A/S	Glostrup, Denmark

Hematoxylin solution according to Mayer	51275-1L	Merck & Co., Inc.	Kenilworth, NJ, USA
HEPES - PUFFERAN®, buffer grade	HN78.2	Carl Roth GmbH + Co. KG	Karlsruhe, Germany
Hydrochloric acid (2 N)	T134.1	Carl Roth GmbH + Co. KG	Karlsruhe, Germany
Hydrogen Peroxide 30 % - ROTIPURAN® p.a.	8070.2	Carl Roth GmbH & Co. KG	Karlsruhe, Germany
Magnesium chloride hexahydrate	131396.1210	AppliChem GmbH	Darmstadt, Germany
Midori green advance DNA stain	MG04	Nippon Genetics Europe GmbH	Dueren, Germany
Mountant for microscopy - Roti®-Mount	HP68.2	Carl Roth GmbH + Co. KG	Karlsruhe, Germany
Non-woven wipes - Desco wipes	00-915-RD7003-01	Dr. Schumacher GmbH	Malsfeld, Germany
PBS Dulbecco, powder	L182-50	Biochrom GmbH	Berlin, Germany
Phenol/ chloroform/ isoamylalcohol (25: 24: 1)	51371	Biomol GmbH	Hamburg, Germany
RNA*later*® RNA stabilization reagent	1018087	Qiagen GmbH	Hilden, Germany
RNase-free water – peqGOLD	12-RWATER-88	VWR International BVBA	Leuven, Belgium
Roticlear® for histology	A538.2	Carl Roth GmbH + Co. KG	Karlsruhe, Germany
Sodium chloride - Fluka™	31434	Honeywell International Inc.,	Morristown, NJ, USA
Sodium fluoride	S1504	Sigma-Aldrich, Co.	St. Louis, MO, USA
Sodium hydroxide solution	5587.2500	Merck KGaA	Darmstadt, Germany
TRIS/ TRIS-HCl - PUFFERAN® p. a.	4855.2/ 9090.3	Carl Roth GmbH + Co. KG	Karlsruhe, Germany
Tri-sodium citrate dihydrate	4088.3	Carl Roth GmbH + Co. KG	Karlsruhe, Germany
TRIzol® reagent - ambion®	15596018	Life Technologies Corp.	Carlsbad, CA, USA
Tween® 20 - PanReac	A4974	AppliChem GmbH	Darmstadt, Germany
β-mercaptoethanol	4227.3	Carl Roth GmbH + Co. KG	Karlsruhe, Germany

2.1.4 Cell Culture

Table 4: Cell culture components

Component	Catalogue number	Supplier	Location
A83-01	72022	STEMCELL Technologies	Vancouver, Canada

B27 Supplement (50 x), serum free	17504-044	Life Technologies Corporation	Grand Island, NY, USA
Collagen I, Rat Tail	ALX-522-435-0100	Enzo Life Sciences, Inc.	Farmingdale, NY, USA
Collagenase from Clostridium histolyticum	C9697-50MG	Merck & Co., Inc.	Kenilworth, NJ, USA
Dimethyl sulfoxide (DMSO)	D8418-100ML	Merck & Co., Inc.	Kenilworth, NJ, USA
Dispase II	D4694-1G	Merck & Co., Inc.	Kenilworth, NJ, USA
Dulbecco's Modified Eagle Medium (DMEM) - gibco®	41965-039	Life Technologies Corp.	Paisley, UK
Dulbecco's Modified Eagle Medium/Nutrient Mixture F-12 (DMEM/F-12)	11330-032	Thermo Fisher Scientific	Waltham, MA, USA
Fetal bovine serum (FBS) - gibco®	10270-106	Life Technologies Corp.	Paisley, UK
Gastrin I human	G9020-250UG	Merck & Co., Inc.	Kenilworth, NJ, USA
GlutaMAX™ Supplement - gibco®	35050-061	Thermo Fisher Scientific	Waltham, MA, USA
HEPES Buffer solution	15630-056	Thermo Fisher Scientific	Waltham, MA, USA
Matrigel® growth factor reduced basement membrane matrix, phenol red-free - Corning®	356231	VWR International GmbH	Darmstadt, Germany
MEM Non-Essential Amino Acids (NEAA) - gibco®	11140-035	Life Technologies Corp.	Paisley, UK
Na_3PO_4	342483-500G	Merck & Co., Inc.	Kenilworth, NJ, USA
N-Acetyl-l-cysteine	A7250-10G	Merck & Co., Inc.	Kenilworth, NJ, USA
Nicotinamide	N0636-100G	Merck & Co., Inc.	Kenilworth, NJ, USA
Recombinant Human FGF-10	100-26	Pepro-Tech	Rocky Hill, NJ, USA
Recombinant Mouse R-Spondin 1 Protein, CF	3474-RS-050	R&D Systems, Inc.	Minneapolis, Mn, USA
Recombinant Murine Epidermal Growth Factor (mEGF)	315-09	Pepro-Tech	Rocky Hill, NJ, USA
Recombinant Murine Noggin	250-38	Pepro-Tech	Rocky Hill, NJ, USA
ROCK Inhibitor Y27632 Dihydrochlorid-Monohydrat	Y0503-5MG	Merck & Co., Inc.	Kenilworth, NJ, USA
Penicillin-streptomycin	P0781	Merck & Co., Inc.	Kenilworth, NJ, USA

Trypsin-EDTA 0.5 % (10 x) - gibco®	15400-054	Life Technologies Corp.	Paisley, UK

Table 5: Cells

Cell type	Source
KPC tumor cells	Department of Gastroenterology and Gastrointestinal Oncology, UMG

2.1.5 Kits

Table 6: Kits

Kit	Catalogue number	Supplier	Location
ImmPACT DAB Peroxidase (HRP) Substrate	SK-4105	VECTOR LABORATORIES, Inc.	Burlingame, CA, USA
Masson's Trichrome Stain Kit	25088	Polyscience, Inc.	Warrington, PA, USA
peqGold total RNA kit	12-6834-02	VWR International BVBA	Leuven, Belgium
Picrosirius Red Stain Kit 500 ml	24901-500	Polysciences, Inc.	Warrington, PA, USA
VECTASTAIN ABC Kit (Rabbit IgG)	PK-4001	VECTOR LABORATORIES, Inc.	Burlingame, CA, USA

2.1.6 Antibodies

Table 7: Antibodies

	AB	Species	Target tissue	Catalogue number	Supplier
1° AB	CDA	rabbit	h/m	ab82346	Abcam plc, Cambridge, UK
	DCK	rabbit	h/m	ab96599	Abcam plc, Cambridge, UK
	HA Binding Protein, Bovine Nasal Cartilage, Biotinylated	bovine	h/m	385911-50UG	Merck Millipore, Billerica, MA, USA
	NT5C1A	rabbit	h/m	C15296	Assay Biotechnology Company Inc., Sunnyvale, CA, USA
	Podoplanin	syrian hamster	m	CVL-MAB50714	Axxora, LLC, Farmingdale, NY, USA

2° AB	Anti-rabbit	goat	E0432	*Dako* Denmark A/S, Glostrup, Denmark
	Anti-syrian hamster	goat	BA-9100	VECTOR LABORATORIES Inc., Burlingame, CA, USA

(AB= antibody)

2.1.7 Anesthetics and analgetics

Table 8: Anesthetics and analgetics

Drug	Approval number	Supplier	Location
Carprieve (carprofen)	401182.00.00	Norbrook Laboratories Limited	Newry, UK
Forene® 100 % (V/V)	2594.00.00	AbbVie Deutschland GmbH & Co. KG	Ludwigshafen, Germany
Temgenic (buprenorphine)	345928	Indivior Eu Ltd.	Berkshire, UK

2.1.8 Primers for qRT-PCR

Table 9: Primers for qRT-PCR

Target	Direction	Sequence (5'-3')
hCDA	forward reverse	AGGAGCTGCAATCGTGTCTG TAGGGGCAGTAGGCTGACTT
mCda	forward reverse	AAGGCCATCTCCGAAGGGTA CAGTCGGTGCCAAACTCTCT
hDCK	forward reverse	GAGCGCGGCTTGAGGAG GGTGTCGGGGTTTGACTTTG
mDck	forward reverse	CAAGACTGGCACGACTGGAT CAGAGTCCGATGAAGGAGCC
hDCTD	forward reverse	CGGACCCAACATGAGTGAAGT GCCGACCTGGGAATTTGGAT
mDctd	forward reverse	GGACCCTGCTCTGACGTATG GCCATTGTACCCGATCCCAA
hNT5C1A	forward reverse	GAGAAGGCCCACGAGAACAA GGTACGAATTGGGCACTCCA
mNt5c1A	forward reverse	ACGAGAATGAGCCCTTCAGC TGAGACGAACTCCCACCTGA
hRRM1	forward reverse	GGAACAAGGTATGCTCCATGAATTG TGCCAAGGCTCCAGGTAAAT
hRRM2	forward reverse	AGGCGGAAGTTGGAATCAGG AGGAAATGGTCTGAGCTGGC
mRrm1	forward	GCCGAGAGAGGTGCTTTCAT

	reverse	AACCCTGCTTCCAACCGTAG
mRrm2	forward reverse	TGTGACTTTGCCTGCCTGAT CTCCAGCATAAGCCTGTCGG
hSLC29A1 (ENT1)	forward reverse	CCTGTTGCAGCCTCTCTTCC CCTGCTGCTGAGACTTTGGA
hSLC29A2 (ENT2)	forward reverse	TGGAGCCTCTCACTTCTCCA CCCGGGAGTGCTCTCATAATC
mSlc29a1 (Ent1)	forward reverse	TAGGGAGCTATCGTCGGTGG TGACTGGTTGTCATGGCTCC
mSlc29a2 (Ent2)	forward reverse	TTCATTCTGGGACTGGGCAC CTGCTGTTGGTCCCTGCTAA
XS-13 (h/m)	forward reverse	TGGGCAAGAACACCATGATG AGTTTCTCCAGAGCTGGGTTGT

2.1.9 Software

Table 10: Software

Software	Supplier	Location
cellSens Entry (Microscopy software)	Olympus Europa	Hamburg, Germany
GraphPad Prism 6.05/7.03	GraphPad Software Inc.	La Jolla, CA, USA
ImageJ 1.50b/ Fiji	Wayne Rasband, National Institute of Health (Schindelin et al. 2012)	USA
Leica LAS X - Application Suite X	Leica Microsystems CMC GmbH	Wetzlar, Germany
Microsoft Office 2016 (Word und Excel)	Microsoft Corp.	Redmond, WA, USA
Nucleotide BLAST	National Center for Biotechnology Information/ U.S. National Library of Medicine	Bethesda, MD, USA
PVC Viewer v1.5.3.1	Intas Science Imaging Instruments GmbH	Goettingen, Germany
Statistica v13.3	TIBCO Software Inc.	Palo Alto, CA, USA
StepOne v2.3	Life Technologies Corp.	Carlsbad, CA, USA

2.1.10 Animals

Table 11: Animals' genotype and type of tissue used

Murine genotype	Category	Supplier	Location
C57BL/6-J	living mice	Charles River Laboratories, Inc.	Wilmington, MA, USA
KPC	archived tissue	AG Neesse	
KPC SPARC$^{-/-}$	archived tissue		

PDX	Archived tissue	AG Hessmann	Department of Gastroenterology and gasotrointestinal Oncology, University Medicine, Goettingen, Germany

2.2 Methods

2.2.1 Cell culture

All cells were cultured in an incubator at 37 °C and 5 % CO_2. Experiments were performed under a sterile safety cabinet.

2.2.1.1 Cell culture conditions for adherent cells

In this study, archived $Kras^{G12D}$; $p53^{R172C/+}$; Pdx-1-Cre (KPC) cells derived from KPC Bl6 mice were used. According to the established protocols in the Neesse lab, cells were thawed, cultured, split, and isolated.

To take cells into culture, cell stocks from the -80 °C freezer were placed on ice. Culture medium was prepared and placed into a 37 °C water bath. After 10 ml of medium was pipetted into a 50 ml falcon, the cell stock was quickly thawed and the total volume (1 ml) was transferred to the conical tube. Then, the suspension was vortexed and centrifuged at 1200 rpm for 3 minutes at room temperature (RT). The supernatant was discarded and the cell pellet was resuspended in 12ml culture medium, transferred to a T75 flask and placed inside an incubator.

To expand cell lines, cells were split according to their growth rate. First, the medium was aspirated and washed with 8 ml of PBS. After discarding the PBS, cells were trypsinized in 2 ml and incubated at 37 °C for approximately 3 minutes for total detachment from the surface. The reaction was stopped with 8 ml of medium containing FCS and, subsequently, a volume according to the split ratio 1:10 was transferred to a new T75 flask.

Table 12: Composition of 2D cell culture media

Medium	Composition	Amount	Concentration
KPC medium	Dulbecco's Modified Eagle's medium (DMEM)	500 ml	
	FCS	50 ml	10 %
	Non-Essential Amino Acids (NEAA)	5 ml	1 %

2.2.1.2 PSC-conditioned medium experiments

Human cancer cell lines (MIA PaCa and L3.6) and human PSC cell line were thawed and cultured in DMEM supplemented with 10 % FCS (Hessmann et al. 2018). Cells were split and seeded onto 6-well plates according to established protocols in the Neesse lab. Having reached

a confluency of 60-80 %, the medium of the PSCs was replaced by serumfree DMEM. After 24 hours, the PSC conditioned medium (PSC-CM) was aspirated and provided to human cancer cell lines, which had also reached a confluency of approximately 60-80 %. Following an incubation time of 48 hours, cells were harvested and ribonucleid acid (RNA) was isolated for qRT-PCR using the peqGold total RNA kit and following the manufactur's instructions.

2.2.1.3 Culture of tumor cells on type I collagen

To generate collagen-coated plates, 1.1 ml type I collagen from rat tail (concentration 5 mg/ml) was suspended in 8.9 ml acetic acid and 40 ml autoclaved H_20. After mixing, 1.5 ml of type I collagen suspension was added to each well of a 6-well plate. Subsequently, the coated plates were incubated under the hood overnight (o/n). The next day, wells were washed twice with 1 x PBS and again incubated for 2 hours. Finally, plates were collected and stored at 4 °C prior to use.

Table 13: Composition of collagen-coated plates

Composition	Amount
Collagen I, Rat Tail	1.1 ml
Acetic Acid, 50 µM	8.9 ml
H_20, autoclaved	40 ml

Cells were seeded on collagen-coated plates for 24 and 48 hours aiming to reach a confluency of 60-80 % at the time point of isolation. After incubation, cells were washed with 1 x PBS and incubated with trypsin for dissociation, which was subsequently stopped by addition of medium. The cell suspension was collected in a 50 ml falcon tube, centrifuged for 3 minutes prior to removal of supernatant and resuspension of the cell pellet in 1 x PBS. Following another centrifugation step, cells were lysated with RNA lysis buffer and the protocol for RNA extraction from cells (chapter 2.2.5.1) was followed.

2.2.2 Animal studies

2.2.2.1 KPC mice

Tissue was obtained from previous preclinical studies (Neesse et al. 2013; Neesse et al. 2014). Tumor development of mice was confirmed by ultrasound and tissue was harvested and preserved according to established protocols (Neesse et al. 2013).

2.2.2.2 PDX mice

The study was approved by the ethics committee vote of the UMG and is listed as number 11/5/17. Archived tissue from AG Hessmann was used. Human biopsies from PDAC patients

(*f0-generation*) were subcutaneously transplanted into both flanks of female NMRI Foxn1^{nu} mice. Once tumor biopsies reached a size of 500 mm^3, mice were sacrified. Tumor pieces were harvested and again, transplanted into nude mice, and labelled *f1 generation*. Further transplantion procedures lead to f2 or higher generations.

Table 14: Overview of hPRT and PDX mice tissue samples

Patient No.	Block No.	PDX No.	Mouse No.	Generation	location
P6904/18	1-9	GöPDX4	5180	F1	right flank
P7328/18	1-7	GöPDX5	5373	F4	right flank
P8974/18	2-8	GöPDX8	5219	F1	left flank
P10136/18	1-12	GöPDX11	5209	F1	not spec.
P10446/18	3-9	GöPDX12	5326	F2	not spec.
P11045/18	1-8	GöPDX13	5321	F3	right flank
P11978/18	1-9	GöPDX14	5233	F1	left flank
P13247/18	1-5	GöPDX15	5231	F1	right flank
P20717/18	3-7	GöPDX18	5317	F1	right flank
P21923/18	6-11	GöPDX19	5322	F1	left flank
P26104/18	1-6	GöPDX21	5318	F1	right flank
P27971/18	1-9	GöPDX23	5333	F1	right flank

(hPRT = human primary resected tissue; No. = number; not spec. = not specified; PDX = patient-derived xenograft)

2.2.2.3 Orthotopic mouse model

Orthotopic transplantations were performed in 8-week-old male C57BL/6-J mice which were ordered from Charles River Laboratories, Germany. In this study, KPC tumor cells were used for transplantation. Before surgery, cells were splitted and counted. For this procedure, 150,000 viable cells were suspended in 20 µl medium and 20 µl matrigel, leading to a total application volume of 40 µl per mice.

2.2.2.4 Orthotopic transplantation procedure

30-45 minutes prior to surgery, Buprenorphin (200 µl/20 g body weight) was injected intraperitoneally. Mic were placed into a chamber. Anesthesia was induced by applying isoflurane (2-3 %) into the chamber until deep sedation occurred. After transferal to the surgical platform with continued isoflurane inhalation via a nose cone, eye cream was applicated and mice were shaved and injected with Caprieve (100 µl/20 g body weight) subcutaneously (s.c). During surgery, mice were kept on a warming plate. After disinfection, the mouse abdomen was opened with a scalpel, the spleen was pulled out and 40 µl of the cell/matrigel suspension was injected into the tail of the pancreas. To close of the abdomen, the peritoneum was stitched and the skin was closed with clips. Upon awaking from anesthesia, mice were transferred in the cage and provided with

mash food. On the day of transplantation, the condition of the mice was checked frequently. Follow-up examinations included daily checks for general behavior and body weight measurements three times a week. All procedures were conducted according to the local animal fare regulations and were registered under the animal test number 15/2057.

2.2.2.5 Housing conditions

All mice were kept at a 12 hours dark and 12 hours light cycle. Housing conditions were in accordance with the local fare regulations and registered under the animal test number 15/2057.

2.2.2.6 Sonography

Tumor development of OTMs was evaluated through high-resultion ultrasound. Mice were checked on day 13 and day 19 after orthotopic transplantation. Prior to sonography, mice were anesthetized with isoflurane (3-4 %). While keeping the nose of the mice in a cone with isoflurane, the fur of the abdomen was removed using a shaver and hair-removing cream. Sonography was conducted by using a Visual Sonics Vevo 2100 High Resolution Ultrasound System according to an established protocol (Goetze et al. 2018).

2.2.2.7 Endpoint criteria

Mice which either showed signs of pain or loss of body weight > 20 % were sacrificed. Additionally, OTMs were sacrificed when tumors detected by sonography were adequate in size and volume of about 75 mm^3 or after 21 days at the latest.

2.2.2.8 Tissue harvesting, fixation and embedding

After isoflurane (5 %) anesthesia, mice were euthanized by cervical dislocation and heart puncture. Following disinfection, the abdomen was opened up and the general appearance was examined. The pancreas was isolated and pieces were cut in a petri dish. Subsequently, tissue pieces were snap frozen and later transferred to -80 °C storage. Furthermore, other parts of tumor tissue were incubated in a cryo vial containing 1 ml RNA later® and kept at 4 °C for 24 hours. After removing the solution, samples were also transferred to -80 °C storage. To establish cell lines, tumor tissue was either placed in a falcon containing 7 ml 1 x PBS or a petri dish, both on ice. Finally, the remaining tumor tissue, together with samples of spleen, intestine, and liver; were placed into 10 % buffered neutral formalin solution o/n for fixation and subsequent paraffin embedding.

2.2.3 Human studies

2.2.3.1 Primary resected PDAC tissue

Primary resected tissue from PDAC patients: Archived tissue was obtained from Dr. Mark-Sebastian Boeshertz, Institute of Pathology, Goettingen (Table 14).

2.2.4 Tissue processing for stainings

2.2.4.1 Paraffin-embedment

For tissues, isolated sections were placed into a histology cassette followed by storage in formalin until the dehydration process. All samples were dehydrated by being passed through a Leica tissue processor. Followed by embedment in paraffin, sections of 4 µl were cut using a Rotary Microtome. After slides were allowed to lay on a heating plate, they were stored at 37 °C o/n before beeing were stored in the dark until staining.

2.2.4.2 Hematoxylin and eosin (H&E) staining

Prior to being passed through a gradient alcohol row for 1 minute each (99 %, 99 %, 96 %, 80 %, 50 %) for rehydration, slides were incubated in roticlear twice for 10 minutes to remove paraffin. Slides were then washed in tap water and placed in hematoxylin for 6 minutes. Next, tissues were kept in tap water for 5 minutes until the color turned blue and, subsequently, acidophile structures were dyed in eosin y solution for additional 3 minutes. Repeatedly, slides were incubated in tap water for 15 seconds prior to the dehydration process in an ascending ethanol row (30 seconds in 70 %, 1.5 minutes in 96 %, 2 minutes in 99 %) ending in roticlear for > 20 minutes. Stained tissue sections were mounted with rotimount and a cover slip was then placed under the hood for solidification.

2.2.4.3 Immunohistochemistry (IHC)

Similarly to H&E staining, slides were incubated in roticlear for 10 minutes twice before being exposed to a rehydration process with equal concentrations for 4 minutes each. To conduct unmasking of antigens, slides were placed into a beaker containing citrate buffer ph 6.0 and cooked for different time periods depending on the primary antibody (AB) used. Afterwards, tissue sections were allowed to first cool down in the microwave for 10 minutes followed by additional 20 minutes on ice and a washing step in tap water. As endogenous peroxidases could induce additional background staining, slides were incubated in 3 % freshly prepared H_2O_2 for 15 minutes prior to another washing step in tap water. Next, tissue sections were aligned in a SequenzaTM Slide Rack using TBST and, subsequently, washed with TBST three times. To reduce unspecific binding of the AB, slides were incubated with 200 µl blocking solution (BS) consisting of TBST supplemented with 10 % goat serum and 1 % BSA in TBST for 1 hour. Meanwhile, the primary AB was diluted either in BS or 1 % BSA, and again 200 µl of suspension were added to each slide. Cadenza systems were placed at 4 °C o/n. The next day, slides were washed with TBST three times, 200 µl of 1:200 diluted secondary AB were added to each slide and incubated at 37 °C for 1 hour. During incubation, AB complex was prepared and incubated for 30 minutes at RT. Followed by another washing step of TBST three times, tissue sections were incubated with 200 µl AB complex/slide for an additional hour prior to being washed with TBST for the last time, removed from SequenzaTM Slide Rack, and placed in tap water. For staining, tissue sections were exposed to 3,3'- diaminobenzidine (DAB) staining for a defined

time depending on the primary AB used (Table 17). The reaction was stopped by placing the slides in tap water. For counterstaining, slides were then stained with hematoxylin for five minutes prior to placement into tap water until the color turned blue. As for H&E staining, slides were exposed to a dehydration process (70 %, 80 %, 96 %, 99 % ethanol) for 5 minutes each and finally ending in roticlear, followed by a mounting and drying process.

Table 15: Composition of epitope-retrieval and washing buffers for IHC

Buffer	Composition	Amount
BS	TBST	
	Goat serum (normal)	10 %
	BSA in TBST	1 %, 10 %
Citrate buffer ph 6.0	Citric acid monohydrate	2.1 g
TBS (10x)	Tris	4.24 g
	Tris-HCl	26.0 g
	NaCl	292.7 g
TBST	TBS (1x)	1 L
	Tween 20	1 ml

(BS = blocking solution)

2.2.4.4 Masson's trichrome staining

According to H&E/IHC stainings, paraffin was removed by roticlear followed by rehydration of tissue slides. Subsequently, slides were incubated in Bouin's solution at RT o/n to further fix the tissue and improve the quality of the staining. The next day, slides were washed under tap water for 5 minutes, followed by staining of all basophilic structures upon placement into Weigert's haematoxylin for 15 minutes. After repeated washing steps in tap water for 5 minutes, slides were placed into Biebrich-Scarlet Acid solution for 5 minutes to stain all acidophilic structures. To remove red staining of collagen, tissue sections were briefly placed in destilled water prior to placement in phosphomolybdic-phosphotungstic acid solution for 5 minutes. Followed by instant placement into aniline blue to stain for collagen for 8 minutes, tissue sections were washed in destilled water three times and further processed into 1 % acetic acid to fix the staining. To avoid bleeching, the dehydration process of slides was reduced to 95 % and 99 % ethanol for 30 seconds each and roticlear process to 1-2 minutes. Finally, slides were covered with rotimount and a cover slip, and allowed to dry o/n.

2.2.4.5 Picrosirius staining

Slides were passed through roticlear and ethanol for paraffin removement and rehydration as described above. Next, tissue sections were stained in Weigert's haematoxylin for nuclei staining and further processed into 2 % acid ethanol for 10 seconds. Afterwards, tissue sections were placed in tap water and then destilled water. Subsequently, slides were immersed in Phosphomolybdic acid (Solution A) for 2 minutes. Repeatedly, slides were rinsed in destilled water and further incubated in picrosirius Red F3BA Stain (Solution B) for 60 minutes to stain type I and III collagen fibers in red. Afterwards, slides were placed in 0.1 N Hydrochloride Acid (Solution C) for fixation for 1 minute followed by a short incubation with 70 % ethanol for 45 seconds. Dehydration and fixation processes of tissue sections were conducted as described above.

Table 16: Staining procedure for each antibody used for IHC

Target	Buffer	BS	C. 1°AB	Med. 1°AB	C. 2°AB	Med. 2°AB	TD (sec)
CDA	Citrate buffer pH 6	10 % Goat serum + 1 % BSA in TBST	1:100	1 % BSA in TBST	1:200	1 % BSA in TBST	180
DCK							50
HA	-	10 % BSA in TBST			-	-	120
NT5C1A	Citrate buffer pH 6	10 % Goat serum + 1% BSA in TBST		10 % Goat serum + 1 % BSA in TBST	1:200	1 % BSA in TBST	120
Podoplanin				1 % BSA in TBST			90

(AB = antibody; BS = blocking solution; C = concentration; Med = medium; TD = time development)

2.2.4.6 Histological quantification analysis

All stainings were planimetrically analyzed using the software Fiji (v1.52p) (Schindelin et al. 2012). To ensure comparability among samples, pictures for each staining were taken with the same focal aperture setting, exposure time, contrast and white balance mode. For enzyme stainings (CDA, DCK, NT5C1A), 10 pictures per mouse (200 x) were taken, while stromal markers (hyaluronan-binding protein, Masson's trichrome, picrosirius, podoplanin) were evaluated with 7 pictures per mouse (100 x). Areas of necrosis, artefacts and overdyed border areas were not included.

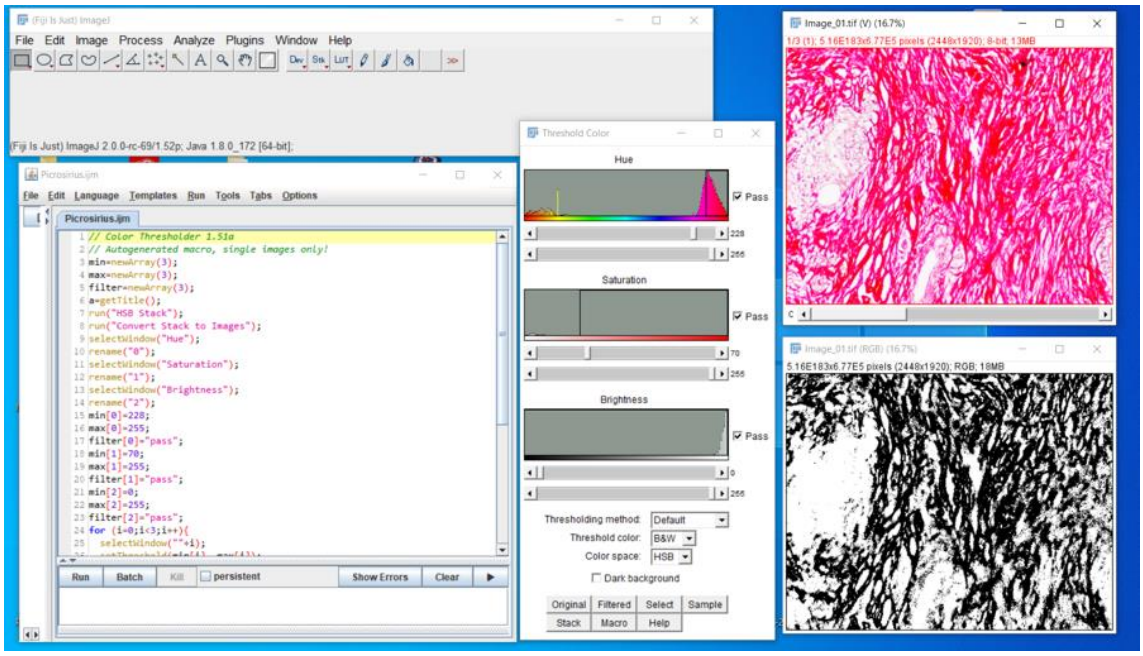

Figure 6: Collagen quantification via picrosirius staining both without and with applied macro. Using Fiji, a macro for each staining was designed. In this process, small batches of slides were analyzed to adjust staining intensity, contrast, and brightness. Thus, the macro detects positively stained areas (black pixels) while the remaining area is left out and not quantified (white pixels).

Prior to the main analysis, small batches of slides were analyzed and a macro displaying the staining most adequately was designed. The macros were written and provided by Benjamin Steuber (Figure 6).

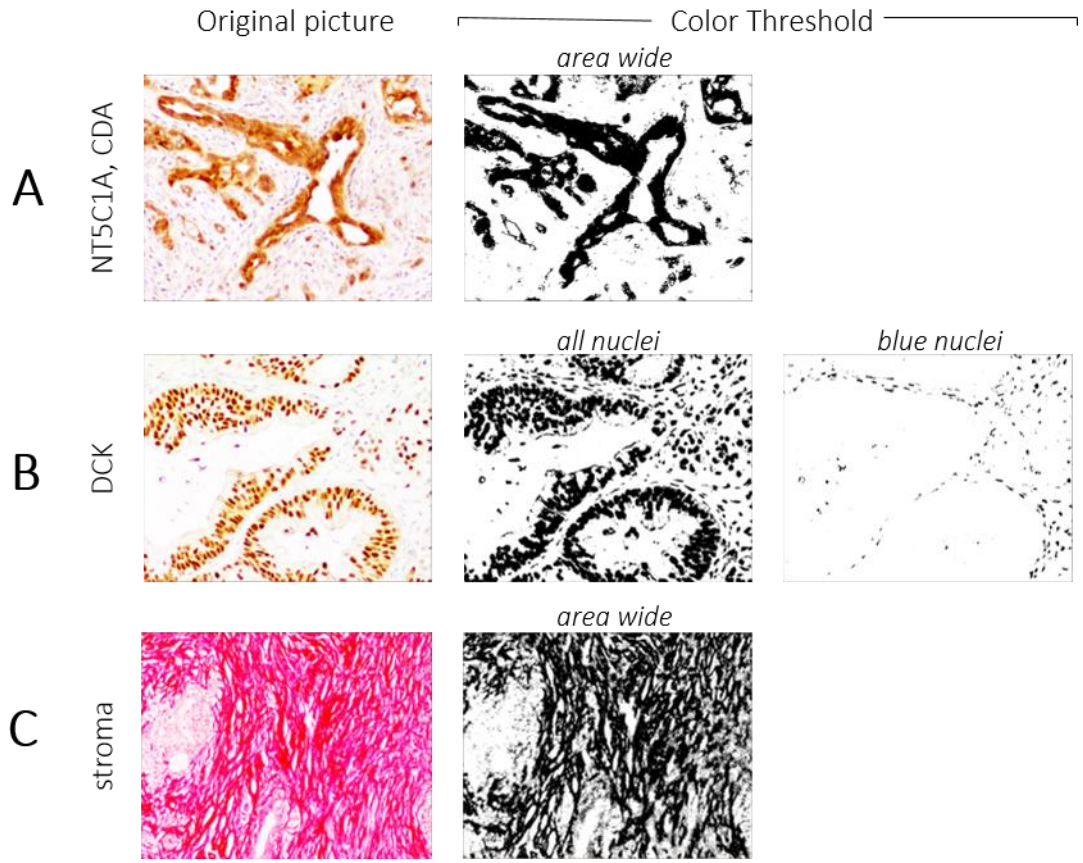

Figure 7: Application of macro for each type of quantification. To analyze enzyme stainings, total area stainings (NT5C1A, CDA) and nuclear stainings (DCK) were quantified. DCK quantification was performed by using two macros: The amount of blue (= negative) nuclei was subtracted from the total amount (= positive + negative) nuclei to determine the amout of brown (= positive) nuclei. Stromal stainings were all quantified by total area macros.

To assess enzyme staining (CDA, DCK, NT5C1A) and stromal stainings (hyaluronan-binding protein, Masson's trichrome, picrosirius, podoplanin), the procedure of Color Threshold was applied ("Image ►Color Threshold"). For this, the staining intensity, contrast and brightness were set individually to define the positivity or negativity of a staining. Stained pixels were translated into black pixels which were then relatively set to the total amount of pixels (Figure 7A,C)

Regarding DCK, two macros were used counting either the total nuclei number [(A) in Table 17] or the blue (negative) nuclei [(B) in Table 17]. Consequently, the number of blue nuclei was subtracted from the total nuclei count to receive the brown (positive) nuclei count (Figure 7B).

Table 17: Overview of all conducted stainings

Staining	Tissue (n)				Magni-fication	Ex-poure time (ms)	No of pictures	Fiji settings			
	KPC	OTM	hPRT	PDX				Procedure	Hue	Satura-tion	Bright-ness
CDA	12	13	12	12	200 x	25	10	DAB CD	0 ; 250	34 ; 255	0 ; 244
DCK	12	13	12	12	200 x	25	10	Color Threshold	(A) 0 ; 255	0 ; 255	0 ; 244
									(B) 126 ; 200	0 ; 255	0 ; 244
NT5C1A	12	13	12	12	200 x	25	10	DAB CD	0 ; 255	35 ; 255	0 ; 255
HA	12	13	12	12	100 x	10	7	Color Threshold	0 ; 80	0 ; 255	0 ; 228
MT	12	13	12	12	100 x	20	7		133 ; 215	0 ; 255	0 ; 235
Picrosirius	12	13	12	12	100 x	15, 63	7		228 ; 255	100 ; 255	0 ; 255
Podoplanin	12	13			100 x	15,63	7		0 ; 111	0 ; 255	0 ; 218

(A) Total nuclei count, (B) blue nuclei count *(MT = Masson's trichrome; OTM = orthotopically trans-planted mouse; PDX = patient-derived xenografi; hPRT = human primary resected tissue)*

2.2.4.7 Statistical analysis

Following the quantification processes, results were further evaluated using linear regression models by Statistica (v13.3). Data was plotted by both Statistica (v13.3) and Graph Pad Prism (v6.05/7.03). Data are presented with ± standard deviation (SD). If not indicated otherwise, unpaired student t-test was used. Statistical significances are indicated with * $p < 0.05$, ** $p < 0.01$, and *** $p < 0.001$.

For other statistical analysis in this work, significance levels were calculated with different statistical tests, depending on the experimental design and the distribution of the calculated values. The exact test used is stated in the figure legends and corresponding chapter. Statistical analysis was performed in collaboration with the Medical Statistics Unit of the UMG and Dr. Christoph Ammer-Herrmenau from the Neesse group.

2.2.5 Molecular methods

2.2.5.1 RNA extraction from 2D-cultured cells

To isolate RNA from 2D cell lines, the PeqLab Gold Total RNA was used according to the manufactur's instructions.

After the medium was discarded, cells were washed with PBS followed by adding 1 ml of Cell Recovery Solution and placing the dish on ice. After 2 minutes, the solution was collected into a 50 ml falcon tube, and after another washing step, incubated on a rocking plate at 4 °C for 60 minutes. Then, cells were centrifuged at 200-300 xg at 4 °C for 5 minutes before being resuspended in cold PBS and centrifuged repeatedly at the same conditions. Subsequently, the supernatant was discarded and cells were resuspended in 200 µl RNA lysis buffer and vortexed before being further processed with the PeqLab Gold Total RNA kit according to the manufactur's instructions.

2.2.5.2 RNA extraction from tissue

Pieces of tissue were placed into Eppendorf cups which were prepared with 1 ml of TRIzol in advance. With the use of short sonification impulses, the tissue was homogenized. After addition of 200 µl of cholorform, samples were vortexed and incubated at RT for 5 minutes. Followed by a centrifugation step at 14000 rpm, 4 °C and 5 minutes, the upper transparent phase containing the RNA was carefully transferred to a new Eppendorf cup. 500 µl of isopropanol was added to each sample, and after a short incubation time at RT, the samples were again centrifuged at the same conditions for 30 minutes. Subsequently, the supernatant was discarded and the pellet washed with 1 ml of 75 % ethanol. After mixing and centrifugation at 13000 rpm, 4 °C for 5 minutes, the supernatant was repeatedly discarded and the pellet resuspended in 50 µl Ampuwa. At last, RNA concentrations from all samples were determined by using the INTAS nanophotometer.

2.2.5.3 cDNA preparation

To obtain a cDNA concentration of 6.4 ng, RNA was prepared with Ampuwa and 1 µl recombinant RNasin® ribonuclease inhibitor to a volume of 9 µl. After incubating at 65 °C for 10 minutes, samples were supplemented with a variety of reagents (Table 18). For the transcription process, samples were incubated at 38 °C for one hour, followed by another step at 72 °C for 10 minutes. Subsequently, cDNA was placed on ice and 60 µl of Ampuwa was added. In the end, 6.4 ng cDNA were obtained.

Table 18: Composition of cDNA Master Mix for one sample

Composition	Amount
5 x First Strand Buffer	8 µl
Primer $p(dt)_{15}$ (nmol)	8 µl
dNTPs 10 nM	8 µl
DTT	4 µl
MMLV-Reverse	2 µl

2.2.5.4 qRT-PCR

Quantitative real time polymerase chain reaction (qRT-PCR) was conducted to compare gene expression levels. The procedure was conducted using three technical replicates for each sample. After the preparation of the master mix containing SYBR Green, Ampuwa, and specific messenger ribonucleid acids (mRNA) primers (Table 9/19), 9 µl of master mix and 1 µl of cDNA were added to a 96-well-plate. Subsequently, plates were sealed with a film, centrifuged shortly, and then placed in a StepOne Real-Time PCR system following a certain thermoprofile (Table 20).

Table 19: Composition of qRT-PCR Master Mix for one sample

Composition	Amount
FAST SYBR	5 µl
Ampuwa	2.8 µl
Primer forward	0.6 µl
Primer reverse	0.6 µl

Table 20: Thermoprofile for qRT-PCR

	Temperature	Time
40 x	95 °C	15 sec.
	60 °C	60 sec.

(sec. = seconds)

3 Results

In this work, we investigated the expression of GME in different pancreatic model systems. In the first part, we addressed the expression of GME. Moreover, based on the findings from the IHC stainings, we extended the focus and also included the TME which is abundantly present in PDAC (Neesse et al. 2011). The second part provided insights into the role of cell-cell interactions and cell-matrix interactions and evaluated whether cellular and extracellular components of the TME regulate expression of GME. By conducting experiments both *in vitro* and *in vivo*, we aimed to examine the role of the stroma in PDAC chemoresistance towards gemcitabine.

3.1 Expression of gemcitabine metabolizing enzymes in different pancreatic cancer model systems

Previously, our group and others have shown that GME play a crucial role in mediating gemcitabine resistance (Patzak et al. 2019). In recent years, various model systems for PDAC were postulated, however, the comparability of the model with the endogenous human tumor remains largely uninvestigated (Frese and Tuveson 2007). Nevertheless, the choice of the most appropriate model system is crucial when developing new treatment strategies. Therefore, we aimed to investigate the expression of GME in two different cohorts comprising two experimental systems each. On the one hand, we compared expression of GME in transgenic KPC mice with endogenous pancreatic tumors, and B6 mice which underwent orthotopic transplantation with tumor cells previously isolated from KPC mice referred as OTMs. On the other hand, we investigated whether the expression of GME in resected tissue from PDAC patients, hPRT, alters when it is subcutaneously transplanted into the flanks of nude mice, PDX mice.

To evaluate GME expression, IHC stainings of NT5C1A, CDA and DCK were performed. As NT5C1A and CDA were area-wide stainings, the percentage of total area was quantified. Since DCK showed a nuclear staining (Kerr et al. 2014), the total amount of brown (= positive) stained nuclei was indirectly counted through substraction of blue (= negative) nuclei stained from all nuclei stained.

3.1.1 Orthotopic transplanted mice demonstrate less expression of gemcitabine metabolizing enzymes

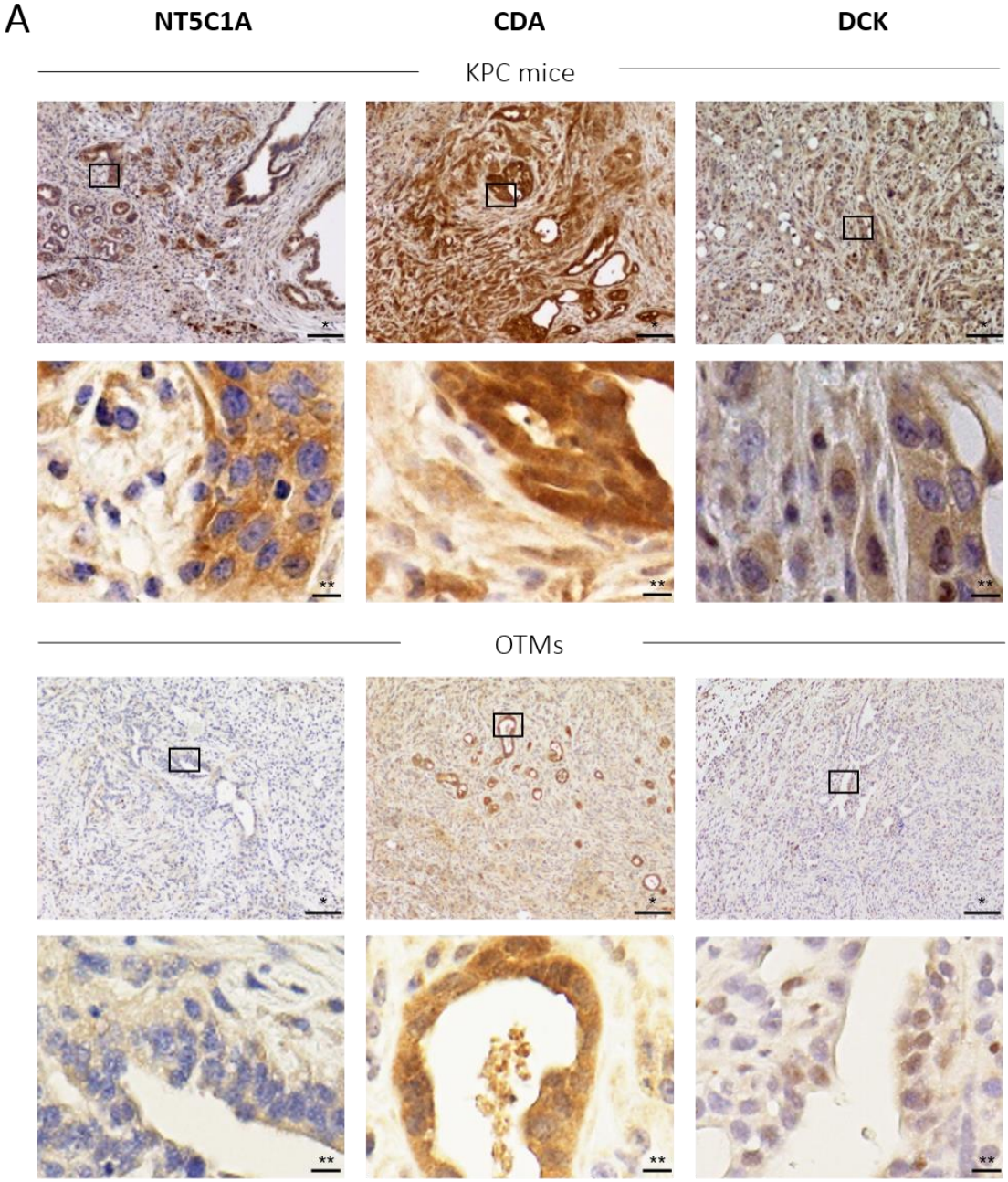

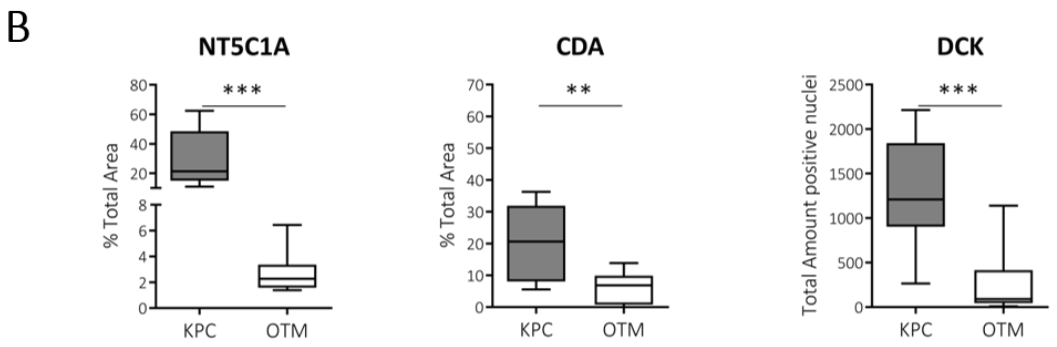

Figure 8: Expression and quantification of GME in KPC mice and OTMs. (A) Representative immuno-histochemical stainings of GME in KPC mice and OTMs, respectively. Scale bars indicate * 100 µm and ** 20 µm, respectively. (B) Enzyme expression (± SD) in KPC mice (n = 12) and OTMs (n = 13) [NT5C1A (*** p), CDA (** p), DCK (*** p)]. P-value was calculated using Mann-Whitney test; * $p < 0.05$, ** $p < 0.01$, *** $p < 0.001$. *[CDA = cytidine deaminase; DCK = deoxycytidine kinase; (KPC = LSL-Kras$^{G12D/+}$; LSL-Trp53$^{R172\ H/+}$; Pdx-1-Cre); NT5C1A = 5'-nucleotidase, cytosolic 1A; OTM = orthotopically transplanted mouse]*

Stainings of GME were compared between independent cohorts of 12 KPC mice and 13 OTMs (Figure 8A). Interestingly, OTMs revealed a significantly lower expression of all three GME compared to the KPC cohort [NT5C1A (*** p), CDA (** p), DCK (*** p)] (Figure 8B).

3.1.2 Human primary resected tissue and corresponding PDX mice demonstrate no significant difference in expression of gemcitabine metabolizing enzymes

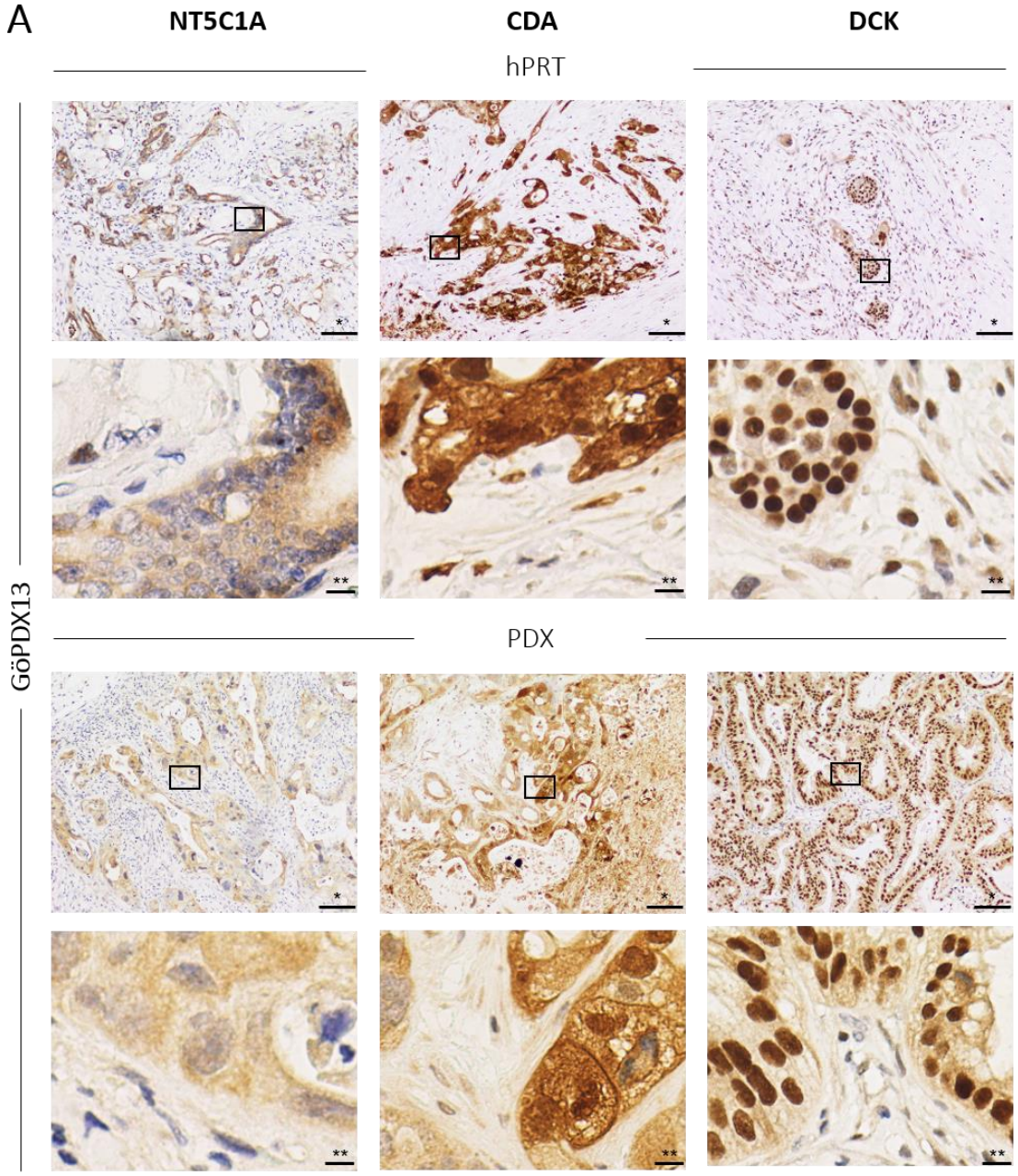

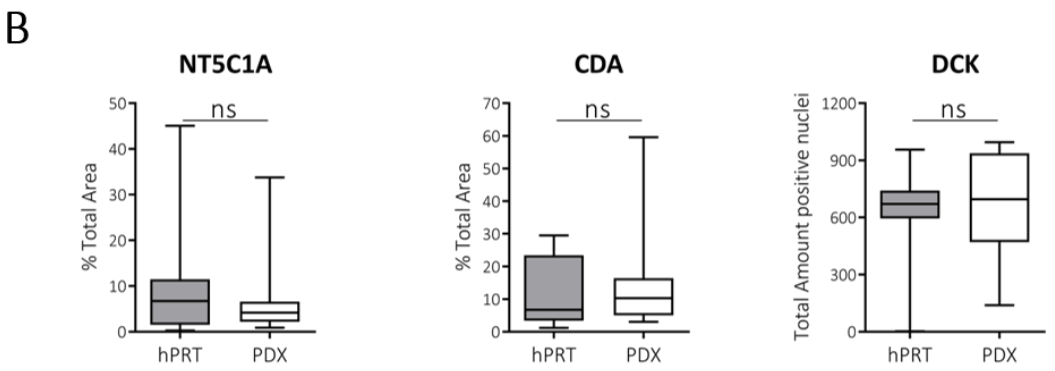

Figure 9: Expression and quantification of GME in hPRT and PDX mice. (A) Representative immuno-histochemical stainings of GME in hPRT and corresponding PDX belonging to GöPDX13. The example demonstrates a medium to high expression of all GME in PDAC bulk tissue. Scale bars indicate * 100µm and ** 20µm, respectively. (B) Enzyme expression (± SD) in n = 12 pairs of hPRT and PDX mice [NT5C1A (ns), CDA (ns), DCK (ns)]. P-value was calculated using Wilcoxon matched-pairs signed rank test; * $p < 0.05$, ** $p < 0.01$, *** $p < 0.001$ *[CDA = cytidine deaminase; DCK = deoxycytidine kinase; (KPC = LSL-KrasG12D/+; LSL-Trp53R172 H/+; Pdx-1-Cre); ns = not significant; NT5C1A = 5'-nucleotidase, cytosolic 1A; PDX = patient-derived xenograft; hPRT = human primary resected tissue]*

Similar to KPC mice and OTMs, IHC stainings were performed in 12 pairs of hPRT and PDX mice, respectively. Except for one patient (GöPDX5), none of the remaining patients received chemotherapeutic treatment prior to resection. As seen in Figure 9A, sample GöPDX13 exhibited a medium to high expression of GME in both hPRT and PDX mouse, respectively. Quantification analysis of the cohorts revealed no significant change in GME expression when hPRT is transplanted and grown subcutaneously in PDX mice as shown above (Figure 9B).

3.2 Stromal expression in different pancreatic cancer model systems

PDAC is a highly desmoplastic cancer exhibiting an abundant stroma environment (Neesse et al. 2019), and different stromal markers have been described to be highly expressed within the tumor mass. Hence, stainings for the extracellular components HA and type I collagen were performed. Type I collagen expression was evaluated using staining protocols for picrosirius (collagen red) and Masson's trichrome (collagen blue). Furthermore, an IHC staining protocol for podoplanin which is known to be expressed on the surface of CAFs and associated with poor survival in other cancer entities (Quintanilla et al. 2019), was conducted. For all stromal components, the total stained area was quantified.

3.2.1 CAFs are significantly reduced in orthotopically transplanted mice compared to KPC mice

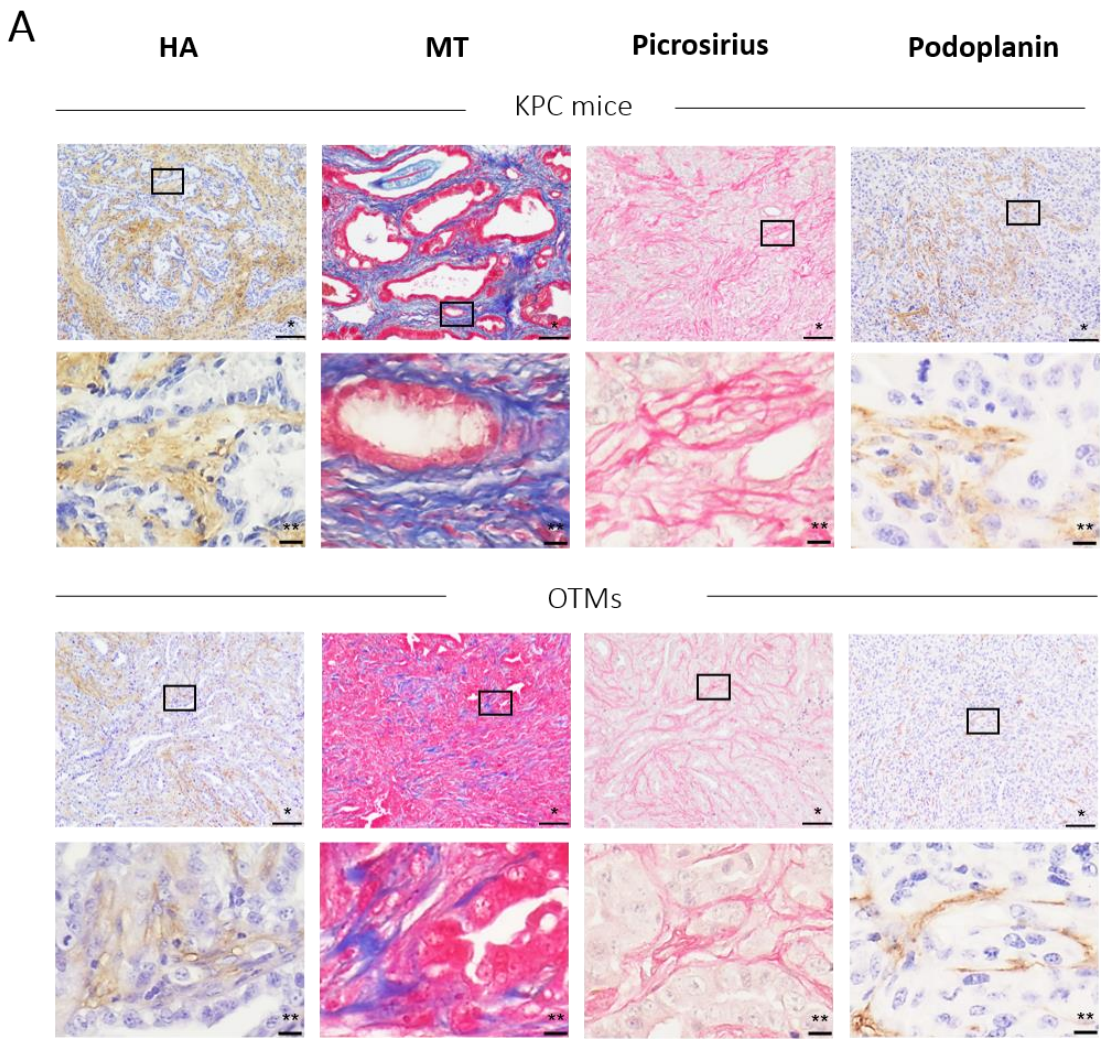

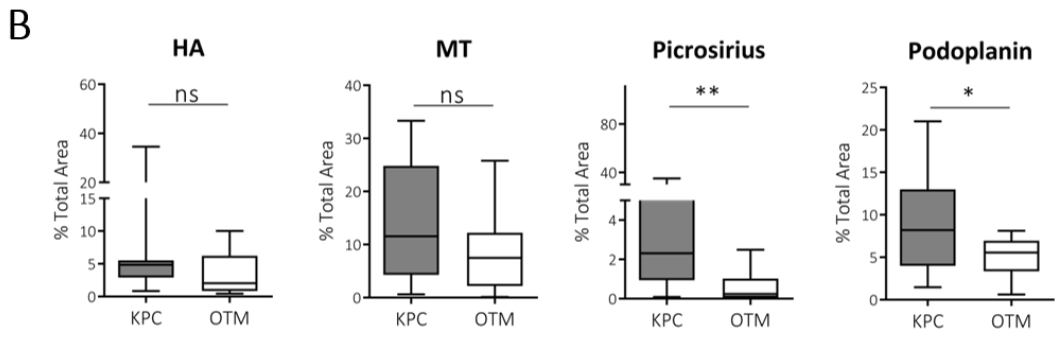

Figure 10: Expression of stromal markers in KPC mice and OTMs. (A) Representative stainings of stromal components in KPC mice and OTMs. Scale bars indicate * 100µm and ** 20µm, respectively. (B) Expression of stromal components (± SD) in KPC mice (n = 12) and OTMs (n = 13) [HA (ns); MT, blue area (ns); picrosirius (** p); podoplanin (* p)]. P-value was calculated using Mann-Whitney test; * $p < 0.05$, ** $p < 0.01$, *** $p < 0.001$. *[HA = hyaluronic acid; (KPC = LSL-Kras$^{G12D/+}$; LSL-Trp53$^{R172\ H/+}$; Pdx-1-Cre); MT = Masson's trichrome; ns = not significant; OTM = orthotopically transplanted mouse]*

Stainings revealed a reduced expression of all stromal components in OTMs compared to KPC mice (Figure 10A). Moreover, quantification analysis revealed a non-significant change in levels of HA and type I collagen in MT staining but a significant reduction in picrosirius staining in OTMs (** p). In addition, the CAF marker podoplanin was expressed significantly lower in OTMs compared to KPC mice (* p) (Figure 10B).

3.2.2 PDX mice reveal reduced amounts of stromal components compared to human primary resected tissue

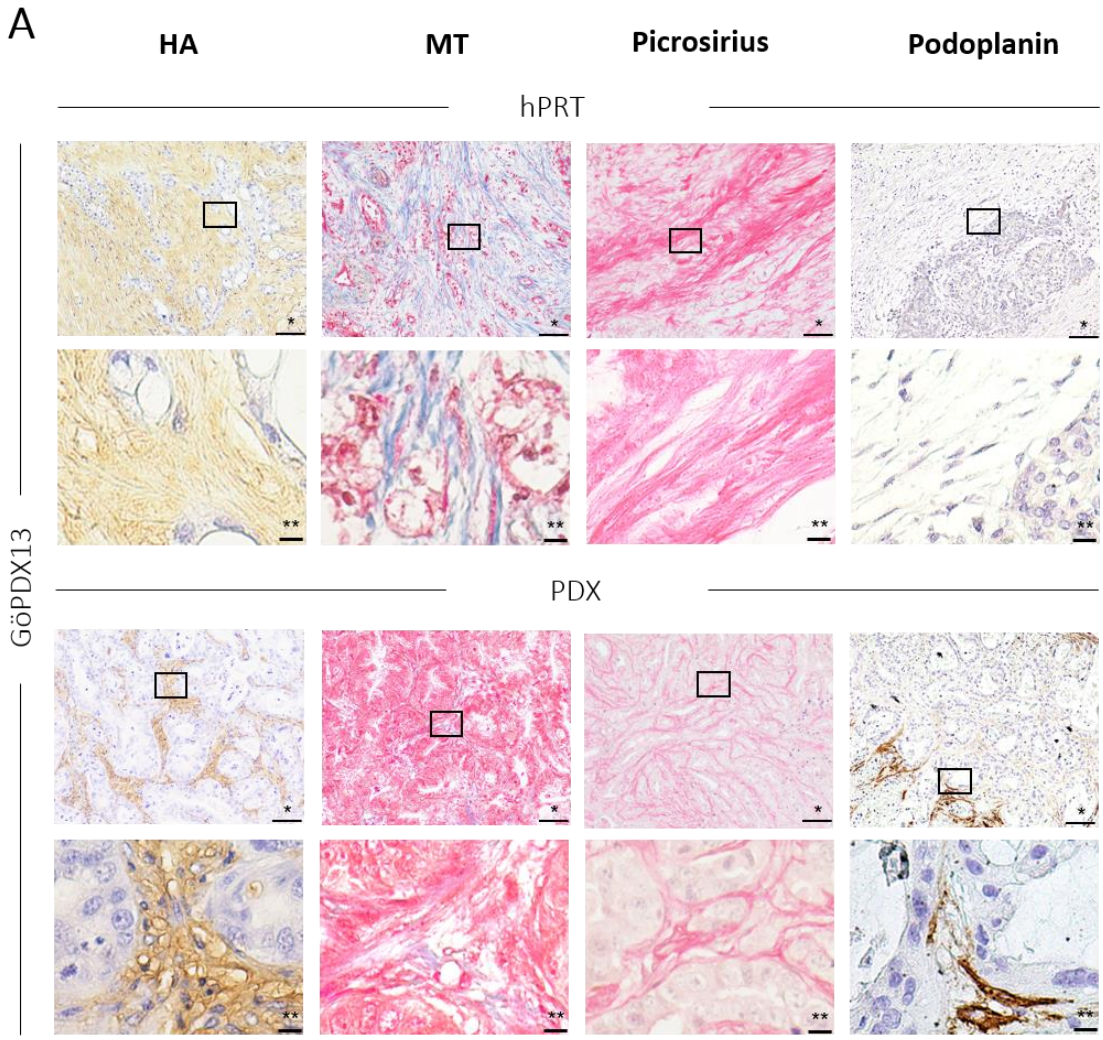

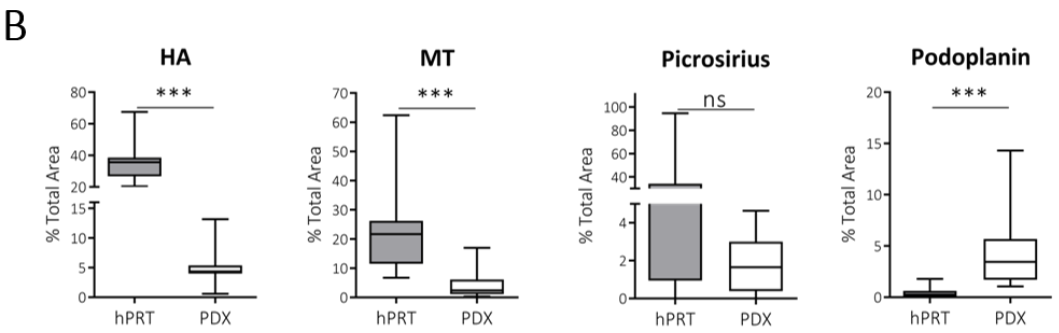

Figure 11: Expression of stromal components in hPRT and PDX mice. (A) Representative stainings of stromal components in hPRT and corresponding PDX belonging to GöPDX13. PDX tumors display less expression of stromal components and more epithelial cells. Scale bars indicate * 100µm and ** 20µm, respectively. (B) Expression of stromal components (± SD) in n = 12 pairs of hPRT and PDX mice [HA (*** p); MT, blue area (*** p); picrosirius, red area (ns); podoplanin (*** p)]. P-value was calculated using Wilcoxon matched-pairs signed rank test; * $p < 0.05$, ** $p < 0.01$, *** $p < 0.001$. *(HA = hyaluronic acid; MT = Masson's trichrome; ns = not significant; PDX = patient-derived xenograft; hPRT = human primary resected tissue)*

Following stainings of GME expression, stainings for stromal components HA, type I collagen and podoplanin were conducted in respective 12 pairs of hPRT and PDX mice (Figure 11A). Quantification analysis demonstrated a significant reduction of HA content in PDX mice (*** p). Furthermore, type I collagen was found significantly lower in PDX mice in MT staining (*** p), but not in the Picrosirus staining. In contrast, PDX mice revealed a significantly higher expression of podoplanin (*** p) which is a marker for CAFs (Figure 11B).

3.3 Association between gemcitabine metabolizing enzymes and stromal components

To investigate an association between GME and stromal components, the statistic software Statistica (v13.3) was used. Based on the hypothesis that GME might be associated with the extent of stromal expression, stromal components were set as the independent variable (x) and GME NT5C1A, CDA and DCK as the dependent variable, respectively (y). Moreover, this analysis was conducted for both KPC vs. OTMs, and hPRT and corresponding PDX mice, respectively.

Table 21: Statistical correlation between gemcitabine metabolizing enzymes and stromal components

		HA		MT		Picrosirius		Podoplanin	
	GME	τ	p	τ	p	τ	p	τ	p
KPC	**NT5C1A**	-.212	.337	-.273	.217	-.333	.131	-.182	.411
	CDA	-.333	.131	-.030	.900	.212	.337	.364	.100
	DCK	-.182	.411	-.243	.273	-.243	.273	-.273	.217
OTM	**NT5C1A**	.103	.635	-.231	.272	-.026	.903	-.282	.180
	CDA	.026	.903	-.051	.807	0	1.0	-.103	.625
	DCK	0	1.0	-.026	.903	-.180	.393	-.026	.903
hPRT	**NT5C1A**	0	1.0	.152	.493	-.030	.891	.091	.681
	CDA	-.394	.075	.364	.100	.061	.784	-.061	.784
	DCK	.152	.493	0	1.0	-.182	.411	-.121	.584
PDX	**NT5C1A**	-.485	.029	-.303	.170	-.242	.273	-.212	.337
	CDA	-.364	.100	-.182	.411	.242	.273	-.212	.337
	DCK	-.091	.681	-.152	.493	-.030	.891	.121	.584

Kendall's Tau (τ) correlation coeffizient and significance value p were calculated by using Kendall rank correlation. *[CDA = cytidine deaminase; DCK = deoxycytidine kinase; HA = hyaluronic acid; (KPC = LSL-Kras$^{G12D/+}$; LSL-Trp53$^{R172\ H/+}$; Pdx-1-Cre); MT = Masson's trichrome; NT5C1A = 5'-nucleotidase, cytosolic 1A; OTM = orthotopically transplanted mouse; PDX = patient-derived xenograft; hPRT = human primary resected tissue]*

The majority of the stromal components and GME did not demonstrate a significant correlation(Table 21). However, a significant negative correlation between NT5C1A and HA (τ = -.485, p = .03) was seen in KPC mice. As this indicated repressive effects of HA on the expression of NT5C1A, we further aimed to investigate the role of stromal components in regulating GME in follow-up *in vitro* and *in vivo* experiments.

3.4 Impact of soluble and solid components of the tumor microenvironment on gemcitabine metabolizing enzymes in tumor cells

The previous analysis showed that OTMs demonstrated less stromal components than KPC mice. In particular, the CAF marker podoplanin was significantly reduced in orthotopic tumors compared to endogenous KPC tumors. This is interesting since PSCs are able to both directly and indirectly interact with tumor cells through paracrine secretion of soluble factors, e. g. CXCL12 and CXCL14 (Bhowmick et al. 2004), thus possibly influencing gene expression. To investigate if soluble factors alter GME expression, human PSCs were incubated

with serumfree medium for 24 hours before the supernatant was transferred on human tumor cell lines L3.6 and MIA PaCa. After incubation for 48 hours, RNA was isolated and mRNA expression was analyzed performing qRT-PCR (Figure 12A).

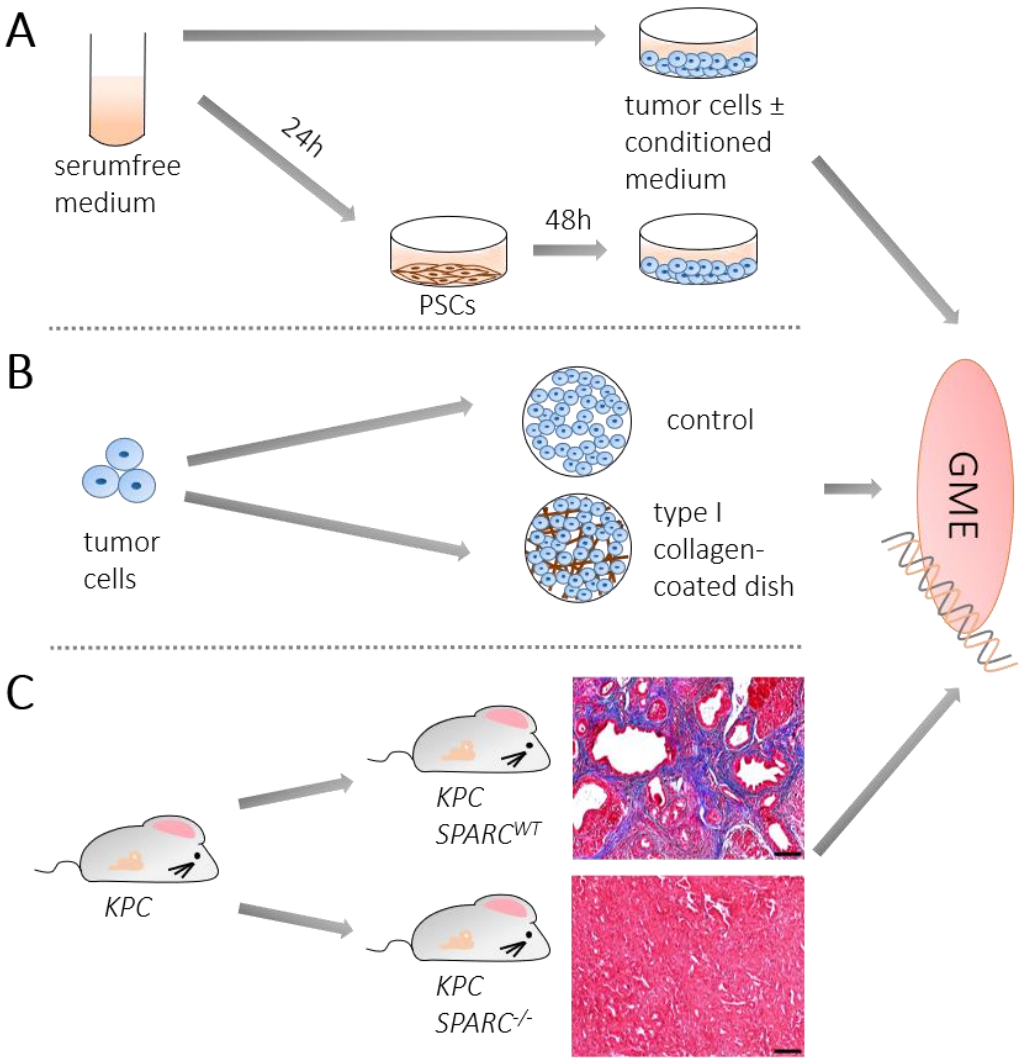

Figure 12: Work flow of *in vitro* and *in vivo* experiments to investigate the influence of soluble and solid (type I collagen) factors on GME expression. Work flow of (A) PSC-CM and (B) type I collagen-coated dish, experiments of human and murine tumor cell lines. (C) The KPC mouse model can be further crossed with SPARC$^{-/-}$ mice to receive KPC SPARC$^{-/-}$. Scale bars indicate 100 µm. *[GME = gemcitabine metabolizing enzymes; (KPC = LSL-Kras$^{G12D/+}$; LSL-Trp53$^{R172\ H/+}$; Pdx-1-Cre); PSC-CM = pancreatic stellate cell-conditioned medium; SPARC = secreted protein acidic and rich in cysteine]*

Though KPC mice and OTMs did not reveal a significant difference in GME expression, *in vitro* and *in vivo* approaches were used to investigate the role of type I collagen in GME expression. Notably, type I collagen is not only considered to mediate a high intratumoural pressure within the tumor mass, but also to increase proliferation and reduce apoptosis of tumor cells (Armstrong 2004; Egeblad et al. 2010; Chauhan et al. 2013).

To further investigate the role of type I collagen and GME expression, the orthotopically transplanted murine tumor cell line TB32047 and human tumor cell lines BXPC3, L3.6, MIA PaCa and Panc-1 were grown on type I collagen or tissue-coated plastic (TCP) for 24 hours and 48 hours, respectively. Afterwards, cells were harvested and the RNA isolated for further analysis (Figure 12B).

Furthermore, an additional *in vivo* approach was used to assess the role of type I collagen. Previously, our group introduced an advanced KPC mouse model which exhibits a deletion of the SPARC protein (Ramu et al. 2019). Resulting KPC SPARC$^{-/-}$ mice demonstrate a reduced amounts of mature type I collagen within the tumor mass that is characterized by less organized and dense collagen fibers (Figure 12C).

3.4.1 Conditioned medium of PSCs does not affect expression of GME in human tumor cells *in vitro*

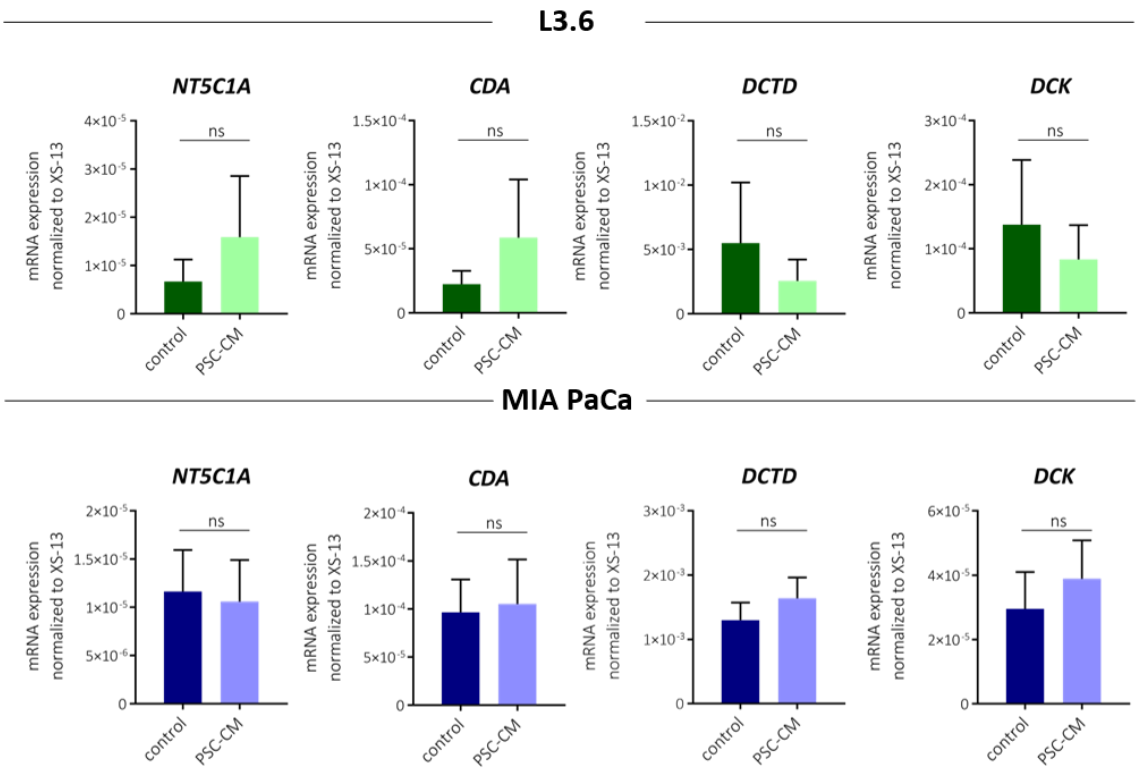

Figure 13: Conditioned medium of human PSC cells does not affect expression of GME in human tumor cells. Human tumor cell lines L3.6 and MIA PaCa were incubated with PSC-CM for 48 hours. Afterwards, RNA was isolated and qRT-PCR (± SD) was performed. P-value was calculated with unpaired student-test; * $p < 0.05$, ** $p < 0.01$, *** $p < 0.001$. *(CDA = cytidine deaminase; DCK = deoxycytidine kinase; ns = not significant; DCTD = deoxycytidylate deaminase; NT5C1A = 5'-nucleotidase, cytosolic 1a; PSC-CM = pancreatic stellate cell conditioned medium)*

To investigate the role of PSC secreted factors on GME expression at the mRNA level, experiments with PSC-CM, as described before, were performed. To this end, I analysed the

expression of four different enzymes. In particular, NT5C1A, CDA and DCTD are gemcitabine inactivating enzymes while DCK is the rate limiting step of gemcitabine activation (Mini et al. 2006). Despite some varibality between the two human PDAC cell lines, no significant changes were found upon incubation with PSC-CM. (Figure 13). Therefore, PSC-CM plays no prominent role in regulation of GME expression.

3.4.2 Type I collagen does not affect expression of GME in murine and human tumor cell lines

Next, we investigated the influence of type I collagen on expression of GME. TCP dishes were coated with type I collagen on which tumor cells can be grown. For each cell line, cells were seeded onto two 6-well-plates, one coated with type I collagen and one control plate (TCP). Three wells were harvested after 24 hours and 48 hours per plate, respectively (Figure 14).

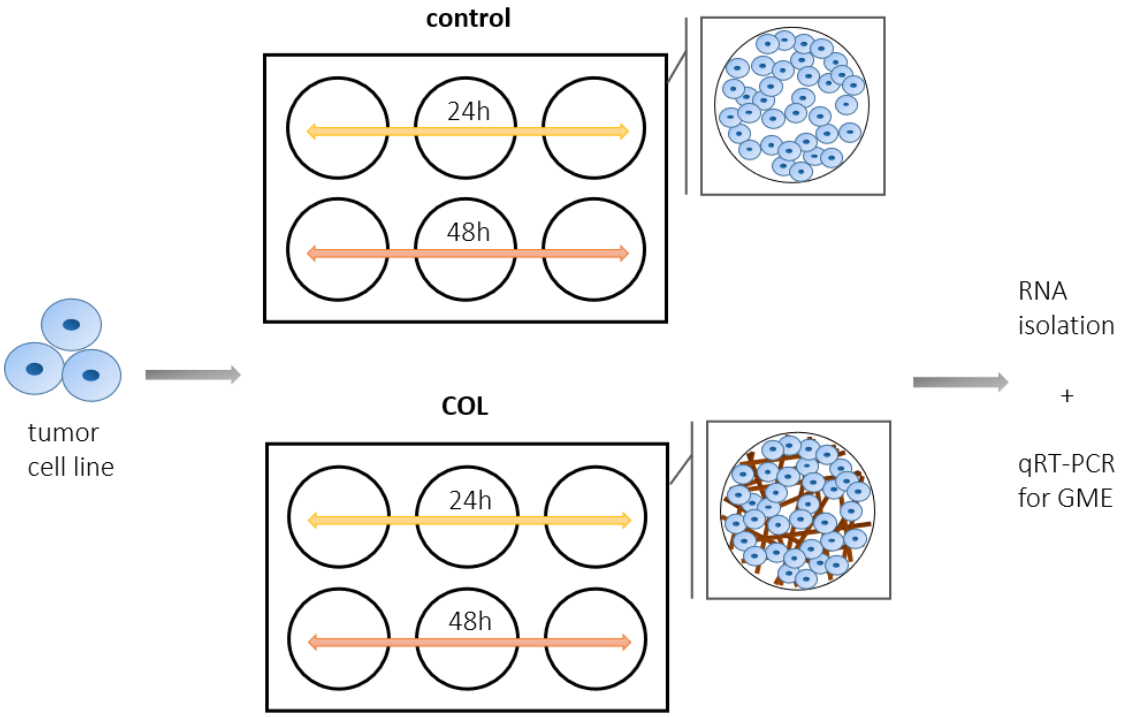

Figure 14: Experimental design of cell lines cultured on control and type I collagen-coated plates. Tumor cells were seeded onto control (TCP) and COL (collagen) plates, respectively. Three wells of each plate were harvested after 24 hours and 48 hours, respectively. RNA was isolated, subsequently, qRT-PCR was conducted. *(COL = collagen; GME = gemcitabine metabolizing enzymes; TCP = tissue-coated plastic)*

After 24 hours of incubation on type I collagen and TCP, the KPC TB 32047, BXPC3, MIA PaCa and Panc-1 cell lines demonstrated differences in cell morphology. Cells grown on type I collagen showed a flatter and more stretched shape while control cells tended to show a rather round and condensed morphology (Figure 15).

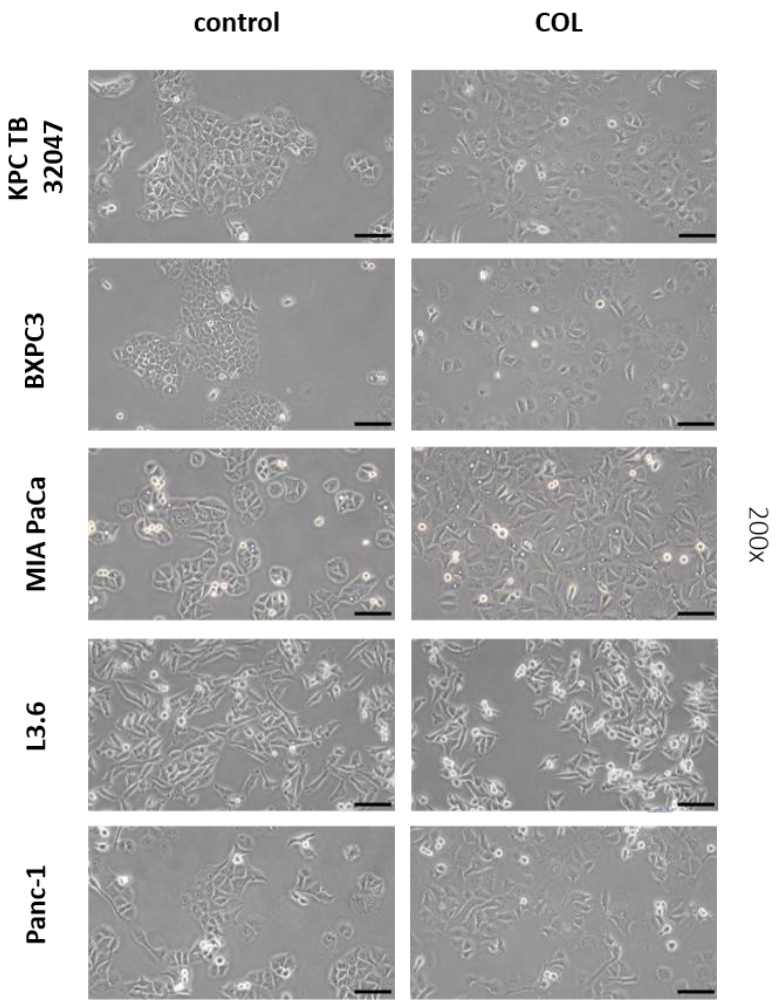

Figure 15: Effect of type I collagen on cell morphology of tumor cell lines. Exemplary pictures of cell morphology after incubation on control (TCP) and COL for 24 hours, respectively. Scale bars indicate 50 µm. *(COL = collagen)*

To investigate whether gene expression of certain enzymes involved in gemcitabine metabolism change when tumor cells are cultured on type I collagen, qRT-PCR was peformed. For one, gene expression levels of DCK, NT5C1A, DCTD and CDA were analysed. Additionally, ENT1 and 2 involved in cellular uptake of gemcitabine were inspected. Moreover, RR catalytic subunits M1 and M2 (RRM1/2), which are important in activating cytidine nucleotides and inhibited through dFdCDP, were included (Figure 16).

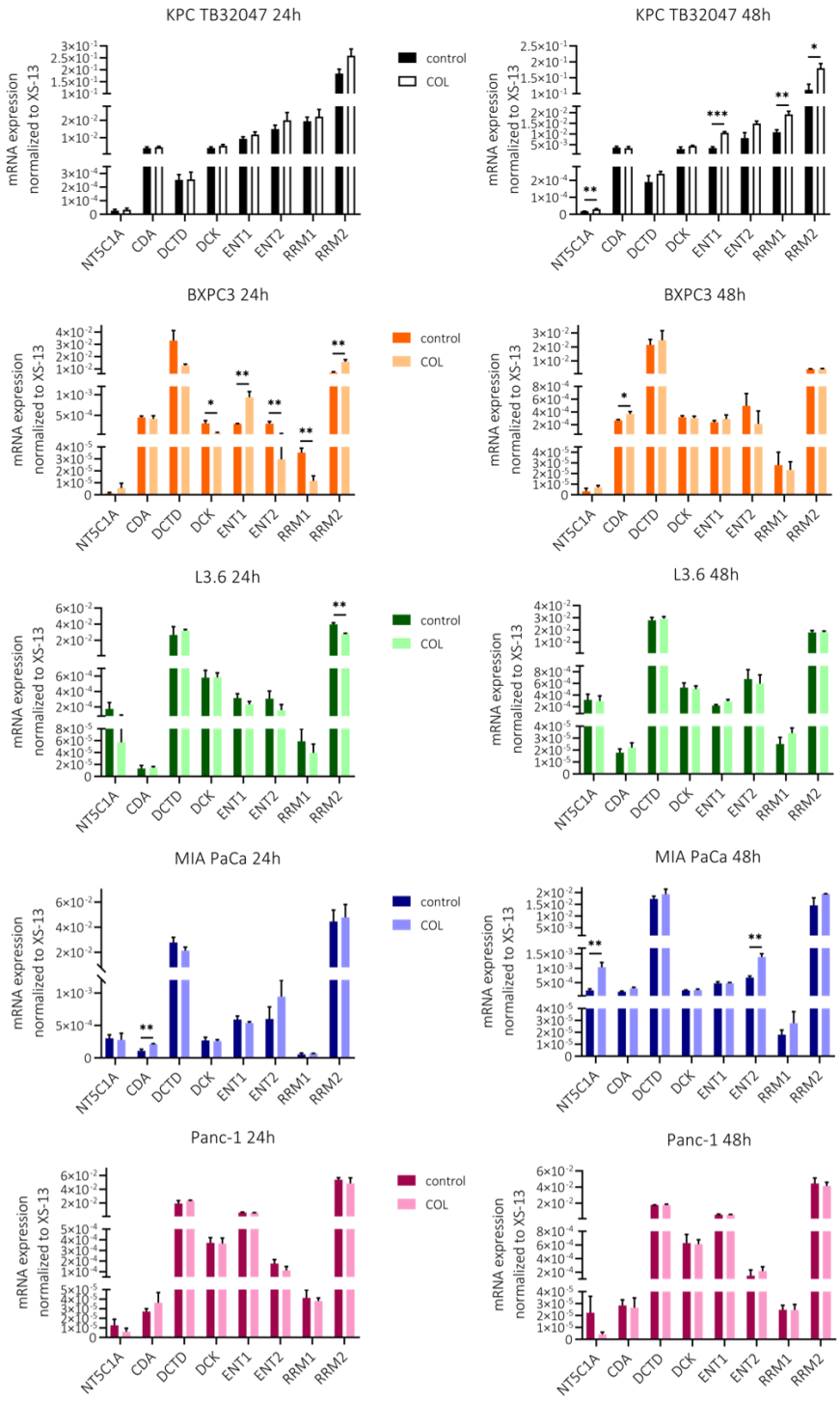

Figure 16: Effect of type I collagen on GME gene expression of tumor cell lines. Murine tumor cell line and human tumor cell lines were cultured on type I collagen for 24 hours and 48 hours, respectively. Gene expression of various GME (± SD) was analyzed by performing qRT-PCR. Subsequently, gene expression was normalized to control. P-value was calculated using unpaired student t-test and Bonferroni correction; * $p < 0.05$, ** $p < 0.01$, *** $p < 0.001$. *(COL = collagen; GME = gemcitabine metabolizing enzymes; CDA = cytidine deaminase; DCK = deoxycytidine kinase; ns = not significant; DCTD = deoxycytidylate deaminase; ENT1/2 = equilibrative nucleoside transporter 1/2; NT5C1A = 5'-nucleotidase, cytosolic 1a; RRM1/2 = ribonucleotide reductase catalytic subunit M1/2)*

Though certain tumor cell lines demonstrated an upregulation of genes when being cultured on type I collagen, this trend could not be observed for all tumor cell lines and all genes investigated (Figure 16). For instance, KPC TB32047 showed an upregulation of NT5C1A, however, L3.6 and Panc-1 showed a downregulation, and only minor changes can be seen in MIA PaCa and BXPC3 tumor cells. Overall, the influence of type I collagen on mRNA expression was not consistent between different cell lines and genes coding for GME.

3.4.3 Depletion of SPARC does not affect expression of GME *in vivo*

Next, we investigated the influence of type I collagen in an *in vivo* model by using archived murine tissue from the Neesse group (Figure 12C). In particular, SPARC is a matricellular protein in fibroblasts and a marker for activated tumor stroma in pancreatic cancer (Sato et al. 2003; Moffitt et al. 2015). Prior to this work, the KPC mouse model was further crossed with a mouse harboring a germline knock-out for SPARC resulting in a novel KPC $SPARC^{-/-}$ mouse model with reduced deposits of mature collagen I compared to KPC $SPARC^{WT}$ mice as established by Ramu et al. in 2019.

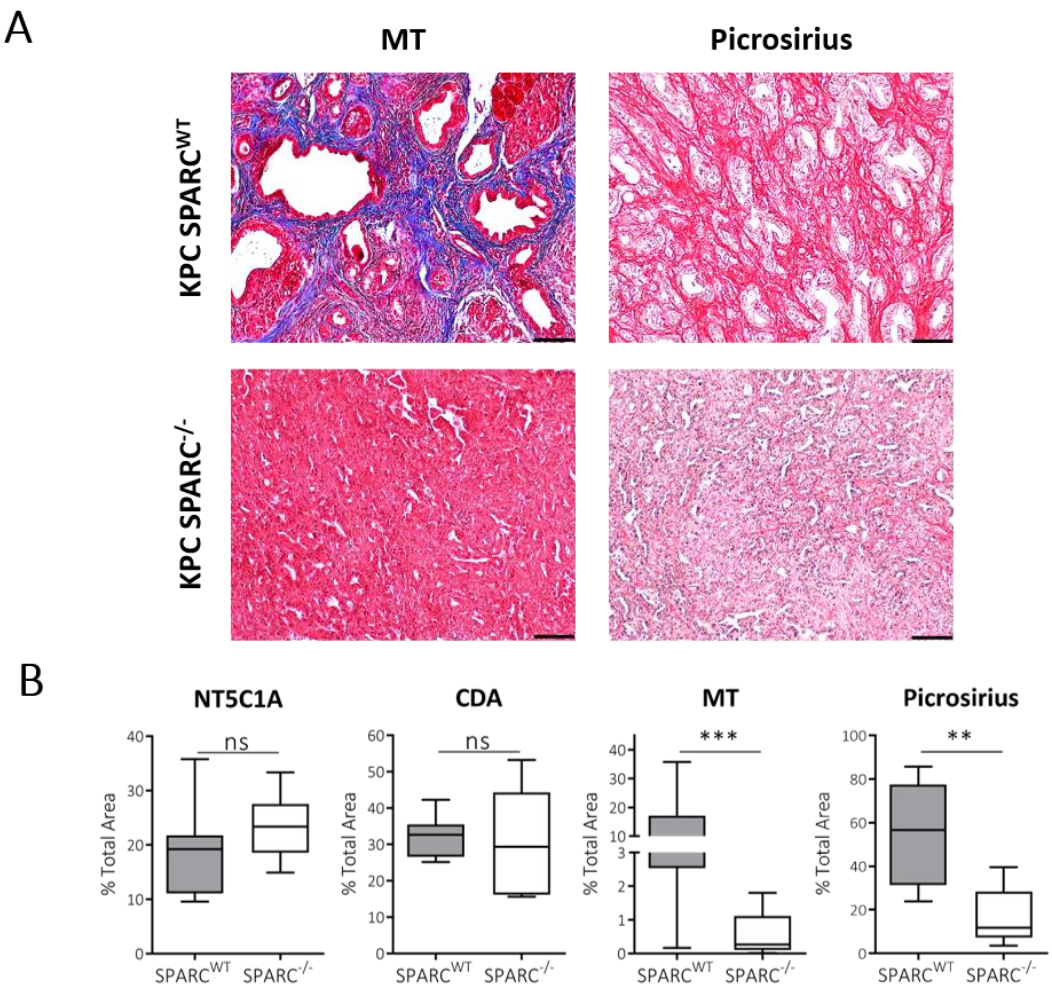

Figure 17: SPARC-knockout promotes the depletion of type I collagen in the KPC mouse model. (A) Representative stainings of stromal components in KPC SPARC^{WT} and KPC SPARC$^{-/-}$ mice. Scale bars indicate 100 µm. (B) Expression of GME and stromal components (± SD) in KPC SPARC^{WT} (n = 7) and KPC SPARC$^{-/-}$ (n = 7) mice [NT5C1A (ns), CDA (ns), MT (*** p) and picrosirius (** p)]. P-value was calculated using Mann-Whitney test; * $p < 0.05$, ** $p < 0.01$, *** $p < 0.001$. *(CDA = cytidine deaminase; GME = gemcitabine metabolizing enzymes; (KPC = LSL-Kras$^{G12D/+}$; LSL-Trp53$^{R172\ H/+}$; Pdx-1-Cre); ns = not significant; NT5C1A = 5'-nucleotidase, cytosolic 1a; MT = Masson's trichrome)*

First, picrosirius and Masson's trichrome stainings and subsequent quantification in KPC SPARC^{WT} and KPC SPARC$^{-/-}$ confirmed prior observations of type I collagen depletion [MT (*** p), picrosirus (** p)]. However, there were no significant changes in expression levels of NT5C1A and CDA when comparing the two cohorts (Figure 17).

4 Discussion

Today, patients diagnosed with pancreatic cancer face a dismal prognosis (Siegel et al. 2019). Therefore, both preclinical and clinical research focus on early tumor detection and novel targets for effective treatment strategies. In this context, the field of pharmacogenetics has evolved significantly in recent years and marks a crucial contribution to personalized therapy (Wong et al. 2009; Relling and Evans 2015).

Gemcitabine has been used for decades in treating PDAC. However, it was found not to be as effective in patients as in preclinical studies (Burris et al. 1997). This can be due to several factors. First, the heterogeneity of enzyme expression in patients might be responsible for the overall little benefit of gemcitabine (Patzak et al. 2019), thus calling for a more tailored therapy based on specific expression patterns of activating and inactivating enzymes of gemcitabine. In addition to the heterogeneous expression of GME between patients, it has been found that high expression of NT5C1A in tumor cells in patients is significantly reduced in 2D cultures (Patzak et al. 2019). This highlights the need for other cell culture options or *in vivo* models to re-evaluate the effects of gemcitabine treatment. In this manner, stromal components which are completely absent *in vitro* and variably expressed *in vivo* dependent on the respective model might be crucial for gemcitabine efficacy. Morever, as pancreatic cancer exhibits an abundant desmoplastic reaction that has often been linked to chemoresistance, this work focuses on potential factors within the TME that might play an important role in the regulation GME expression, and possible differences among different experimental model systems.

4.1 GME in pancreatic cancer

In our study, we observed heterogeneous GME protein expression in different pancreatic cancer model systems. The rate-limiting step of gemcitabine activation is the phosphorylation step of dFdC to dFdCMP, catalyzed by DCK (Mini et al. 2006). Previous studies showed that higher levels of DCK led to longer OS of patients due to an increased activation of the prodrug, thus causing higher apoptosis rate in tumors (Bergman et al. 1999; Pan et al. 2008). Moreover, elevated levels of the gemcitabine inactivating enzyme CDA were linked to shorter PFS and OS of patients, respectively (Bengala et al. 2005). In line with this, it has been recently published that another gemcitabine inactivating enzyme, NT5C1A, is highly expressed in a significant number of PDAC patients, and that overexpression leads to gemcitabine resistance and reduced OS (Patzak et al. 2019). However, the mechanisms underlying the differences in gene expression and heterogeneity in patients are still unknown.

4.2 KPC mice and OTMs differ in stromal composition and GME expression

Our study demonstrates that the transgenic KPC mouse model exhibits a higher expression of GME and stromal components than the corresponding OTMs which were generated from KPC cells orthotopically transplanted into the tail of the pancreas of B6 mice.

In general, GEMMs like KPC mice recapitulate the nature of human PDAC the closest and are currently considered to be the most appropriate preclinical model (Sharpless and DePinho 2006). Importantly, KPC tumors are mostly resistant to gemcitabine treatment, a scenario that is often encounterd in PDAC patients (Neesse et al. 2013; Neesse et al. 2015; Neesse et al. 2019). However, KPC colonies are expensive due to lengthy breeding, genotyping and maintenance costs.

Therefore, a more feasible and cost-effective *in vivo* approach might be a promising alternative. In particular, mouse models can be established in many ways, e. g. by injecting murine tumor cells into the pancreas of mice from the same genetic background, or subcutaneously transplanting human tumor tissue into the flanks of nude mice, generating OTMs or PDX mice, respectively (Jiang et al. 2014; Dorado et al. 2018). In addition, it is also possible to transplant several cell lines or cell types (e. g. tumor cells and fibroblasts) simultaneously to investigate the cross-talk between them (Bachem et al. 2005). In contrast to KPC mice, the success rate of establishing OTMs is nearly 100 %, allowing for reliable planning of experiments (Jiang et al. 2014). Notably, most OTMs harboring pancreatic tumors primarily respond to gemcitabine therapy, although the response can considerably vary depending on the transplanted cell line. Therefore, there is currently no consensus on whether the KPC or OTM model is better suited for preclinical drug testing.

In our study, we observed that OTMs revealed a reduced expression of both GME and stromal components compared to KPC mice. Notably, alterations of the stromal architecture with less abundant stromal compartments and reduced distance between blood vessels were also been described by other studies (Boj et al. 2015). However, expression of GME was never systematically assessed in KPC mice and OTMs before. In conclusion, these findings provide a rationale for the observed treatment differences where OTMs generally show a better response to gemcitabine monotherapy.

4.3 PDX mice differ in stromal composition but not GME expression compared to hPRT

We observed that the PDX model does not significantly differ in enzyme expression from corresponding hPRT, although the deposition of stromal components was reduced. Therefore, the PDX model could be of further interest in preclinical drug testing. It harbors several advantages. The generation of PDX mice is more feasible and less difficult compared to KPC mice and OTMs (Jiang et al. 2014). Studies showed that tumors are stable in chemotherapy

response after several generations of passaging (Rubio-Viqueira et al. 2006). Moreover, tumor histology and proliferation are stable along passaging several generations (Dorado et al. 2018). Nevertheless, generation of PDX models is only effective in approximately 60-70 %, and generation from tissue pieces after neoadjuvant treatment of patients is less effective (Thomas et al. 2015; Dorado et al. 2018). In addition to that, the clinical research group (KFO, *deutsch Klinische Forschungsgruppe*) 5002 project which is involved in PDX generation in our clinic also made the observation that tumors exhibit different growth rates prior to re-transplantation, or that tumors undergo growth arrest. Considering the late diagnosis and high aggressiveness of PDAC, it is challenging but not impossible to employ PDX mice for tailored drug testing in the same patient (Tsai et al. 2018). Moreover, as human tissue is transplanted in a murine recipient, human cells from the TME (e. g. fibroblasts, endothelial cells, immune cells) are progressively replaced by murine cells (Kelland 2004; Dorado et al. 2018). Through this, the physiological interaction between the TME and tumor cells is progressively lost which might influence a potential drug response (Sharpless and DePinho 2006).

In this study, OTMs and PDX mice demonstrated a reduced stromal compartment compared to KPC mice and hPRT. Additionally, we showed for the first time that the PDX model accurately displays expression of enzymes involved in gemcitabine metabolism while expression of such enzymes is reduced in OTMs. In line with these findings, we did not find a change of GME expression in multiple *in vitro* and *in vivo* approaches. This indicates that expression levels of GME may not be associated with single stromal components but rather independently contribute to chemoresistance in murine and human PDAC. However, the complete absence of microenvironmental factors in 2D-cultured cells may still affect expression of GME, as previously shown for NT5C1A (Patzak et al. 2019).

To conclude, we found that PDX mice accurately recapitulate expression of GME compared to hPRT, thus providing a useful platform to study gemcitabine metabolism and treatment response in this model. However, as the tumor stroma is progressively altered in PDX tumors compared to desmoplastic human tumors, it will be challenging to study cross-talks between GME and components of the tumor stroma in these mice.

4.4 Alternative mechanisms and models of chemoresistance

In this work, we demonstrated that PDX mice exhibited stable expression of GME although stromal components were significantly reduced compared to the corresponding human PDAC tissue. Besides GME and stromal mechanisms of therapy resistance, epigenetic mechanisms might regulate GME expression, hence possibly favoring chemoresistance in pancreatic cancer. For instance, bromodomain and extra-terminal motif (BET) proteins have been implicated in gemcitabine resistance in pancreatic cancer by regulating gene transcription and therapeutic resistance (Mazur et al. 2015), therefore inhibition might be a promising novel therapeutic approach in subgroups of patients. However, investigating a subgroup of patients

emphasizes the limitation of large phase III trials (Qin et al. 2019). It would be more suitable to perform so called basket trials in which patients are subjected to tailored treatment strategies based on certain transcriptional or genetic characteristics (McNeil 2015). Interestingly, basket trials offer the opportunity to include patients with the same genetic mutations but different cancer entities and to evaluate whether targeting of novel genomic features is actually efficient clinically (Qin et al. 2019). Exemplarily, a study investigated tumors harboring the germline mutation breast cancer gene 1 and 2 (BRCA1/2) in different tumor entities including breast, ovarian, pancreatic and prostate cancer. It was shown that an overall response to the poly (adenosine diphosphate-ribose) polymerase (PARP) inhibitor olaparib was present in all tumor entities (Kaufman et al. 2015). Therefore, basket trials can be an important first trial method to validate efficacy of preclinically hypothesized targeted therapies.

Further studies then exclusively focused on the role of DNA-damage repair genes (including BRCA) in PDAC. In general, a small percentage of PDAC patients (about 5 %) harbor germline mutations of BRCA1/2 (Sugarman et al. 2019). It was shown that these patients treated with a platinum-based therapy revealed a significantly longer PFS than patients who received a non-platinum-based-therapy (12.6 months vs. 4.4 months) (Park et al. 2020). In addition, the Polo trial provided first evidence that PDAC patients with BRCA mutations that responded to platinum-based chemotherapies could be successfully maintained with olaparib (Golan et al. 2019). These results highlight the importance of basket and subsequent clinical trials in further evaluation of targeted therapies.

Besides *in vivo* approaches, *in vitro* organoid models are a rapidly emerging concept in preclinical research. Intriguingly, multiple drugs demonstrated increased chemoresistance in 3D culture although prior testing in 2D culture predicted sensitivity (Lee et al. 2013). Accordingly, human and murine pancreatic tumor cells cultured in 3D showed an increased resistance to drugs compared to 2D-cultured control cells including gemcitabine (Hou et al. 2018). Interestingly, a recent study investigated if patient-derived organoid cultures can predict chemotherapeutic response in patients (Tiriac et al. 2018). Five out of six organoid cultures showed similar responses towards chemotherapeutics, and the corresponding patients showed a prolonged PFS of 332 days compared to expected 180 days (Tiriac et al. 2018). Moreover, longitudinal testing of one patient identified an amplification of the *KRAS* allele during disease progression which was accompanied by acquired resistance to gemcitabine and two other chemotherapeutics (Tiriac et al. 2018). Intriguingly, the exact mechanism of chemoresistance was not further elucidated, and it is unknown whether dysregulated GME may have played a role. Even though longitudinal assessment of drug resistance in organoids is associated with high financial costs, transcriptional alterations likely contribute to chemotherapeutic responsiveness.

Considerung the increasing incidence and mortality of pancreatic cancer, it is undoubtly clear that novel therapies and model systems are urgently needed to bridge the gap between bench

and bed. Organoids certainly constitute a promising and powerful new approach that may pave the way for rapid and faithful drug testing allowing the implementation of personalized treatment strategies for PDAC patients. Therefore, GME expression should be investigated in cancer cells which are cultured in 3D culture.

4.5 The tumor microenvironment and its diverse functions in PDAC

The interaction of tumor cells with the sorrounding TME has an profound impact on tumor progression and aggressiveness (Sugarman et al. 2019). Since PDAC demonstrates an abundant desmoplastic reaction, it is crucial to investigate the TME in detail (Neesse et al. 2011). In recent years, multiple studies revealed a complex architecture of the tumor stroma and multiple interactions among the various components within the TME and cancer cells (Öhlund et al. 2017; Elyada et al. 2019).

4.5.1 Subtyping cancer-associated fibroblasts

The TME in pancreatic cancer exhibits cancer-associated fibroblasts, commonly referred to as CAFs. Interestingly, earlier studies indicate both tumor-promoting and tumor-suppressing functions (Özdemir et al. 2014; Rhim et al. 2014; Neesse et al. 2019). Although all CAFs express the novel marker podoplanin (Elyada et al. 2019; Quintanilla et al. 2019), researchers identified an immense heterogeneity of CAFs which differ in expression of other molecular markers depending upon location and pathway (Neuzillet et al. 2019).

In particular, CAFs closely located to tumor cells were categorized as myoepithelial CAFs (myCAFs) showing high expressions of α-smooth muscle actin (α-SMA) and transforming growth factor-β (TGF-β) (Öhlund et al. 2017). The counterpart was found more distantly and classified as inflammatory CAFs (iCAFs). iCAFs are characterized by secretion of pro-inflammatory cytokines such as interleukin (IL)-6 and IL-11 (Öhlund et al. 2017). Previous studies suggested a tumor-promoting and pro-inflammatory effect of fibroblasts when cultured distant to tumor cells and decreased TGF-β levels (Flaberg et al. 2011; Laklai et al. 2016), therefore, myCAFs might represent tumor-restraining properties while iCAFs tend to show pro-tumorigenic functions (Hessmann et al. 2020). Besides myCAFs and iCAFs, further studies identified antigen-presenting CAFs (apCAFs) showing certain similarities to antigen-presenting cells (APCs) by presenting MHC class-II related antigenes, e. g. cluster of differentiation (CD) 74 (Elyada et al. 2019). Although the exact function of apCAFs in pancreatic cancer remains to be investigated, it is hypothesized that they present tumor antigens yet without a costimulatory signal to $CD4^+$ T cells, thus leading to a state of anergy or differentiation status of regulatory T cells (T_{Reg}s) (Elyada et al. 2019). Consequently, proliferation of T cells is inhibited, marking a potential pathway of immune escape (Elyada et al. 2019).

In addition, CAFs demonstrate a high plasticity through different features. First, besides the development from endothelial cells and MDSCs (Garcia et al. 2012; Öhlund et al. 2014),

PSCs are the main source of CAFs which have been shown to have the ability to transdifferentiate in either myCAFs or iCAFs depending on the location within the tumor (Apte et al. 2004; Öhlund et al. 2017). Secondly, plasticity is promoted through different factors including IL-1 supporting the iCAF subtype, while TGF-β presence suppresses IL-1 receptors on CAFs, subsequently favoring the subtype of myCAFs (Biffi et al. 2019). Thirdly, differenct cell culture methods promote distinct CAF subtypes. Specifically, both iCAFs and apCAFs lose their distinct expression of molecular markers and instead exhibit features of myCAFs when cultured in 2D while the iCAF subtype is preserved exclusively in 3D (Öhlund et al. 2017; Elyada et al. 2019). In other words, early studies which included cultivation of CAFs *in vitro* preferably investigated a mostly homogenous myCAF population and did not present the full spectrum of CAF heterogeneity present in pancreatic cancer (Hessmann et al. 2020).

Evidence indicates that the term CAF describes a heterogenous cell type with both promoting and restraining functions along with a high plasticity in pancreatic cancer. Podoplanin is a pan-CAF marker and captures various CAF subtypes (Quintanilla et al. 2019). In our study, we solely quantified the presence of CAFs by IHC staining of podoplanin in tumor bulk tissue and did not additionally investigate the distribution between subtypes. Therefore, we cannot conclude whether certain CAF subtypes might influence GME expression. As a consequence, the question whether the examined *in vivo* models recapitulate the CAF population similar to patients (Elyada et al. 2019) was not thematisized in this work and remains to be answered. This is important since changes in distribution of CAF subtypes might result in shifts of tumor biology, e. g. invasiveness, caused by oppossing functions of CAFs. One can postulate that OTMs largely exhibit iCAFs and apCAFs leading to a more undifferentiated tumor histology, higher aggressiveness and an increased metastatic rate while immunodefient PDX mice mostly harbor myCAFs resulting in rather slowly growing, well-differentiated tumors.

Future efforts may aim at reprograming iCAFs and apCAFs into myCAFs or even quiescent PSCs, thus changing tumor biology (Hessmann et al. 2020). Murine data from the Tuveson group showed that the vitamin D receptor (VDR) is expressed in CAFs of pancreatic tumors and that treatment with calcipotriol, a synthetic VDR ligand, significantly ablated tumor stroma and inflammation (Sherman et al. 2014). The authors provided evidence that VDR controls the transcriptional regulation of CAFs and supports the quiescent state and that treatment with calcipotriol improved therapeutic response to gemcitabine and resulted in smaller and less desmoplastic pancreatic mouse tumors (Sherman et al. 2014). In this context, another interesting study using the plant-derived compound minnelide demonstrated a reduction of ECM components, e. g. HA and collagen, in KPC and PDX mice upon treatment (Banerjee et al. 2016). A follow-up study showed that treatment with minnelide favors the transition from an activated to an quiescent state of CAFs, accompanied by downregulaton of α-SMA expression and TGF-β signaling, and reduced proliferation of tumor cells (Dauer et al. 2018). Since CAFs were cultured in 2D in this study, the CAF population possibly consisted of mostly myCAFs. Intriguingly, it is indicated that myCAFs might not be solely

tumor-suppressive, but exhibit also tumor-promoting features. Therefore, targeting of particular pathways in CAFs (e. g. TGF-β signaling) might be far more promising than broad depletion of all CAFs which led to reduced OS in mice as demonstrated in earlier studies (Özdemir et al. 2014). Nonetheless, the question of whether minnelide demonstrates an overall benefit in treatment of pancreatic cancer is currently being investigated in an ongoing phase II clinical trial (NCT03117920). The study specifically aims to examine if minnelide treatment attenuates tumor growth of treatment-refractory pancreatic cancers.

Moreover, it is also unknown whether CAF subtypes show the same behavior both in humans and mice and if replacement of human stroma with murine stroma is associated with changes in subtype function in PDX mice. Furthermore, incubation with PSC-CM in our study did not change GME expression in different tumor cell lines. However, the PSCs that were used in our study were immortalized and were not cocultured with pancreatic cancer cells. Therefore, our PSCs cannot be considered as true CAFs and might likely have a distinct secretome from CAFs. These findings are in line with other studies which showed that the different molecular subtypes of PDAC are characterized by upregulations of certain signaling pathways and that stromal cells themselves exhibit a distinct pathway pattern which support tumor cell biology in turn (Bailey et al. 2016; Nicolle et al. 2017). Therefore, stromal cells might be primed by tumor cells to synergistically promote tumorigenesis (Nicolle et al. 2017). As a consequence, coculture of tumor cells and PSCs may stimulate a different secretome with a distinct CM composition, subsequently leading to a different effect on GME expression than observed in our experiments. In addition, we did not address interactions between cellular and acellular components of the TME in our study. Crucially, this might also influence tumor behavior. Exemplarily, CAFs secrete different ECM components including HA and collagen and that transition to a quiescent state induced by minnelide results in a downregulation of ECM components and increased drug delivery (Banerjee et al. 2016). Taken together, future experiments need to focus intensively on the heterogeneity of CAFs along with choosing the appropriate cell culture method for each subtype (e. g. 3D organoids for iCAFs) to recapitulate the opposing functions of CAFs in pancreatic cancer as faithfully as possible.

4.5.2 Acellular components impair drug delivery and have tumor suppressive and pro-tumorigenic functions in pancreatic cancer

As previously mentioned, Olive et al. demonstrated that, by inhibiting interactions between tumor cells and CAFs, a higher vascularization and drug delivery was achieved. Importantly, the authors targeted the hedgehog (Hh) pathway which is essential for collagen synthesis (Olive et al. 2009). Indeed, acellular components like collagen and HA contribute to a high intratumoural pressure which results in impaired drug delivery (Provenzano et al. 2012; Chauhan et al. 2013; Jacobetz et al. 2013). Therefore, the importance of the ECM within the TME was highlighted. In fact, studies showed that only small micelles had a sufficient anti-

tumoral effect in characteristically desmoplastic pancreatic cancer and that higher accumulation of drugs can be achieved by decompression of blood vessels (Cabral et al. 2011; Stylianopoulos and Jain 2013). In contrary to these promising preclinical findings, clinical trials failed to show an advantage of the Hh-inhitor vismodegib in combination with gemcitabine compared to gemcitabine monotherapy and even had to be stopped early because of shortened survival of patients (Kim et al. 2014; Catenacci et al. 2015). Subsequent preclinical studies demonstrated that Hh-knockout tumors showed undifferentiated tumor pathology along with increased proliferation of tumor cells and reduced survival (Rhim et al. 2014), highlighting anti-tumorigenic properties of collagen. Likewise, clinical trials targeting HA through a combination of a hyaluronidase and gemcitabine failed to show an advantage over gemcitabine monotherapy after preclinical success (Jacobetz et al. 2013; Van Cutsem et al. 2020). However, there is still no general agreement on whether collagen and HA promote tumor progression or have restraining properties in pancreatic cancer (Xu et al. 2019). Therefore, the development of drugs which are e. g. optimized in size and accumulative rate might be a more promising approach to target stroma-rich tumors than direct modification of stroma, which is the main goal of nanomedicine (de Souza et al. 2015; Adiseshaiah et al. 2016). Nanomedicine allows the modification of drug-delivering vectors which need to be adjusted to different cancer types. Exemplarily, the application of gemcitabine packed in liposomes led to higher apoptosis rate than free gemcitabine in tumor cells *in vitro* (Lin et al. 2019), thus capsuled treatment may be superior in treatment efficacy highlighting an advantage of nanomedice over chemotherapy currently applied.

In our study, we observed that tumor cells cultured on type I collagen showed a more stretched and spindle-shaped morphology compared to control cells. Nevertheless, alteration in GME expression was neither demonstrated in *in vitro* nor in *in vivo* experiments. Previous studies showed that type I collagen promotes EMT in colon and pancreatic cancer cells that is paralleled by profound transcriptional changes, e. g. induction of vimentin and zinc finger e-box binding homeobox 1 (ZEB1) expression (Kirkland 2009). Cells undergoing EMT also demonstrate increased chemoresistance in pancreatic cancer (Zhou et al. 2019). Since we observed that type I collagen did not impact GME mRNA expression in tumor cells, chemoresistance might be acquired through alternative mechanisms.

Morever, the TME in pancreatic cancer is hypoxic, subsequently leading to an upregulation of hypoxia-inducible factor 1α (HIF1α) which in turn promotes transcription of the lysyl oxidase (LOX) family (Saatci et al. 2020). Critically, LOX is involved in collagen maturation (Neesse et al. 2019) and promotes gemcitabine resistance by increasing proliferation and reducing apoptosis in tumor cells at the same time (Le Calvé et al. 2016). In addition, gemcitabine concentrations were lower in hypoxic regions of tumors (Fanchon et al. 2020). A recent study demonstrated that a lipid-coated polymer containing gemcitabine and small interfering RNA (siRNA) targeting HIF1α reduced tumor size to a greater content than control drugs which were not capsuled and capsules containing gemcitabine alone (Lin et al. 2019). In comparison to that, a trial with the LOX-inhibitor simtuzumab and gemcitabine did not

show a significant benefit in patients although prior *in vivo* studies were successful (Miller et al. 2015; Benson et al. 2017). The discrepancy between these findings indicates that inhibition of pathways other than LOX-associated signaling pathways, but regulated by HIF1α, are instead responsible for antitumoral effects. These findings demonstrate that nanomedicine offers the opportunity to further potentiate therapeutic efficacy by the simultaneous application of multiple compounds exposing synergistic effects.

In conclusion, these findings spark the question whether gemcitabine itself is not ineffective in patients, but rather the method of how it is applied and transported to the tumor. Thus, further research should investigate a potential role of nanomedicine in treatment strategies. However, even if gemcitabine is applied differently in patients, the question how GME expression is regulated remains because high expression of gemcitabine inactivating enzymes favors a negative outcome for patients.

4.5.3 Infiltrating components of immune- and nervous systems potentiate tumor complexity

In this work, we exclusively concentrated on a limited number of components of the TME. Notably, it was found that the majority of non-epithelial cells (~ 80 %) within the TME are myeloid and lymphoid cells comprised of macrophages and T cells among other cell types, while CAFs mark a fraction of about 2 % (Elyada et al. 2019). Consequently, other cellular components such as immune cells have gained attention in pancreatic cancer research. Furthermore, pancreatic cancer is sourrounded by an abundant neural cell population and the subsequent tumor-neuron interplay results in increased proliferation rates of both populations (Dai et al. 2007; Demir et al. 2021). Moreover, neural invasion of tumor cells is associated with a reduced OS in patients (Demir et al. 2015).

In general, tumor-associated macrophages (TAMs) can be subcategorized into two polarization states M1 and M2, and the latter is predominantly present in both primary and metastatic lesions of the pancreas (Mantovani et al. 2002; Biswas and Mantovani 2010). Intriguingly, infiltration of TAMs was inversely correlated to survival of patients in different tumor entities including pancreatic cancer (Di Caro et al. 2016). Among the involvement in pro-inflammatory processes (Biswas and Mantovani 2010), TAMs also take part in multiple tumor-promoting pathways. For instance, exposure to the anti-inflammatory cytokine IL-35 led to elevated expression of CXCL1 and CXCL8 important in angiogenesis (Huang et al. 2018). In line with this, depletion of TAMs from tumors resulted in impaired angiogenesis and a reduction in metastatic formation (Griesmann et al. 2017). Furthermore, TAMs were shown to support the activity of CDA, thus promoting gemcitabine resistance (Weizman et al. 2014; Buchholz et al. 2020). Our findings of different GME expression levels might be explained by different numbers of TAMs present in *in vivo* models and hPRT.

Besides pro-tumorigenic functions of the innate immunity, tumor cells actively suppress T cells which are the predominant part of the adaptive immune system (Bailey et al. 2016). In

particular, tumor cells demonstrated expression of coinhibitory T cell receptors (TCR) along with programmed cell death protein 1 (PD-1) and programmed death-ligand 1 (PD-L1) which are inversely associated with OS in PDAC (Loos et al. 2008; Shibuya et al. 2014). Likewise, apCAFs also interact with $CD4^+$ T cells, thus marking a dual suppression from both tumor and stroma cells (Elyada et al. 2019). As as consequence, the overall T cell response is reduced (Hessmann et al. 2020). Again, different expression levels of suppressive receptors might be responsible for patients' outcome along with GME expression.

In addition, the field of tumor-neuron interactions has gained more attention. Important studies demonstrated a correlation between hyperinnervation and grades of desmoplasia and stromal activity in PDAC (Demir et al. 2015). Importantly, close location to nerves resulted in increased proliferation rates and OS in tumor cells *in vitro* (Dai et al. 2007). This may pose a problem in our PDX mice and OTMs as we cannot be certain that we transplanted the tumor or injected the tumor cells in close vicinity to neural cells. As a consequence, we might have observed different proliferation rates due to variation between mice. Moreover, as neural invasion of tumor cells differs between GEMMs such as KPC mice and human pancreatic cancer, the establishment of further mouse models accurately displaying the nerve systeme is important (Demir et al. 2015; Hessmann et al. 2020).

It is obvious that the experiments of this work were restricted to certain methods and components of the TME. It could be that only the interplay between several components or even the sum of those TME components attributes to a change in GME.

4.6 Key findings

In this work, we investigated GME expression in several pancreatic cancer model systems including KPC mice, OTMs, hPRTs and PDX mice. Until now, it has not been described that GME protein expression is significantly reduced in OTMs compared to KPC mice. These findings correlate with the generally higher sensitivity of OTMs towards chemotherapy than corresponding KPC mice (Olive et al. 2009). Likewise, the stability of GME expression in PDX mice compared to respected hPRTs has not been observed yet, and the PDX model might be a promising approach for evaluating effective treatment strategies preclinically before being applied to patients. Based on our experiments which included several tumor cell lines of human and murine origin, type I collagen does not impact GME gene and protein expression *in vitro* and *in vivo*.

In conclusion, these results suggest that the tumor stroma and expression of GME are likely independent from each other, yet, simultaneous targeting could have synergistic effects. For example, parallel therapeutic targeting of the ECM to increase drug delivery in combination with targeting of epigenetic regulation mechanisms of GME could sensitize tumors to gemcitabine treatment. Whereas the KPC model is likely the most appropriate model to experimentally probe stromal depletion strategies, PDX mice closely recapitulate the expression GME of corresponding human tumors.

4.7 Research limitations

Overall, we solely described an association between stromal components and GME expression in these pancreatic cancer systems. Whether this data suggests a fundamental causality remains to be investigated, and can only partly be answered for type I collagen in this thesis. Several limitations from the conducted experiments should be mentioned and great care shoud be paid to not overinterpret the experimental data.

4.7.1 Tumor models

One limitation of this work is the quantity of tissue samples used. Analysis included 12 KPC mice, 13 OTMs and 12 pairs of hPRTs and PDX mice, respectively. If a higher amount of tissue samples were included, results may have shown a correlation between stromal components and GME expression.

However, the use of each model is restricted to a certain extent. For one, the breeding of the KPC mouse model requires high financial efforts and time for planning which was also present in the course of this work. In particular, successful breeding itself is not trivial, but dependent on many factors, e. g. availability of mice and rate of gravidity. After birth, samples from newborn mice need to undergo genotyping to investigate whether mice demonstrate the intended genotype, and subsequently, whether these mice develop pancreatic tumors over the course of the next months.

In case of OTMs, the tumor development rate is near to 100 %, allowing the generation of a great quantity of tumor samples. However, this work showed that the tumor architecture of OTMs does not adequately recapitulate the one found in KPC mice. One reason could be the injection of a cell suspension which only consists of tumor cells and not e. g. CAFs or other acellular components of the TME. One improvement of this model could be the simultaneous injection of both tumor cells and stromal components, e. g. CAFs, type I collagen or HA, to investigate the tumor-stromal interplay and possible effects on GME expression. Another reason could be the injection of 2D-cultured cells. Studies which were earlier described showed that gene expression significantly changes when cells are isolated and cultured in 2D (Birgersdotter et al. 2007). A promising compromise might be the establishment of OTMs with 3D-cultured cells. It has been shown that 3D-cultured cells are both more similar in gene expression to origin cells and tend to build a similar architecture (Birgersdotter et al. 2007; Boj et al. 2015). We did attempt establishing organoid cultures, but due to lack of additional time, this experimental approach was not pursued further. Therefore, future experiments should include the establishment of either heterogenous cell suspensions or 3D-cultured tumor cells with the aim to establish a model which might be more adequate for preclinical research experiments.

PDX mice might be a promising approach in the future. Nonetheless, the subsequent replacement with murine stroma along with overall stromal reduction compared to hPRT marks a difficulty in investigating the tumor-stroma crosstalk within these mice. In addition,

both hPRT and PDX mice tissue samples need to be available to allow for comparison of the two. In contrast to the sufficient availability of hPRT tissue, PDX mice tissue sample availability was limited due to relatively small tumors. Even though tumors could be harvested at a later time point allowing the tumors to grow larger, it needs to be considered that a higher tumor burden would impair PDX mice's health and quality of life (e. g. movements) to an unjustifiable extent.

Besides the limitations of tumor models themselves, experimental alterations of the carefully optimized staining protocols must also be taken into account. For instance, type I collagen content was quantified by MT and picrosirius stainings. The analysis between KPC mice and OTMs demonstrated a non-significant difference for MT, but for picrosirius, and the opposite effect was seen for hPRT and PDX mice. Likewise, hPRT exhibited a significant lower expression of podoplanin than corresponding PDX mice. These findings could have been experimentally affected by different binding properties of the AB for human and mouse ECM targets.

4.7.2 TME components and use of cell culture method

Since desmoplasia shows an abundant presence in pancreatic cancer, it possibly contributes to tumorigenesis. Therefore, our aim was to investigate whether single components of the TME had an impact upon GME expression. As our group just began investigating the influence of stromal components upon GME expression, the amount of potential TME components was limited. We worked with immortalized PSCs and CAFs utilizing expertise and resources from our research group. CAFs could have also been isolated as part of these experiments. However, as they represent a cellular fraction of only about 2 % within the TME (Elyada et al. 2019), fresh isolation would have required multiple KPC tumors and pooling by flow cytometry. Both procedures are time-consuming and connected to both high financial and personal efforts. Moreover, CAFs were cultivated in 2D mono cell culture which is probably the most feasible, cost-effective, and least time-consuming cell culture method. Importantly, findings suggest a shift in CAF subtypes dependent on used cell culture methods (Öhlund et al. 2017; Elyada et al. 2019), thus conducted experiments might have favored a certain CAF subtype and subsequent GME expression. As CAFs did not undergo subtyping, this is a simple hypothesis that highlights the importance of CAF subtyping in future experiments. In the same manner, tumor cells were cultivated on a layer of type I collagen in 2D cell culture rather than in a 3D cell culture. As mentioned earlier, if a 3D cell culture had been applied, it could have shown completely different results. Furthermore, *in vitro* experiments did not include simultaneous coculture of multiple TME components such as cellular, acellular components e. g. type I collagen and HA, and tumor cells. However, this could stimulate a different secretome with a distinct CM composition, subsequently leading to a different effect on GME expression than observed in our experiments.

As a consequence, future experiments should include the fresh isolation of CAFs and subsequent characterization into subgroups by molecular markers to investigate the effects of different subtypes on GME expression in tumor cells. Furthermore, more components of the TME which are postulated to effect tumor biology, e. g. macrophages and neural cells, should be included in the studies to display a broader picture *in vitro*. Importantly, rather than using CM, TME components and tumor cells should be cocultured, at best in 3D cell culture.

5 Summary

Pancreatic cancer still exhibits a dismal five-year overall survival rate of 9 % and is foreseen to even increase in incidence and mortality rates in the future. This is due to unspecific symptoms leading to late diagnosis, and a lack of effective screening procedures and treatment strategies. The chemotherapeutic drug gemcitabine is frequently used as a backbone agent in the clinical setting, but has failed to be as effective as in preclinical trials. One reason for this could be the discrepancy in expression of gemcitabine metabolizing enzymes between patients and *in vitro* and *in vivo* models. Moreover, the tumor microenvironment includes different cellular and acellular components of the stroma that have been implicated in chemoresistance. Recently, various *in vivo* models for pancreatic cancer have been established in the preclinical research setting to investigate mechanisms of therapeutic resistance. In particular, the transgenic KPC mouse model, the orthotopically transplanted mouse and the patient-derived xenograft mouse model are of current use.

This work investigated the expression of gemcitabine metabolizing enzymes and stromal components in different pancreatic cancer model systems. This was achieved by immunohistochemistry for stromal components and gemcitabine metabolizing enzymes performed in *in vivo* models and human primary resected tissue. Another aim was to investigate whether single soluble and solid components of the tumor microenvironment had an impact on the expression of gemcitabine metabolizing enzymes in tumor cells *in vitro* and *in vivo*. Hence, conditioned medium experiments, cultivation of tumor cells on type I collagen and evaluation of a KPC mouse model devoid of mature collagen, were performed.

It was shown that gemcitabine metabolizing enzyme expression in KPC mice was significantly higher than in mice orthotopically transplanted with 2D-cultured KPC tumor cells. Notably, orthotopically transplanted tumors revealed reduced amounts of stromal components as compared to endogenous tumors from KPC mice. Moreover, gemcitabine metabolizing enzyme expression levels in patient-derived xenograft mice did not significantly differ from original human primary resected tissue although patient-derived xenograft mice exhibited a significantly lower number of stromal components. In line with the results from the *in vivo* models, subsequent *in vitro* experiments did not reveal a significant effect of fibroblast conditioned medium or type I collagen on gemcitabine metabolizing enzyme expression in human and murine tumor cells. The expression of gemcitabine metabolizing enzymes was not significantly altered in the collagen-depleted KPC mouse model compared to control mice.

In conclusion, this work contributed to a deeper understanding of tumor-stroma crosstalk within pancreatic cancer. Whereas expression of gemcitabine metabolizing enzymes varies between KPC mice and orthotopically transplanted mice, the patient-derived xenograft mouse model displayed comparable levels of gemcitabine metabolizing enzymes despite different amounts of tumor stroma. In conjunction with the obtained *in vitro* experiments, our results suggest that the tumor stroma and gemcitabine metabolizing enzymes are likely two

separate therapeutic targets in pancreatic cancer that could be targeted synergistically, e. g. by depletion of tumor stroma to increase drug delivery, and parallel epigenetic targeting of gemcitabine metabolizing enzymes to sensitize tumors to gemcitabine. Whereas the KPC model is likely the most appropriate model to experimentally probe stromal depletion strategies, patient-derived xenografts closely recapitulate the expression of gemcitabine metabolizing enzymes in corresponding human tumors.

6 Zusammenfassung

Das Pankreaskarzinom geht bis heute mit einer fünf-Jahres-Überlebensrate von 9 % einher. Für die Zukunft ist zudem ein Anstieg der Inzidenzraten und der Mortalität zu erwarten. Zugrundeliegend dafür sind unspezifische klinische Symptome und dadurch bedingte späte Diagnosestellung sowie ein Mangel an Früherkennungsmaßnahmen und effektiven Therapiemaßnahmen. Gemcitabin wird zurzeit als Backbone Chemotherapeutikum bei der Behandlung von vielen Patienten im klinischen Alltag verwendet, zeigt jedoch häufig keine hohe Effektivität im Vergleich zu präklinischen Studien. Ein Grund für die unterschiedliche Chemosensitivität auf Gemcitabin könnte die Diskrepanz in der Expression von Gemcitabin metabolisierenden Enzymen zwischen Patient:innen und *in vitro* und *in vivo* Modellen sein. Desweiteren könnte das ausgeprägte Tumorstroma im Pankreaskarzinom, welches häufig mit Therapieresistenz in Verbindung gebracht wird, die Expression von Gemcitabin metabolisierenden Enzymen regulieren und hierüber die Chemotherapieresistenz regulieren. Zur Untersuchung von Mechanismen der Therapieresistenz wurden vielzählige *in vivo* Tumormodelle für das Pankreaskarzinom in der präklinischen Forschung etabliert. Unter anderem werden das transgene KPC Mausmodell, das orthotope Mausmodell und das aus Patientenmaterial-abgeleitete Xenograftmodell alltäglich angewendet.

In dieser Arbeit wurde die Expression von Gemcitabin metabolisierenden Enzymen in verschiedenen pankreatischen Modelsystemen untersucht. Dafür wurden immunohistochemische Färbungen für verschiedene Komponenten des Tumorstromas und von Gemcitabin metabolisierenden Enzymen in *in vivo* Modellen und humanen Pankreaskarzinomgeweben durchgeführt. Ein weiteres Ziel war es zu untersuchen, ob einzelne lösliche oder feste Komponenten des Tumormikromilieus einen Einfluss auf die Expression von Gemcitabin metabolisierenden Enzymen in Tumorzellen *in vivo* und *in vitro* haben. Dafür wurden Versuche mit konditioniertem Medium von Fibroblasten, Kultivierung von Tumorzellen auf Kollagen Typ I und Immunhistochemie in einem genetisch modifizierten KPC Mausmodell mit reduziertem intratumoralen Kollagengehalt durchgeführt.

Es konnte gezeigt werden, dass die Expression von Gemcitabin metabolisierenden Enzymen in KPC-Mäusen signifikant höher war als in Mäusen, die orthotop mit 2D-kultivierten KPC-Zellen transplantiert wurden. Auffallend war zudem ein verminderter Umfang von stromalen Komponenten im orthotopen Mausmodell im Vergleich zu den Tumoren der KPC-Mäuse. Die Expression der Gemcitabin metabolisierenden Enzyme unterschieden sich zwischen den aus Patientenmaterial-abgeleiteten Xenograftmodellen und humanen Ursprungsgewebe nicht signifikant, auch wenn im Mausmodell eine signifikante Reduktion des stromalen Kompartiments zu beobachten war. Weiterführende Experimente zeigten keinen signifikant positiven oder negativen Effekt von Fibroblasten-konditionierten Medium und Kollagen Typ I auf die Expression von Gemcitabin metabolisierenden Enzymen in humanen und murinen Tumorzellen *in vitro*. Es wurde auch kein Unterschied der Enzymexpression zwischen KPC-

Mäusen mit reduziertem intratumoralen Kollagengehalt und Kontroll-KPC-Mäusen beobachtet.

Zusammenfassend konnte diese Arbeit einen Beitrag zum besseren Verständnis der Interaktion zwischen Tumorzellen und Tumorstroma im Pankreaskarzinom leisten. Während die Expression von Gemcitabin metabolisierenden Enzymen zwischen KPC-Mäusen und orthotop transplantierten Mäusen variiert, zeigte das aus Patientenmaterial-abgeleitete Xenograft-Mausmodell trotz unterschiedlichem Stromagehalt eine vergleichbare Expression von Gemcitabin metabolisierenden Enzymen. In Verbindung mit den *in vitro* Experimenten deuten unsere Ergebnisse darauf hin, dass das Tumorstroma und Gemcitabin metabolisierende Enzyme wahrscheinlich zwei separate therapeutische Ziele des PDAC darstellen, die synergistisch angegangen werden könnten. Beispielsweise könnten eine therapeutische Stromadepletion, um die Anflutung von Chemotherapeutika zu erhöhen, und eine Beeinflussung (z.B. durch epigenetische Ansätze) der Gemcitabin metabolisierenden Enzyme parallel ablaufen, um in der Gesamtheit Tumore für Gemcitabin zu sensibilisieren. Während das KPC-Modell das am besten geeignete Modell ist, um Strategien zur therapeutischen Stromadepletion experimentell zu untersuchen, rekapitulieren die aus Patienmaterial-abgeleiteten Xenograftmodelle die Expression von Gemcitabin metabolisiernden Enzymen von humanen Pankreaskarzinomen am besten *in vivo*.

7 References

Adamska A, Domenichini A, Falasca M (2017): Pancreatic Ductal Adenocarcinoma: Current and Evolving Therapies. Int J Mol Sci 18, 1338

Adiseshaiah PP, Crist RM, Hook SS, McNeil SE (2016): Nanomedicine strategies to overcome the pathophysiological barriers of pancreatic cancer. Nat Rev Clin Oncol 13, 750–765

Akram M, Iqbal M, Daniyal M, Khan AU (2017): Awareness and current knowledge of breast cancer. Biol Res 50, 33-133

Almoguera C, Shibata D, Forrester K, Martin J, Arnheim N, Perucho M (1988): Most human carcinomas of the exocrine pancreas contain mutant c-K-ras genes. Cell 53, 549–554

Aparicio S, Hidalgo M, Kung AL (2015): Examining the utility of patient-derived xenograft mouse models. Nat Rev Cancer 15, 311–316

Apte MV, Park S, Phillips PA, Santucci N, Goldstein D, Kumar RK, Ramm GA, Buchler M, Friess H, McCarroll JA, et al. (2004): Desmoplastic Reaction in Pancreatic Cancer: Role of Pancreatic Stellate Cells. Pancreas 29, 179–187

Armstrong T (2004): Type I Collagen Promotes the Malignant Phenotype of Pancreatic Ductal Adenocarcinoma. Clin Cancer Res 10, 7427–7437

Bachem MG, Schünemann M, Ramadani M, Siech M, Beger H, Buck A, Zhou S, Schmid-Kotsas A, Adler G (2005): Pancreatic carcinoma cells induce fibrosis by stimulating proliferation and matrix synthesis of stellate cells. Gastroenterology 128, 907–921

Baharvand H, Hashemi SM, Ashtiani SK, Farrokhi A (2004): Differentiation of human embryonic stem cells into hepatocytes in 2D and 3D culture systems in vitro. Int J Dev Biol 50, 645–652

Bailey P, Chang DK, Forget M-A, Lucas FAS, Alvarez HA, Haymaker C, Chattopadhyay C, Kim S-H, Ekmekcioglu S, Grimm EA, et al. (2016): Exploiting the neoantigen landscape for immunotherapy of pancreatic ductal adenocarcinoma. Sci Rep 6, 35848

Banerjee S, Modi S, McGinn O, Zhao X, Dudeja V, Ramakrishnan S, Saluja AK (2016): Impaired Synthesis of Stromal Components in Response to Minnelide Improves Vascular Function, Drug Delivery, and Survival in Pancreatic Cancer. Clin Cancer Res 22, 415–425

Barcellos-Hoff MH, Aggeler J, Ram TG, Bissell MJ (1989): Functional differentiation and alveolar morphogenesis of primary mammary cultures on reconstituted basement membrane. Development 105, 223–225

Bengala C, Guarneri V, Giovannetti E, Lencioni M, Fontana E, Mey V, Fontana A, Boggi U, Del Chiaro M, Danesi R, et al. (2005): Prolonged fixed dose rate infusion of gemcitabine with autologous haemopoietic support in advanced pancreatic adenocarcinoma. Br J Cancer 93, 35–40

Benson AB, Wainberg ZA, Hecht JR, Vyushkov D, Dong H, Bendell J, Kudrik F (2017): A Phase II Randomized, Double-Blind, Placebo-Controlled Study of Simtuzumab or Placebo in

Combination with Gemcitabine for the First-Line Treatment of Pancreatic Adenocarcinoma. The Oncologist 22, 241-e15

Bergman AM, Pinedo HM, Jongsma APM, Brouwer M, Ruiz van Haperen VWT, Veerman G, Leyva A, Eriksson S, Peters GJ (1999): Decreased resistance to gemcitabine (2',2'-difluorodeoxycitidine) of cytosine arabinoside-resistant myeloblastic murine and rat leukemia cell lines: role of altered activity and substrate specificity of deoxycytidine kinase. Biochem Pharmacol 57, 397–406

Bhowmick NA, Neilson EG, Moses HL (2004): Stromal fibroblasts in cancer initiation and progression. Nature 432, 332–337

Biankin AV, Waddell N, Kassahn KS, Gingras M-C, Muthuswamy LB, Johns AL, Miller DK, Wilson PJ, Patch A-M, Wu J, et al. (2012): Pancreatic cancer genomes reveal aberrations in axon guidance pathway genes. Nature 491, 399–405

Biffi G, Oni TE, Spielman B, Hao Y, Elyada E, Park Y, Preall J, Tuveson DA (2019): IL1-Induced JAK/STAT Signaling Is Antagonized by TGFβ to Shape CAF Heterogeneity in Pancreatic Ductal Adenocarcinoma. Cancer Discov 9, 282–301

Birgersdotter A, Baumforth KRN, Porwit A, Sundblad A, Falk KI, Wei W, Sjöberg J, Murray PG, Björkholm M, Ernberg I (2007): Three-dimensional culturing of the Hodgkin lymphoma cell-line L1236 induces a HL tissue-like gene expression pattern. Leuk Lymphoma 48, 2042–2053

Biswas SK, Mantovani A (2010): Macrophage plasticity and interaction with lymphocyte subsets: cancer as a paradigm. Nat Immunol 11, 889–896

Boj SF, Hwang C-I, Baker LA, Chio IIC, Engle DD, Corbo V, Jager M, Ponz-Sarvise M, Tiriac H, Spector MS, et al. (2015): Organoid models of human and mouse ductal pancreatic cancer. Cell 160, 324–338

Boj SF, Hwang C-I, Baker LA, Engle DD, Tuveson DA, Clevers H (2016): Model organoids provide new research opportunities for ductal pancreatic cancer. Mol Cell Oncol 3, e1014757

Bradford JR, Farren M, Powell SJ, Runswick S, Weston SL, Brown H, Delpuech O, Wappett M, Smith NR, Carr TH, et al. (2013): RNA-Seq Differentiates Tumour and Host mRNA Expression Changes Induced by Treatment of Human Tumour Xenografts with the VEGFR Tyrosine Kinase Inhibitor Cediranib. PloS One 8, e66003

Buchholz SM, Goetze RG, Singh SK, Ammer-Herrmenau C, Richards FM, Jodrell DI, Buchholz M, Michl P, Ellenrieder V, Hessmann E, Neesse A (2020): Depletion of Macrophages Improves Therapeutic Response to Gemcitabine in Murine Pancreas Cancer. Cancers 12, E1978

Burris HA, Moore MJ, Andersen J, Green MR, Rothenberg ML, Modiano MR, Cripps MC, Portenoy RK, Storniolo AM, Tarassoff P, et al. (1997): Improvements in survival and clinical benefit with gemcitabine as first-line therapy for patients with advanced pancreas cancer: a randomized trial. J Clin Oncol 15, 2403–2413

Cabral H, Matsumoto Y, Mizuno K, Chen Q, Murakami M, Kimura M, Terada Y, Kano MR, Miyazono K, Uesaka M, et al. (2011): Accumulation of sub-100 nm polymeric micelles in poorly permeable tumours depends on size. Nat Nanotechnol 6, 815–823

Catenacci DVT, Junttila MR, Karrison T, Bahary N, Horiba MN, Nattam SR, Marsh R, Wallace J, Kozloff M, Rajdev L, et al. (2015): Randomized Phase Ib/II Study of Gemcitabine Plus Placebo or Vismodegib, a Hedgehog Pathway Inhibitor, in Patients With Metastatic Pancreatic Cancer. J Clin Oncol 33, 4284–4292

Chauhan VP, Martin JD, Liu H, Lacorre DA, Jain SR, Kozin SV, Stylianopoulos T, Mousa AS, Han X, Adstamongkonkul P, et al. (2013): Angiotensin inhibition enhances drug delivery and potentiates chemotherapy by decompressing tumour blood vessels. Nat Commun 4, 2516

Cheng X-B, Sato N, Kohi S, Yamaguchi K (2013): Prognostic Impact of Hyaluronan and Its Regulators in Pancreatic Ductal Adenocarcinoma. PLoS ONE 8, e80765

Collisson EA, Sadanandam A, Olson P, Gibb WJ, Truitt M, Gu S, Cooc J, Weinkle J, Kim GE, Jakkula L, et al. (2011): Subtypes of pancreatic ductal adenocarcinoma and their differing responses to therapy. Nat Med 17, 500–503

Conroy T, Desseigne F, Ychou M, Bouché O, Guimbaud R, Bécouarn Y, Adenis A, Raoul J-L, Gourgou-Bourgade S, de la Fouchardière C, et al. (2011): FOLFIRINOX versus Gemcitabine for Metastatic Pancreatic Cancer. N Engl J Med 364, 1817–1825

Conroy T, Hammel P, Hebbar M, Ben Abdelghani M, Wei AC, Raoul J-L, Choné L, Francois E, Artru P, Biagi JJ, et al. (2018): FOLFIRINOX or Gemcitabine as Adjuvant Therapy for Pancreatic Cancer. N Engl J Med 379, 2395–2406

Dai H, Li R, Wheeler T, Ozen M, Ittmann M, Anderson M, Wang Y, Rowley D, Younes M, Ayala GE (2007): Enhanced survival in perineural invasion of pancreatic cancer: an in vitro approach. Hum Pathol 38, 299–307

Dauer P, Zhao X, Gupta VK, Sharma N, Kesh K, Gnamlin P, Dudeja V, Vickers SM, Banerjee S, Saluja A (2018): Inactivation of Cancer-Associated-Fibroblasts Disrupts Oncogenic Signaling in Pancreatic Cancer Cells and Promotes Its Regression. Cancer Res 78, 1321–1333

de Sousa Cavalcante L, Monteiro G (2014): Gemcitabine: Metabolism and molecular mechanisms of action, sensitivity and chemoresistance in pancreatic cancer. Eur J Pharmacol 741, 8–16

de Souza PC, Ranjan A, Towner RA (2015): Nanoformulations for therapy of pancreatic and liver cancers. Nanomedicine 10, 1515–1534

Delitto D, Pham K, Vlada AC, Sarosi GA, Thomas RM, Behrns KE, Liu C, Hughes SJ, Wallet SM, Trevino JG (2015): Patient-derived xenograft models for pancreatic adenocarcinoma demonstrate retention of tumor morphology through incorporation of murine stromal elements. Am J Pathol 185, 1297–1303

Demir IE, Friess H, Ceyhan GO (2015): Neural plasticity in pancreatitis and pancreatic cancer. Nat Rev Gastroenterol Hepatol 12, 649–659

Demir IE, Reyes CM, Alrawashdeh W, Ceyhan GO, Deborde S, Friess H, Görgülü K, Istvanffy R, Jungwirth D, Kuner R, et al. (2021): Future directions in preclinical and translational cancer neuroscience research. Nat Cancer 1, 1027–1031

DGVS (2013): Kurzversion S3-Leitlinie Exokrines Pankreaskarzinom, Kurzversion 1.0 2013, 40-41. https://www.awmf.org/uploads/tx_szleitlinien/032-010OLk_S3_Exokrines_Pankreaskarzinom_21112013-abgelaufen.pdf; accessed on 24.11.2021

Di Caro G, Cortese N, Castino GF, Grizzi F, Gavazzi F, Ridolfi C, Capretti G, Mineri R, Todoric J, Zerbi A, et al. (2016): Dual prognostic significance of tumour-associated macrophages in human pancreatic adenocarcinoma treated or untreated with chemotherapy. Gut 65, 1710–1720

Dorado MR-M, Gómez LMM, Sánchez DA, Arenas SP, Praena-Fernández JM, Martín JJB, López FF, Bravo MÁG, Relat JM, Ruiz JP (2018): Translational pancreatic cancer research: A comparative study on patient-derived xenograft models. World J Gastroenterol 24, 794–809

Edmondson R, Broglie JJ, Adcock AF, Yang L (2014): Three-Dimensional Cell Culture Systems and Their Applications in Drug Discovery and Cell-Based Biosensors. Assay Drug Dev Technol 12, 207–218

Edwards BK, Ward E, Kohler BA, Eheman C, Zauber AG, Anderson RN, Jemal A, Schymura MJ, Lansdorp-Vogelaar I, Seeff LC, et al. (2010): Annual report to the nation on the status of cancer, 1975-2006, featuring colorectal cancer trends and impact of interventions (risk factors, screening, and treatment) to reduce future rates. Cancer 116, 544–573

Egeblad M, Rasch MG, Weaver VM (2010): Dynamic interplay between the collagen scaffold and tumor evolution. Curr Opin Cell Biol 22, 697–706

Elyada E, Bolisetty M, Laise P, Flynn WF, Courtois ET, Burkhart RA, Teinor JA, Belleau P, Biffi G, Lucito MS, et al. (2019): Cross-Species Single-Cell Analysis of Pancreatic Ductal Adenocarcinoma Reveals Antigen-Presenting Cancer-Associated Fibroblasts. Cancer Discov 9, 1102–1123

Erkan M, Michalski CW, Rieder S, Reiser-Erkan C, Abiatari I, Kolb A, Giese NA, Esposito I, Friess H, Kleeff J (2008): The activated stroma index is a novel and independent prognostic marker in pancreatic ductal adenocarcinoma. Clin Gastroenterol Hepatol 6, 1155–1161

Esposito I, Konukiewitz B, Schlitter AM, Klöppel G (2012): [New insights into the origin of pancreatic cancer. Role of atypical flat lesions in pancreatic carcinogenesis]. Pathologe 33 Suppl 2, 189–193

Fanchon LM, Russell J, Pillarsetty N, O'Donoghue I, Gangangari K, Yu KH, Humm JL (2020): Comparing the intra-tumoral distribution of Gemcitabine, 5-Fluorouracil, and Capecitabine in a murine model of pancreatic ductal adenocarcinoma. PloS One 15, e0231745

Feig C, Gopinathan A, Neesse A, Chan DS, Cook N, Tuveson DA (2012): The Pancreas Cancer Microenvironment. Clin Cancer Res 18, 4266–4276

Feldmann G, Maitra A (2008): Molecular Genetics of Pancreatic Ductal Adenocarcinomas and Recent Implications for Translational Efforts. J Mol Diagn 10, 111–122

Feldmann G, Beaty R, Hruban RH, Maitra A (2007): Molecular genetics of pancreatic intraepithelial neoplasia. J Hepatobiliary Pancreat Surg 14, 224–232

Flaberg E, Markasz L, Petranyi G, Stuber G, Dicső F, Alchihabi N, Oláh È, Csízy I, Józsa T, Andrén O, et al. (2011): High-throughput live-cell imaging reveals differential inhibition of tumor cell proliferation by human fibroblasts. Int J Cancer 128, 2793–2802

Frappart P-O, Walter K, Gout J, Beutel AK, Morawe M, Arnold F, Breunig M, Barth TF, Marienfeld R, Schulte L, et al. (2020): Pancreatic cancer-derived organoids – a disease modeling tool to predict drug response. United European Gastroenterol J 8, 594–606

Frese KK, Tuveson DA (2007): Maximizing mouse cancer models. Nat Rev Cancer 7, 654–658

Garcia J, Sandi MJ, Cordelier P, Binétruy B, Pouysségur J, Iovanna JL, Tournaire R (2012): Tie1 deficiency induces endothelial–mesenchymal transition. EMBO Rep 13, 431–439

Goetze R-G, Buchholz SM, Patil S, Petzold G, Ellenrieder V, Hessmann E, Neesse A (2018): Utilizing High Resolution Ultrasound to Monitor Tumor Onset and Growth in Genetically Engineered Pancreatic Cancer Models. J Vis Exp 134, 56979

Golan T, Hammel P, Reni M, Van Cutsem E, Macarulla T, Hall MJ, Park J-O, Hochhauser D, Arnold D, Oh D-Y, et al. (2019): Maintenance Olaparib for Germline *BRCA*-Mutated Metastatic Pancreatic Cancer. N Engl J Med 381, 317–327

Greenhalf W, Ghaneh P, Neoptolemos JP, Palmer DH, Cox TF, Lamb RF, Garner E, Campbell F, Mackey JR, Costello E, et al. (2014): Pancreatic cancer hENT1 expression and survival from gemcitabine in patients from the ESPAC-3 trial. J Natl Cancer Inst 106, djt347

Griesmann H, Drexel C, Milosevic N, Sipos B, Rosendahl J, Gress TM, Michl P (2017): Pharmacological macrophage inhibition decreases metastasis formation in a genetic model of pancreatic cancer. Gut 66, 1278–1285

Gurski LA, Petrelli NJ, Jia X, Farach-Carson MC (2010): 3D Matrices for Anti-Cancer Drug Testing and Development. Oncol Issues 25, 20–25

Hahn SA, Schutte M, Hoque ATMS, Moskaluk CA, Costa LT da, Rozenblum E, Weinstein CL, Fischer A, Yeo CJ, Hruban RH, Kern SE (1996): DPC4, A Candidate Tumor Suppressor Gene at Human Chromosome 18q21.1. Science 271, 350–353

Heinemann V, Xu YZ, Chubb S, Sen A, Hertel LW, Grindey GB, Plunkett W (1990): Inhibition of ribonucleotide reduction in CCRF-CEM cells by 2',2'-difluorodeoxycytidine. Mol Pharmacol 38, 567–572

Hessmann E, Patzak MS, Klein L, Chen N, Kari V, Ramu I, Bapiro TE, Frese KK, Gopinathan A, Richards FM, et al. (2018): Fibroblast drug scavenging increases intratumoural gemcitabine accumulation in murine pancreas cancer. Gut 67, 497–507

Hessmann E, Buchholz SM, Demir IE, Singh SK, Gress TM, Ellenrieder V, Neesse A (2020): Microenvironmental Determinants of Pancreatic Cancer. Physiol Rev 100, 1707-1751

Hingorani SR, Petricoin EF, Maitra A, Rajapakse V, King C, Jacobetz MA, Ross S, Conrads TP, Veenstra TD, Hitt BA, et al. (2003): Preinvasive and invasive ductal pancreatic cancer and its early detection in the mouse. Cancer Cell 4, 437–450

Hingorani SR, Wang L, Multani AS, Combs C, Deramaudt TB, Hruban RH, Rustgi AK, Chang S, Tuveson DA (2005): Trp53R172H and KrasG12D cooperate to promote chromosomal instability and widely metastatic pancreatic ductal adenocarcinoma in mice. Cancer Cell 7, 469–483

Hingorani SR, Zheng L, Bullock AJ, Seery TE, Harris WP, Sigal DS, Braiteh F, Ritch PS, Zalupski MM, Bahary N, et al. (2018): HALO 202: Randomized Phase II Study of PEGPH20 Plus Nab-Paclitaxel/Gemcitabine Versus Nab-Paclitaxel/Gemcitabine in Patients With Untreated, Metastatic Pancreatic Ductal Adenocarcinoma. J Clin Oncol 36, 359–366

Hishinuma S, Ogata Y, Tomikawa M, Ozawa I, Hirabayashi K, Igarashi S (2006): Patterns of recurrence after curative resection of pancreatic cancer, based on autopsy findings. J Gastrointest Surg 10, 511–518

Hou S, Tiriac H, Sridharan BP, Scampavia L, Madoux F, Seldin J, Souza GR, Watson D, Tuveson D, Spicer TP (2018): Advanced Development of Primary Pancreatic Organoid Tumor Models for High-Throughput Phenotypic Drug Screening. SLAS Discov 23, 574–584

Hruban RH, Goggins M, Parsons J, Kern SE (2000): Progression Model for Pancreatic Cancer. Clinical Cancer Res 6, 2969-2972

Huang C, Li Z, Li N, Li Y, Chang A, Zhao T, Wang X, Wang H, Gao S, Yang S, et al. (2018): Interleukin 35 Expression Correlates With Microvessel Density in Pancreatic Ductal Adenocarcinoma, Recruits Monocytes, and Promotes Growth and Angiogenesis of Xenograft Tumors in Mice. Gastroenterology 154, 675–688

Huang L, Holtzinger A, Jagan I, BeGora M, Lohse I, Ngai N, Nostro C, Wang R, Muthuswamy LB, Crawford HC, et al. (2015): Ductal pancreatic cancer modeling and drug screening using human pluripotent stem cell– and patient-derived tumor organoids. Nat Med 21, 1364–1371

Imamura T, Iguchi H, Manabe T, Ohshio G, Yoshimura T, Wang Z, Suwa H, Ishigami S, Imamura M (1995): Quantitative Analysis of Collagen and Collagen Subtypes I, III, and V in Human Pancreatic Cancer, Tumor-Associated Chronic Pancreatitis, and Alcoholic Chronic Pancreatitis. Pancreas 11, 357–364

Jacobetz MA, Chan DS, Neesse A, Bapiro TE, Cook N, Frese KK, Feig C, Nakagawa T, Caldwell ME, Zecchini HI, et al. (2013): Hyaluronan impairs vascular function and drug delivery in a mouse model of pancreatic cancer. Gut 62, 112–120

Jacobs E, Rathmann W: Epidemiologie des Diabetes in Deutschland. In: Deutsche Diabetes Gesellschaft (DDG) und diabetesDE - Deutsche Diabetes-Hilfe (Eds.): Deutscher Gesundheitsbericht Diabetes 2019. Verlag Kirchheim + Co GmbH; Mainz 2019, 9-20

Jiang Y-J, Lee C-L, Wang Q, Zhou Z-W, Yang F, Jin C, Fu D-L (2014): Establishment of an orthotopic pancreatic cancer mouse model: Cells suspended and injected in Matrigel. World J Gastroenterol 20, 9476–9485

Jones S, Zhang X, Parsons DW, Lin JC-H, Leary RJ, Angenendt P, Mankoo P, Carter H, Kamiyama H, Jimeno A, et al. (2008): Core Signaling Pathways in Human Pancreatic Cancers Revealed by Global Genomic Analyses. Science 321, 1801–1806

Kaufman B, Shapira-Frommer R, Schmutzler RK, Audeh MW, Friedlander M, Balmaña J, Mitchell G, Fried G, Stemmer SM, Hubert A, et al. (2015): Olaparib monotherapy in patients with advanced cancer and a germline BRCA1/2 mutation. J Clin Oncol 33, 244–250

Kawaguchi Y, Cooper B, Gannon M, Ray M, MacDonald RJ, Wright CVE (2002): The role of the transcriptional regulator Ptf1a in converting intestinal to pancreatic progenitors. Nat Genet 32, 128–134

Kedra B, Popiela T, Sierzega M, Precht A (2001): Prognostic factors of long-term survival after resective procedures for pancreatic cancer. Hepatogastroenterology 48, 1762–1766

Kelland LR (2004): "Of mice and men": Values and liabilities of the athymic nude mouse model in anticancer drug development. Eur J Cancer 40, 827–836

Kerr M, Scott HE, Groselj B, Stratford MRL, Karaszi K, Sharma NL, Kiltie AE (2014): Deoxycytidine Kinase Expression Underpins Response to Gemcitabine in Bladder Cancer. Clin Cancer Res 20, 5435–5445

Kim EJ, Sahai V, Abel EV, Griffith KA, Greenson JK, Takebe N, Khan GN, Blau JL, Craig R, Balis UG, et al. (2014): Pilot clinical trial of hedgehog pathway inhibitor GDC-0449 (vismodegib) in combination with gemcitabine in patients with metastatic pancreatic adenocarcinoma. Clin Cancer Res 20, 5937–5945

Kirkland SC (2009): Type I collagen inhibits differentiation and promotes a stem cell-like phenotype in human colorectal carcinoma cells. Br J Cancer 101, 320–326

Kromrey M-L, Bülow R, Hübner J, Paperlein C, Lerch MM, Ittermann T, Völzke H, Mayerle J, Kühn J-P (2018): Prospective study on the incidence, prevalence and 5-year pancreatic-related mortality of pancreatic cysts in a population-based study. Gut 67, 138–145

Laklai H, Miroshnikova YA, Pickup MW, Collisson EA, Kim GE, Barrett AS, Hill RC, Lakins JN, Schlaepfer DD, Mouw JK, et al. (2016): Genotype tunes pancreatic ductal adenocarcinoma tissue tension to induce matricellular fibrosis and tumor progression. Nat Med 22, 497–505

Le Calvé B, Griveau A, Vindrieux D, Maréchal R, Wiel C, Svrcek M, Gout J, Azzi L, Payen L, Cros J, et al. (2016): Lysyl oxidase family activity promotes resistance of pancreatic ductal adenocarcinoma to chemotherapy by limiting the intratumoral anticancer drug distribution. Oncotarget 7, 32100–32112

Lee AYL, Dubois CL, Sarai K, Zarei S, Schaeffer DF, Sander M, Kopp JL (2019): Cell of origin affects tumour development and phenotype in pancreatic ductal adenocarcinoma. Gut 68, 487–498

Lee JJ, Huang J, England CG, McNally LR, Frieboes HB (2013): Predictive Modeling of *In Vivo* Response to Gemcitabine in Pancreatic Cancer. PLoS Comput Biol 9, e1003231

Lee JW, Komar CA, Bengsch F, Graham K, Beatty GL (2016): Genetically Engineered Mouse Models of Pancreatic Cancer: The KPC Model (*LSL-Kras* $^{G12D/+}$ *;LSL-Trp53* $^{R172H/+}$ *;Pdx-1-Cre*), Its Variants, and Their Application in Immuno-oncology Drug Discovery: GEMMs of Pancreatic Cancer. Curr Protoc Pharmacol 73, 14.39.1-14.39.20

Lin C, Hu Z, Yuan G, Su H, Zeng Y, Guo Z, Zhong F, Jiang K, He S (2019): HIF1α-siRNA and gemcitabine combination-based GE-11 peptide antibody-targeted nanomedicine for enhanced therapeutic efficacy in pancreatic cancers. J Drug Target 27, 797–805

Lomberk G, Blum Y, Nicolle R, Nair A, Gaonkar KS, Marisa L, Mathison A, Sun Z, Yan H, Elarouci N, et al. (2018): Distinct epigenetic landscapes underlie the pathobiology of pancreatic cancer subtypes. Nat Commun 9, 1978

Loos M, Giese NA, Kleeff J, Giese T, Gaida MM, Bergmann F, Laschinger M, W Büchler M, Friess H (2008): Clinical significance and regulation of the costimulatory molecule B7-H1 in pancreatic cancer. Cancer Lett 268, 98–109

Mahadevan D, Von Hoff DD (2007): Tumor-stroma interactions in pancreatic ductal adenocarcinoma. Mol Cancer Ther 6, 1186–1197

Maitra A, Adsay NV, Argani P, Iacobuzio-Donahue C, De Marzo A, Cameron JL, Yeo CJ, Hruban RH (2003): Multicomponent Analysis of the Pancreatic Adenocarcinoma Progression Model Using a Pancreatic Intraepithelial Neoplasia Tissue Microarray. Mod Pathol 16, 902–912

Mantovani A, Sozzani S, Locati M, Allavena P, Sica A (2002): Macrophage polarization: tumor-associated macrophages as a paradigm for polarized M2 mononuclear phagocytes. Trends Immunol 23, 549–555

Maréchal R, Bachet J-B, Mackey JR, Dalban C, Demetter P, Graham K, Couvelard A, Svrcek M, Bardier-Dupas A, Hammel P, et al. (2012): Levels of gemcitabine transport and metabolism proteins predict survival times of patients treated with gemcitabine for pancreatic adenocarcinoma. Gastroenterology 143, 664-674.e6

Martin ST, Sato N, Dhara S, Chang R, Hustinx SR, Abe T, Maitra A, Goggins M (2005): Aberrant methylation of the human hedgehog interacting protein (HHIP) gene in pancreatic neoplasms. Cancer Biol Ther 4, 728–733

Martín-Villar E, Megías D, Castel S, Yurrita MM, Vilaró S, Quintanilla M (2006): Podoplanin binds ERM proteins to activate RhoA and promote epithelial-mesenchymal transition. J Cell Sci 119, 4541–4553

Mazur PK, Herner A, Mello SS, Wirth M, Hausmann S, Sánchez-Rivera FJ, Lofgren SM, Kuschma T, Hahn SA, Vangala D, et al. (2015): Combined inhibition of BET family proteins and histone deacetylases as a potential epigenetics-based therapy for pancreatic ductal adenocarcinoma. Nat Med 21, 1163–1171

McNeil C (2015): NCI-MATCH launch highlights new trial design in precision-medicine era. J Natl Cancer Inst 107, djv193

Miller BW, Morton JP, Pinese M, Saturno G, Jamieson NB, McGhee E, Timpson P, Leach J, McGarry L, Shanks E, et al. (2015): Targeting the LOX/hypoxia axis reverses many of the features that make pancreatic cancer deadly: inhibition of LOX abrogates metastasis and enhances drug efficacy. EMBO Mol Med 7, 1063–1076

Mini E, Nobili S, Caciagli B, Landini I, Mazzei T (2006): Cellular pharmacology of gemcitabine. Ann Oncol 17 Suppl 5, v7-12

Modolell I, Guarner L, Malagelada JR (1999): Vagaries of clinical presentation of pancreatic and biliary tract cancer. Ann Oncol 10 Suppl 4, 82-84

Moffitt RA, Marayati R, Flate EL, Volmar KE, Loeza SGH, Hoadley KA, Rashid NU, Williams LA, Eaton SC, Chung AH, et al. (2015): Virtual microdissection identifies distinct tumor- and stroma-specific subtypes of pancreatic ductal adenocarcinoma. Nat Genet 47, 1168–1178

Moore MJ, Goldstein D, Hamm J, Figer A, Hecht JR, Gallinger S, Au HJ, Murawa P, Walde D, Wolff RA, et al. (2007): Erlotinib Plus Gemcitabine Compared With Gemcitabine Alone in Patients With Advanced Pancreatic Cancer: A Phase III Trial of the National Cancer Institute of Canada Clinical Trials Group. J Clin Oncol 25, 1960–1966

Morris JP, Wang SC, Hebrok M (2010): KRAS, Hedgehog, Wnt and the twisted developmental biology of pancreatic ductal adenocarcinoma. Nat Rev Cancer 10, 683–695

Neesse A, Michl P, Frese KK, Feig C, Cook N, Jacobetz MA, Lolkema MP, Buchholz M, Olive KP, Gress TM, Tuveson DA (2011): Stromal biology and therapy in pancreatic cancer. Gut 60, 861–868

Neesse A, Frese KK, Bapiro TE, Nakagawa T, Sternlicht MD, Seeley TW, Pilarsky C, Jodrell DI, Spong SM, Tuveson DA (2013): CTGF antagonism with mAb FG-3019 enhances chemotherapy response without increasing drug delivery in murine ductal pancreas cancer. Proc Natl Acad Sci U S A 110, 12325–12330

Neesse A, Frese KK, Chan DS, Bapiro TE, Howat WJ, Richards FM, Ellenrieder V, Jodrell DI, Tuveson DA (2014): SPARC independent drug delivery and antitumour effects of nab-paclitaxel in genetically engineered mice. Gut 63, 974–983

Neesse A, Algül H, Tuveson DA, Gress TM (2015): Stromal biology and therapy in pancreatic cancer: a changing paradigm. Gut 64, 1476–1484

Neesse A, Bauer CA, Öhlund D, Lauth M, Buchholz M, Michl P, Tuveson DA, Gress TM (2019): Stromal biology and therapy in pancreatic cancer: ready for clinical translation? Gut 68, 159–171

Neoptolemos JP, Dunn JA, Stocken DD, Almond J, Link K, Beger H, Bassi C, Falconi M, Pederzoli P, Dervenis C, et al. (2001): Adjuvant chemoradiotherapy and chemotherapy in resectable pancreatic cancer: a randomised controlled trial. Lancet 358, 1576–1585

Neoptolemos JP, Stocken DD, Bassi C, Ghaneh P, Cunningham D, Goldstein D, Padbury R, Moore MJ, Gallinger S, Mariette C, et al. (2010): Adjuvant Chemotherapy With Fluorouracil Plus Folinic Acid vs Gemcitabine Following Pancreatic Cancer Resection: A Randomized Controlled Trial. JAMA 304, 1073–1081

Neoptolemos JP, Palmer DH, Ghaneh P, Psarelli EE, Valle JW, Halloran CM, Faluyi O, O'Reilly DA, Cunningham D, Wadsley J, et al. (2017): Comparison of adjuvant gemcitabine and capecitabine with gemcitabine monotherapy in patients with resected pancreatic cancer (ESPAC-4): a multicentre, open-label, randomised, phase 3 trial. Lancet 389, 1011–1024

Neuzillet C, Tijeras-Raballand A, Ragulan C, Cros J, Patil Y, Martinet M, Erkan M, Kleeff J, Wilson J, Apte M, et al. (2019): Inter- and intra-tumoural heterogeneity in cancer-associated fibroblasts of human pancreatic ductal adenocarcinoma. J Pathol 248, 51–65

Nicolle R, Blum Y, Marisa L, Loncle C, Gayet O, Moutardier V, Turrini O, Giovannini M, Bian B, Bigonnet M, et al. (2017): Pancreatic Adenocarcinoma Therapeutic Targets Revealed by Tumor-Stroma Cross-Talk Analyses in Patient-Derived Xenografts. Cell Rep 21, 2458–2470

NIH (2021): Surveillance, Epidemiology, and End Results (SEER) Program: Cancer Stat Facts: Pancreatic Cancer: Age-Adjusted Rates of New Cases/Deaths Per 100,000 & 5-Year Relative Survival Percentages. https://seer.cancer.gov/statfacts/html/pancreas.html, accessed on 24.11.2021

Oberstein PE, Olive KP (2013): Pancreatic cancer: why is it so hard to treat? Therap Adv Gastroenterol 6, 321–337

Oettle H, Post S, Neuhaus P, Gellert K, Langrehr J, Ridwelski K, Schramm H, Fahlke J, Zuelke C, Burkart C, et al. (2007): Adjuvant Chemotherapy With Gemcitabine vs Observation in Patients Undergoing Curative-Intent Resection of Pancreatic Cancer: A Randomized Controlled Trial. JAMA 297, 267–277

Öhlund D, Elyada E, Tuveson D (2014): Fibroblast heterogeneity in the cancer wound. J Exp Med 211, 1503–1523

Öhlund D, Handly-Santana A, Biffi G, Elyada E, Almeida AS, Ponz-Sarvise M, Corbo V, Oni TE, Hearn SA, Lee EJ, et al. (2017): Distinct populations of inflammatory fibroblasts and myofibroblasts in pancreatic cancer. J Exp Med 214, 579–596

Okano K (2014): Strategies for early detection of resectable pancreatic cancer. World J Gastroenterol 20, 11230-11240

Olive KP, Tuveson DA, Ruhe ZC, Yin B, Willis NA, Bronson RT, Crowley D, Jacks T (2004): Mutant p53 Gain of Function in Two Mouse Models of Li-Fraumeni Syndrome. Cell 119, 847–860

Olive KP, Jacobetz MA, Davidson CJ, Gopinathan A, McIntyre D, Honess D, Madhu B, Goldgraben MA, Caldwell ME, Allard D, et al. (2009): Inhibition of Hedgehog Signaling Enhances Delivery of Chemotherapy in a Mouse Model of Pancreatic Cancer. Science 324, 1457–1461

Özdemir BC, Pentcheva-Hoang T, Carstens JL, Zheng X, Wu C-C, Simpson TR, Laklai H, Sugimoto H, Kahlert C, Novitskiy SV, et al. (2014): Depletion of Carcinoma-Associated Fibroblasts and Fibrosis Induces Immunosuppression and Accelerates Pancreas Cancer with Reduced Survival. Cancer Cell 25, 719–734

Pan X, Arumugam T, Yamamoto T, Levin PA, Ramachandran V, Ji B, Lopez-Berestein G, Vivas-Mejia PE, Sood AK, McConkey DJ, Logsdon CD (2008): Nuclear factor-kappaB p65/relA silencing induces apoptosis and increases gemcitabine effectiveness in a subset of pancreatic cancer cells. Clin Cancer Res 14, 8143–8151

Park W, Chen J, Chou JF, Varghese AM, Yu KH, Wong W, Capanu M, Balachandran V, McIntyre CA, Dika IE, et al. (2020): Genomic Methods Identify Homologous Recombination Deficiency in Pancreas Adenocarcinoma and Optimize Treatment Selection. Clin Cancer Res 26, 3239–3247

Patzak MS, Kari V, Patil S, Hamdan FH, Goetze RG, Brunner M, Gaedcke J, Kitz J, Jodrell DI, Richards FM, et al. (2019): Cytosolic 5'-nucleotidase 1A is overexpressed in pancreatic cancer and mediates gemcitabine resistance by reducing intracellular gemcitabine metabolites. EBioMedicine 40, 394–405

Porta M, Fabregat X, Malats N, Guarner L, Carrato A, de Miguel A, Ruiz L, Jariod M, Costafreda S, Coll S, et al. (2005): Exocrine pancreatic cancer: Symptoms at presentation and their relation to tumour site and stage. Clin Transl Oncol 7, 189–197

Provenzano PP, Cuevas C, Chang AE, Goel VK, Von Hoff DD, Hingorani SR (2012): Enzymatic Targeting of the Stroma Ablates Physical Barriers to Treatment of Pancreatic Ductal Adenocarcinoma. Cancer Cell 21, 418–429

Qin B-D, Jiao X-D, Liu K, Wu Y, He X, Liu J, Qin W-X, Wang Z, Zang Y-S (2019): Basket Trials for Intractable Cancer. Front Oncol 9, 229

Quante AS, Ming C, Rottmann M, Engel J, Boeck S, Heinemann V, Westphalen CB, Strauch K (2016): Projections of cancer incidence and cancer-related deaths in Germany by 2020 and 2030. Cancer Med 5, 2649–2656

Quintanilla M, Montero-Montero L, Renart J, Martín-Villar E (2019): Podoplanin in Inflammation and Cancer. Int J Mol Sci 20, 707

Rahib L, Smith BD, Aizenberg R, Rosenzweig AB, Fleshman JM, Matrisian LM (2014): Projecting Cancer Incidence and Deaths to 2030: The Unexpected Burden of Thyroid, Liver, and Pancreas Cancers in the United States. Cancer Res 74, 2913–2921

Ramu I, Buchholz SM, Patzak MS, Goetze RG, Singh SK, Richards FM, Jodrell DI, Sipos B, Ströbel P, Ellenrieder V, et al. (2019): SPARC dependent collagen deposition and gemcitabine delivery in a genetically engineered mouse model of pancreas cancer. EBioMedicine 48, 161–168

Reichert M, Rustgi AK (2011): Pancreatic ductal cells in development, regeneration, and neoplasia. J Clin Invest 121, 4572–4578

Relling MV, Evans WE (2015): Pharmacogenomics in the clinic. Nature 526, 343–350

Rhim AD, Oberstein PE, Thomas DH, Mirek ET, Palermo CF, Sastra SA, Dekleva EN, Saunders T, Becerra CP, Tattersall IW, et al. (2014): Stromal Elements Act to Restrain, Rather Than Support, Pancreatic Ductal Adenocarcinoma. Cancer Cell 25, 735–747

RKI, GEKID (Eds.): Bauchspeicheldrüse. In: Krebs in Deutschland für 2015/2016. 12nd edition; Berlin 2020, 52-55

Rubio-Viqueira B, Jimeno A, Cusatis G, Zhang X, Iacobuzio-Donahue C, Karikari C, Shi C, Danenberg K, Danenberg PV, Kuramochi H, et al. (2006): An *In vivo* Platform for Translational Drug Development in Pancreatic Cancer. Clin Cancer Res 12, 4652–4661

Rygaard J, Poulsen CO (1969): Heterotransplantation of a human malignant tumour to "Nude" mice. Acta Pathol Microbiol Scand 77, 758–760

Saatci O, Kaymak A, Raza U, Ersan PG, Akbulut O, Banister CE, Sikirzhytski V, Tokat UM, Aykut G, Ansari SA, et al. (2020): Targeting lysyl oxidase (LOX) overcomes chemotherapy resistance in triple negative breast cancer. Nat Commun 11, 2416

Sato N, Fukushima N, Maehara N, Matsubayashi H, Koopmann J, Su GH, Hruban RH, Goggins M (2003): SPARC/osteonectin is a frequent target for aberrant methylation in pancreatic adenocarcinoma and a mediator of tumor–stromal interactions. Oncogene 22, 5021–5030

Schindelin J, Arganda-Carreras I, Frise E, Kaynig V, Longair M, Pietzsch T, Preibisch S, Rueden C, Saalfeld S, Schmid B, et al. (2012): Fiji: an open-source platform for biological-image analysis. Nat Methods 9, 676–682

Sharpless NE, DePinho RA (2006): The mighty mouse: genetically engineered mouse models in cancer drug development. Nat Rev Drug Discov 5, 741–754

Sherman MH, Yu RT, Engle DD, Ding N, Atkins AR, Tiriac H, Collisson EA, Connor F, Van Dyke T, Kozlov S, et al. (2014): Vitamin D Receptor-Mediated Stromal Reprogramming Suppresses Pancreatitis and Enhances Pancreatic Cancer Therapy. Cell 159, 80–93

Shibuya KC, Goel VK, Xiong W, Sham JG, Pollack SM, Leahy AM, Whiting SH, Yeh MM, Yee C, Riddell SR, Pillarisetty VG (2014): Pancreatic ductal adenocarcinoma contains an effector and regulatory immune cell infiltrate that is altered by multimodal neoadjuvant treatment. PloS One 9, e96565

Siegel RL, Miller KD, Jemal A (2019): Cancer statistics, 2019. CA Cancer J Clin 69, 7–34

Simian M, Bissell MJ (2017): Organoids: A historical perspective of thinking in three dimensions. J Cell Biol 216, 31–40

Singh SK, Chen N, Hessmann E, Siveke J, Lahmann M, Singh G, Voelker N, Vogt S, Esposito I, Schmidt A, et al. (2015): Antithetical NFAT c1–Sox2 and p53–miR200 signaling networks govern pancreatic cancer cell plasticity. EMBO J 34, 517–530

Sironen R, Tammi M, Tammi R, Auvinen P, Anttila M, Kosma V-M (2011): Hyaluronan in human malignancies. Exp Cell Res 317, 383–391

Sohn TA, Yeo CJ, Cameron JL, Koniaris L, Kaushal S, Abrams RA, Sauter PK, Coleman J, Hruban RH, Lillemoe KD (2000): Resected adenocarcinoma of the pancreas-616 patients: results, outcomes, and prognostic indicators. J Gastrointest Surg 4, 567–579

Stylianopoulos T, Jain RK (2013): Combining two strategies to improve perfusion and drug delivery in solid tumors. Proc Natl Acad Sci U S A 110, 18632–18637

Sugarman R, Patel R, Sharma S, Plenker D, Tuveson D, Saif MW (2019): Pharmacokinetics and pharmacodynamics of new drugs for pancreatic cancer. Expert Opin Drug Metab Toxicol 15, 541–552

Swarm RL (1963): Transplantation of a murine chondrosarcoma in mice of different inbred strains. J Natl Cancer Inst 31, 953–975

Tanaka M, Fernández-del Castillo C, Adsay V, Chari S, Falconi M, Jang J-Y, Kimura W, Levy P, Pitman MB, Schmidt CM, et al. (2012): International consensus guidelines 2012 for the management of IPMN and MCN of the pancreas. Pancreatology 12, 183–197

Thomas RM, Truty MJ, Kim M, Kang Y, Zhang R, Chatterjee D, Katz MH, Fleming JB (2015): The canary in the coal mine: the growth of patient-derived tumorgrafts in mice predicts clinical recurrence after surgical resection of pancreatic ductal adenocarcinoma. Ann Surg Oncol 22, 1884–1892

Thota R, Maitra A, Berlin JD (2017): Preclinical Rationale for the Phase III Trials in Metastatic Pancreatic Cancer: Is Wishful Thinking Clouding Successful Drug Development for Pancreatic Cancer? Pancreas 46, 143–150

Tiriac H, Belleau P, Engle DD, Plenker D, Deschênes A, Somerville TDD, Froeling FEM, Burkhart RA, Denroche RE, Jang G-H, et al. (2018): Organoid Profiling Identifies Common Responders to Chemotherapy in Pancreatic Cancer. Cancer Discov 8, 1112–1129

Tsai S, McOlash L, Palen K, Johnson B, Duris C, Yang Q, Dwinell MB, Hunt B, Evans DB, Gershan J, James MA (2018): Development of primary human pancreatic cancer organoids, matched stromal and immune cells and 3D tumor microenvironment models. BMC Cancer 18, 335

Van Cutsem E, Tempero MA, Sigal D, Oh D-Y, Fazio N, Macarulla T, Hitre E, Hammel P, Hendifar AE, Bates SE, et al. (2020): Randomized Phase III Trial of Pegvorhyaluronidase Alfa With Nab-Paclitaxel Plus Gemcitabine for Patients With Hyaluronan-High Metastatic Pancreatic Adenocarcinoma. J Clin Oncol 38, 3185–3194

Van Duyne GD (2001): A Structural View of Cre-loxP Site-Specific Recombination. Annu Rev Biophys Biomol Struct 30, 87–104

Vogelstein B, Fearon ER, Hamilton SR, Kern SE, Preisinger AC, Leppert M, Smits AMM, Bos JL (1988): Genetic Alterations during Colorectal-Tumor Development. N Engl J Med 319, 525–532

Von Hoff DD, Ervin T, Arena FP, Chiorean EG, Infante J, Moore M, Seay T, Tjulandin SA, Ma WW, Saleh MN, et al. (2013): Increased Survival in Pancreatic Cancer with nab-Paclitaxel plus Gemcitabine. N Engl J Med 369, 1691–1703

Vonlaufen A, Joshi S, Qu C, Phillips PA, Xu Z, Parker NR, Toi CS, Pirola RC, Wilson JS, Goldstein D, Apte MV (2008): Pancreatic Stellate Cells: Partners in Crime with Pancreatic Cancer Cells. Cancer Res 68, 2085–2093

Weizman N, Krelin Y, Shabtay-Orbach A, Amit M, Binenbaum Y, Wong RJ, Gil Z (2014): Macrophages mediate gemcitabine resistance of pancreatic adenocarcinoma by upregulating cytidine deaminase. Oncogene 33, 3812–3819

Whatcott CJ, Diep CH, Jiang P, Watanabe A, LoBello J, Sima C, Hostetter G, Shepard HM, Von Hoff DD, Han H (2015): Desmoplasia in Primary Tumors and Metastatic Lesions of Pancreatic Cancer. Clin Cancer Res 21, 3561–3568

Winter JM, Maitra A, Yeo CJ (2006): Genetics and pathology of pancreatic cancer. HPB (Oxford) 8, 324–336

Witkiewicz AK, Balaji U, Eslinger C, McMillan E, Conway W, Posner B, Mills GB, O'Reilly EM, Knudsen ES (2016): Integrated Patient-Derived Models Delineate Individualized Therapeutic Vulnerabilities of Pancreatic Cancer. Cell Rep 16, 2017–2031

Wong A, Soo RA, Yong W-P, Innocenti F (2009): Clinical pharmacology and pharmacogenetics of gemcitabine. Drug Metab Rev 41, 77–88

Wörmann SM, Diakopoulos KN, Lesina M, Algül H (2014): The immune network in pancreatic cancer development and progression. Oncogene 33, 2956–2967

Xu S, Xu H, Wang W, Li S, Li H, Li T, Zhang W, Yu X, Liu L (2019): The role of collagen in cancer: from bench to bedside. J Transl Med 17, 309

Yauch RL, Settleman J (2012): Recent advances in pathway-targeted cancer drug therapies emerging from cancer genome analysis. Curr Opin Genet Dev 22, 45–49

Zhou Yang, Zhou Yunjiang, Wang K, Li T, Zhang M, Yang Y, Wang R, Hu R (2019): ROCK2 Confers Acquired Gemcitabine Resistance in Pancreatic Cancer Cells by Upregulating Transcription Factor ZEB1. Cancers (Basel) 11, 1881

Acknowledgements

The journey of my dissertation was definitely one of the most challenging and instructive times of my life. However, I also experienced so much joy and memorable moments with people I will probably never forget.

In the beginning, I would like to thank Prof. Dr. Ellenrieder who gave me the opportunity to perform my thesis in his clinic. Furthermore, I am very grateful to my first supervisor Prof. Dr. Dr. Albrecht Neesse who let me work in his lab for my thesis. Though not every plan worked out the way it was supposed to be, You - at all times - found a solution and created a new plan. Thank You. Moreover, I would like to thank my second supervisor Prof. Dr. Wolfram-Hubertus Zimmermann who was part of my thesis committee.

I was not only supported by certain people but also by the *Promotionskolleg für Medizinstudiere*, which is led by Prof. Dr. Matthias Dobbelstein and Prof. Dr. Martin Oppermann and organized by then Helen Mayrhofer and now Dr. Daria Witt. To this day, I still believe that this program incorporates money well spent. Firstly, it gives medical students the chance to get to know preclinical research which is not significantly thematized during the course of the regular studies. Through this, it becomes clear that medicine is not only made in Clinics with doctors, nursing staff and other clinical personal, but also in labs where scientists, technicians and PhD students work. Secondly, individual supervision through e. g. workshops is framed by financial support. It is guaranteed that colleagues can continuously focus on their thesis while having the chance for being supported individually.

During my full-time lab work, I was accompanied by the two technicians Jutta Blumberg and Ulrike Wegner. Moreover, PhD student Nina Pfisterer worked on her thesis while I stayed in the lab. Also Dr. Robert Goetze and Dr. Christoph Ammer-Herrmenau supported me in conducting sonography and in statistical analysis. Thank You all for helpful advice and assistance in experiments.

During the development of this thesis, I coorporated also with other labs. For one, I would like to thank AG Ellenrieder, especially Kristina Reutlinger, Dr. Geske Schmidt and Dr. Sercan Mercan, for the support in mice breeding as well as experiments. In this manner, I also like to mention Tobias Kaiser for his excellent care. Secondly, I would like to thank AG Hessmann, especially Prof. Dr. Elisabeth Hessmann, Waltraut Kopp and Jessica Spitalieri who gave me the opportunity to include the PDX model in this work and were also helpful in scientic manners. Furthermore, I would like to thank Benjamin Steuber and Dr. Marie Hasselluhn for both supervision in the quantification process and individually.

Besides the labs of the Clinic for Gastroenterology, gastrointestinal Oncology & Endocrinology, I would like to thank Prof. Dr. Philipp Stroebel and Dr. Mark-Sebastian Boesherz who provided the primary resected tissue from patients and supported me in experiments with organoids.

Moreover, I would like to thank Prof. Dr. Wolfram-Hubertus Zimmermann and Marcel Zoremba for the opportunity of using the sonography equipment.

A special thanks goes out to the team of the Medical Statistics Unit of the UMG which assisted me in statistical analysis.

Danksagung

Der Weg meiner Dissertation war sicherlich eine der lehrreichsten und fordernsten Zeiten meines bisherigen Lebensweges. Dennoch verbinde ich mit diesem Weg viel Freude und Momente mit Menschen, die ich wahrscheinlich für immer in Erinnerung behalten werde.

Am Anfang möchte ich mich bei Herrn Prof. Dr. Volker Ellenrieder bedanken, welcher mir die Gelegenheit gab in seiner Klinik zu promovieren. Besonders dankbar bin ich meinem direkten Doktorvater Herrn Prof. Dr. Dr. Albrecht Neeße, in dessen Arbeitsgruppe ich arbeiten durfte. Obwohl nicht jeder Plan so funktionerte wie Wir Uns das vorstellten, fanden Sie – über die ganze Zeit – stets eine Lösung und hatten einen neuen Plan in der Tasche. Ich danke Ihnen. Zudem danke ich meinem Zweitbetreuer Herrn Prof. Dr. Wolfram-Hubertus Zimmermann, der Teil meines Betreuungsausschusses war.

Die individuelle Unterstützung, die ich erfahren durfte, wurde durch das *Promotionskolleg für Medizinstudierende* ergänzt, welches von Herrn Prof. Dr. Matthias Dobbelstein und Herrn Prof. Dr. Martin Oppermann geleitet und einst von Frau Helen Mayrhofer und derzeit von Frau Dr. Daria Witt organisiert wird. Ich glaube bis zu diesem Tag daran, dass dieses Programm jeden Cent seines Fördergeldes wert ist. Zum einen gibt es Medizinstudent:innen die Chance die präklinische Forschung kennenzulernen, welche im Studium nicht gesondert thematisiert wird. Dadurch wird deutlich, dass Medizin nicht nur in den verschiedenen (Fachbereichs-) Kliniken durch ärztliches, pflegerisches und weiterem Personal, sondern gleichwertig in den Forschungslaboren von Forschern, technischen Assistenten und PhD-Student:innen tagtäglich praktiziert wird. Zum anderen wird individuelle Betreuung durch bsp. verschiedenen Lehrangeboten und finanzielle Unterstützung abgerundet. Es wird sichergestellt, dass sich die Kollegiat:innen kontinuierlich auf ihre Dissertation konzentrieren können. Ich würde jederzeit wieder teilnehmen.

Während der zwei Freisemester wurde ich von den beiden medizinisch-technischen Assistentinnen Jutta Blumberg und Ulrike Wegner betreut. Desweiteren arbeitete Nina Pfisterer an ihrer naturwissenschaftlichen Doktorarbeit. Herr Dr. Robert Götze und Herr Dr. Christoph Ammer-Herrmenau halfen mir bei den Ultraschallen und der statistischen Auswertung. Ich danke Euch allen für hilfreiche Ratschläge und Unterstützung bei den Experimenten.

Neben der Arbeitsgruppe des Herrn Prof. Dr. Dr. Albrecht Neeße arbeitete ich auch mit anderen Arbeitsgruppen zusammen. Zum einen möchte ich mich bei AG Ellenrieder und besonders Kristina Reutlinger, Frau Dr. Geske Schmidt und Herrn Dr. Sercan Mercan für die Unterstützung bei der Mauszucht und Experimenten bedanken. An dieser Stelle möchte ich Tobias Kaiser nennen, durch den eine ausgezeichnete Pflege praktiziert wird. Zum anderen möchte ich AG Heßmann mit Frau Prof. Dr. Elisabeth Heßmann, Waltraut Kopp und Jessica Spitalieri meinen Dank aussprechen, wodurch ich das PDX-Modell mit in die Experimente einbinden und wissenschaftliche Fragen klären konnte. Ich danke zudem Benjamin

Steuber und Frau Dr. Marie Hasselluhn, welche mich im Rahmen der Quantifizierungen und auch individuell unterstützten.

Neben den klinik-internen Laboren möchte ich meinen Dank Herrn Prof. Dr. Philipp Ströbel und Herrn Dr. Mark-Sebastian Bösherz für die Bereitstellung von Patientenmaterial und die Unterstützung mit Experimenten von Organoiden aussprechen.

Weiterhin möchte ich mich bei Herrn Prof. Dr. Wolfram-Hubertus Zimmermann und Marcel Zoremba für die Nutzung des Ultraschallequipments bedanken.

Desweiteren bedanke ich mich bei der Medinischen Statistikberatung der UMG, welche mir bei den statistischen Auswertungen half.